

# Accuracy of *ab initio* methods in predicting the crystal structures of metals: review of 80 binary alloys.

Stefano Curtarolo<sup>1,3</sup>, Dane Morgan<sup>2</sup>, Gerbrand Ceder<sup>2</sup>

<sup>1</sup>*Department of Mechanical Engineering and Materials Science, Duke University, Durham, NC 27708*

<sup>2</sup>*Department of Materials Science and Engineering, MIT, Cambridge, MA 02139*

<sup>3</sup>*corresponding author, e-mail: stefano@duke.edu*

(August 29, 2018)

Predicting and characterizing the crystal structure of materials is a key problem in materials research and development. We report the results of *ab initio* LDA/GGA computations for the following systems: AgAu, AgCd, AgMg, AgMo\*, AgNa, AgNb\*, AgPd, AgRh\*, AgRu\*, AgTc\*, AgTi, AgY, AgZr, AlSc, AuCd, AuMo\*, AuNb, AuPd, AuPt\*, AuRh\*, AuRu\*, AuSc, AuTc\*, AuTi, AuY, AuZr, CdMo\*, CdNb\*, CdPd, CdPt, CdRh, CdRu\*, CdTc\*, CdTi, CdY, CdZr, CrMg\*, MoNb, MoPd, MoPt, MoRh, MoRu, MoTc\*, MoTi, MoY\*, MoZr, NbPd, NbPt, NbRh, NbRu, NbTc, NbY\*, NbZr\*, PdPt, PdRh\*, PdRu\*, PdTc, PdTi, PdY, PdZr, PtRh, PtRu, PtY, PtTc, PtTi, PtZr, RhRu, RhTc, RhTi, RhY, RhZr, RuTi, RuTc, RuY, RuZr, TcTi, TcY, TcZr, TiZr\*, YZr\* (\* = systems in which the *ab initio* method predicts that no compounds are stable). A detailed comparison to experimental data confirms the high accuracy with which *ab initio* methods can predict ground states.

Keywords: Binary Alloys, *Ab initio*, Intermetallics, Transition Metals, Structure Prediction, Phase Stability, Aluminum, Cadmium, Gold, Magnesium, Molybdenum, Niobium, Palladium, Platinum, Rhodium, Ruthenium, Scandium, Silver, Sodium, Titanium, Technetium, Yttrium, Zirconium.

## CONTENTS

I. Introduction	1
II. The library: alloys and structures	2
III. High-throughput First Principles calculations	3
IV. Discussion and summary of results	4
A. Discussion of disagreement between experimental and <i>ab initio</i> results	5
V. Conclusions	6
VI. Alloys without <i>ab initio</i> compounds	8
VII. Alloys with <i>ab initio</i> compounds	9
VIII. Trend for Technetium alloys	45
IX. Acknowledgments	46
X. Tables of Results	47
A. Experimental compounds in agreement with <i>ab initio</i> solutions	47
B. Experimentally unknown, non-identified or speculated compounds and <i>ab initio</i> predictions	48
C. Experimental solid solutions, two-phases and “not studied” regions and possible <i>ab initio</i> predictions	49
D. Experimental compounds that could not be checked by our calculations	51
E. Experimental compounds in disagreement with other <i>ab initio</i> compounds or two-phase regions	52
XI. Appendix: new structure prototypes which are superstructures of FCC, BCC, HCP	53
XII. Appendix: relaxed structure prototypes	53
References	54

## I. INTRODUCTION

First principles computation, whereby the properties of materials are predicted starting from the principles of quantum mechanics, is becoming well integrated with more traditional materials research. A list of *ab initio* studies on binary and ternary alloy phase stability up to 1994 can be found in reference [1]. Since the earliest, completely *ab initio* computation of a binary phase diagram [2], the approaches to compute the total energy of a solid have significantly improved, and computing resources have continued to become faster and less expensive. We believe that a point has been reached where, with a reasonable amount of resources, high throughput first principles studies of a large number of alloys can be performed [3–8]. In this paper we present the results of a first principles study of 14080 computed total energies on 176 crystal structures in 80 binary alloys. To our knowledge this is the largest first principles study of its kind on alloys. As we have compared the results in every system to experimental compilations, this study also offers a statistical test on the accuracy of some current *ab initio* approaches in correctly predicting the structure of materials.

For 89 compounds we find unambiguous agreement between experiment and the *ab initio* computation (Table 5), giving some indication of the predictive power of modern *ab initio* electronic structure methods. For many systems, verification of the *ab initio* results is difficult, as the systems have been poorly or incompletely characterized,

or only high-temperature information is available experimentally. For most of these system, we make predictions that are consistent with the limited available information. Even though our library of 176 crystal structures is, to our knowledge, the largest library of *ab initio* energies ever produced, there are still 27 compounds for which we cannot verify the experimental structures as they are not in our library. We have not included such prototypes because they are extremely rare and complicated (many atoms per unit cell) (Table 8).

Overall, we find remarkably few significant discrepancies between the *ab initio* predictions and the experimental observations (Table 9). Based on the experimental data in references [9,10], we find only nine compounds for which LDA/GGA seems to predict the ground state incorrectly. For four of these nine systems, the experimental ground state is within less than 10meV/atom of the *ab initio* ground state. For the remaining five systems, there are at least two in which further investigation indicates that the experimental structure assignment is poorly justified, leaving three compounds in which a significant disagreement between experiment and *ab initio* LDA/GGA is likely. Such disagreements are addressed in Section (IV).

We believe that the low ratio of unambiguous errors (3) to the number of unambiguous correct predictions (89) is encouraging, and establishes clearly the potential of predicting crystal structure correctly with *ab initio* methods.

We also predict the stability of five new crystal structures which, to the best of our knowledge, have not yet been observed in any system. An AB<sub>3</sub> superstructure of the fcc lattice, stable for CdPt<sub>3</sub>, PdPt<sub>3</sub> and Pd<sub>3</sub>Pt, an AB bcc superstructure for MoTi, an AB<sub>3</sub> bcc superstructure for MoTi<sub>3</sub>, Mo<sub>3</sub>Ti, Nb<sub>3</sub>Tc, RuTi<sub>3</sub> and TcTi<sub>3</sub>, an A<sub>2</sub>B<sub>2</sub> hcp superstructure for RhRu, and an A<sub>2</sub>B<sub>4</sub> hcp superstructure for RhRu<sub>2</sub> (Appendix (XI)). In addition, we find two new crystal structures which are not superstructures of fcc, bcc or hcp: MoZr<sub>3</sub> and Mo<sub>5</sub>Ti (for Mo<sub>5</sub>Ti, MoZr<sub>5</sub>, and Nb<sub>5</sub>Ru) (Appendix (XII)).

## II. THE LIBRARY: ALLOYS AND STRUCTURES

**Binary alloys.** Our calculated library contains 80 binary intermetallic alloys. The alloys include the binaries that can be made from row 5 transition metals, as well as some systems with Aluminum, Gold, Magnesium, Platinum, Scandium, Sodium, Titanium, and Technetium. The alloys are: AgAu, AgCd, AgMg, AgMo\*, AgNa, AgNb\*, AgPd, AgRh\*, AgRu\*, AgTc\*, AgTi, AgY, AgZr, AuCd, AuMo\*, AuNb, AuPd, AuPt\*, AuRh\*, AuRu\*, AuSc, AuTc\*, AuTi, AuY, AuZr, AlSc, CdMo\*, CdNb\*, CdPd, CdPt, CdRh, CdRu\*, CdTc\*, CdTi, CdY, CdZr, CrMg\*, MoNb, MoPd, MoPt, MoRh,

MoRu, MoTc\*, MoTi, MoY\*, MoZr, NbPd, NbPt, NbRh, NbRu, NbTc, NbY\*, NbZr\*, PdPt, PdRh\*, PdRu\*, PdTc, PdTi, PdY, PtRh, PtRu, PtY, PtTc, PdZr, PtTi, PtZr, RhRu, RhTc, RhTi, RhY, RhZr, RuTi, RuTc, RuY, RuZr, TcTi, TcY, TcZr, TiZr\*, YZr\*, where the superscript \* indicates the systems in which the *high throughput ab initio* method predicts that no compounds are stable: 57 alloys form compounds and 23 are non compound forming.

**Structures and their prototypes.** The library contains 176 crystal structures. Many of these have the same structure type but with different compositions of occupancies, for example, AB<sub>3</sub> and A<sub>3</sub>B (also AB and BA if the point groups of atomic positions of A and B are different), so the number of distinct prototypes is 101. The various concentrations are listed in the table below.

Compounds composition	Conc. of B	number of prototypes
A & B	0%	4
A <sub>5</sub> B & AB <sub>5</sub>	16.66%	3
A <sub>4</sub> B & AB <sub>4</sub>	20%	2
A <sub>3</sub> B & AB <sub>3</sub>	25%	27
A <sub>2</sub> B & AB <sub>2</sub>	33.33%	32
A <sub>5</sub> B <sub>3</sub> & A <sub>3</sub> B <sub>5</sub>	37.5%	2
A <sub>3</sub> B <sub>2</sub> & A <sub>2</sub> B <sub>3</sub>	40%	1
A <sub>4</sub> B <sub>3</sub> & A <sub>3</sub> B <sub>4</sub>	42.85%	1
AB (& BA*)	50%	29 (+3)

TABLE 1. Compositions, concentrations and number of prototypes inside the library. The library has 176 structures, and 101 distinct prototypes (\* at composition AB, 3 prototypes have different point groups in atomic positions A and B, therefore they represent distinct structure types).

Of such prototypes, 65 are chosen from the most common intermetallic binary structures in the CRYSTMET database [11] and in the Pauling File [10]. Such prototypes can be described by their Strukturbericht designation and/or natural prototypes [9,10]: A1, A2, A3, A4, A15, B<sub>h</sub>, B1, B2, B3, B4, B8<sub>1</sub>, B8<sub>2</sub>, B10, B11, B19, B27, B32, B33 (B<sub>f</sub>), C<sub>c</sub>, C2, C6, C11<sub>b</sub>, C14, C15, C15<sub>b</sub>, C16, C18, C22, C32, C33, C37, C38, C49, D0<sub>a</sub>, D0<sub>3</sub>, D0<sub>9</sub>, D0<sub>11</sub>, D0<sub>19</sub>, D0<sub>22</sub>, D0<sub>23</sub>, D0<sub>24</sub>, D1<sub>3</sub>, D1<sub>a</sub>, D2<sub>d</sub>, D7<sub>3</sub>, D8<sub>8</sub>, L1<sub>0</sub>, L1<sub>1</sub>, L1<sub>2</sub>, L6<sub>0</sub>, CaIn<sub>2</sub>, CuTe, CuZr<sub>2</sub>, GdSi<sub>2</sub> (1.4), MoPt<sub>2</sub>, NbAs (NbP), NbPd<sub>3</sub>, Ni<sub>2</sub>Si, Ω (with z=1/4), Pu<sub>3</sub>Al (Co<sub>3</sub>V), Ti<sub>3</sub>Cu<sub>4</sub>, W<sub>5</sub>Si<sub>3</sub>, YCd<sub>3</sub>, ZrSi<sub>2</sub>, γ-Ir. The rest of the structures (36) are fcc, bcc or hcp superstructures. Twelve of these superstructures consist of stacking of pure A and B planes along some direction. Of such prototypes, 12 contain a stacking direction, therefore we can name them following the parent lattice and the stacking direction:

$$LATTICE_{stacking}^{direction}. \quad (1)$$

For example the designation  $FCC_{A_2B_2}^{[001]}$  indicates a structure prototype with FCC parent lattice and A2B2

stacking along direction [001]. The 12 prototypes of the library that can be labeled in this manner are:  $BCC_{AB_2}^{[011]}$ ,  $BCC_{AB_2}^{[211]}$ ,  $FCC_{A_2B_2}^{[001]}$ ,  $FCC_{A_2B_2}^{[011]}$ ,  $FCC_{A_2B_2}^{[111]}$ ,  $FCC_{A_2B_2}^{[311]}$ ,  $FCC_{AB_2}^{[100]}$ ,  $FCC_{AB_2}^{[111]}$ ,  $FCC_{AB_3}^{[001]}$ ,  $FCC_{AB_3}^{[011]}$ ,  $FCC_{AB_3}^{[111]}$ . For the FCC superstructures, a conversion table between the lattice-stacking-direction, the Sanchez - de Fontaine notation [12], and the Lu *et al.* designations [13,14] is included below.

	Space Group	Sanchez - de Fontaine [12]	Lu <i>et al.</i> [13,14]	Here and [15]
AB <sub>2</sub>	I4/mmm #139	AB <sub>2</sub> (c)	$\beta 1/\beta 2$	$FCC_{AB_2}^{[100]}$
AB <sub>2</sub>	P $\bar{3}m1$ #164		$\alpha 1/\alpha 2$	$FCC_{AB_2}^{[111]}$
AB <sub>3</sub>	P4/mmm #123		Z1/Z3	$FCC_{AB_3}^{[001]}$
A <sub>2</sub> B <sub>2</sub>	P4/nmm #129	AB(a)	Z2	$FCC_{A_2B_2}^{[001]}$
A <sub>2</sub> B <sub>2</sub>	C2/m #12		W2	$FCC_{A_2B_2}^{[311]}$
AB <sub>3</sub>	Pmmm #47		Y1/Y3	$FCC_{AB_3}^{[011]}$
A <sub>2</sub> B <sub>2</sub>	Pmmn #59	AB(e)	Y2	$FCC_{A_2B_2}^{[011]}$
A <sub>2</sub> B <sub>2</sub>	I4 <sub>1</sub> /amd #141		CH or "40"	$FCC_{A_2B_2}^{[201]}$
AB <sub>3</sub>	R $\bar{3}m$ #166		V1/V3	$FCC_{AB_3}^{[111]}$
A <sub>2</sub> B <sub>2</sub>	R $\bar{3}m$ #166		V2	$FCC_{A_2B_2}^{[111]}$

TABLE 2. Conversion table between the lattice-stacking-direction, the Sanchez - de Fontaine notation [12], and the Lu *et al.* designations [13,14].

The prototypes of stable structures, that cannot be described by Strukturbericht designation, natural prototypes or lattice-stacking-direction convention, are described in Appendix XI. The complete geometrical description of all the fcc, bcc, and hcp superstructures of the library can be found in reference [15].

### III. HIGH-THROUGHPUT FIRST PRINCIPLES CALCULATIONS

**Ultra Soft Pseudopotentials LDA calculations (US-LDA).** Most of the energy calculations of the library were performed using Density Functional Theory in the Local Density Approximation (LDA), with the Ceperley-Alder form for the correlation energy as parameterized by Perdew-Zunger [18] with ultra soft Vanderbilt type pseudopotentials [19], as implemented in VASP [20]. Calculations are at zero temperature and pressure, and without zero-point motion. The energy cutoff in an alloy was set to 1.5 times the larger of the suggested energy cutoffs of the pseudopotentials of the elements of the alloy (suggested energy cutoffs are derived by the method described in [20]). Brillouin zone integrations were done using 2000/(number of atoms in unit cell)  $\mathbf{k}$ -points distributed as uniformly as possible on a Monkhorst-Pack mesh [21,22]. For a sample set of calculations, we verified that with these energy cutoffs and  $\mathbf{k}$ -points meshes the absolute energy is converged

to better than 10 meV/atom. Energy differences between structures are expected to be converged to much smaller tolerances. Spin polarization was used only for magnetic alloys. For the non-magnetic ones, spin polarization was used only to verify the energies of the ground state structures. All structures were fully relaxed. With such methodology, we consider degenerate structures the ones that have energies closer than about 5meV/atom.

We have decided to calculate the entire library within the LDA formalism instead of the PAW-GGA method (discussed below) because of the faster execution speed of LDA.

**PAW-GGA calculations.** When several structures are in close competition for the ground state, we also performed calculations in the Generalized Gradient Approximation (GGA), with Projector Augmented-Wave (PAW) pseudopotentials, as implemented in VASP [20,23,24]. One would expect the PAW-GGA approach to be somewhat more accurate than the US-LDA. For the GGA correlation energy, we used the Perdew-Wang parameterization (GGA-PW91) [25]. Similar to the US-LDA case, all PAW-GGA calculations are performed at zero temperature and pressure, and without zero-point motion. The energy cutoff in each calculation was set to 1.75 times the larger of the suggested energy cutoffs of the pseudopotentials of the elements of the alloy. Brillouin zone integrations were done using at least  $\sim 3500$ /(number of atoms in unit cell)  $\mathbf{k}$ -points distributed as uniformly as possible on a Monkhorst-Pack mesh [21,22]. Spin polarization was used in all calculations. We expect such calculations to be able to distinguish energies of structures previously degenerate. This is because the increased density of the  $\mathbf{k}$ -points mesh, the reduced radial cutoff of the PAW potentials versus the ultrasoft pseudopotentials, and the GGA correlation energy implementation. With such methodology, we consider degenerate structures the ones that have energies closer than  $\lesssim 1$ meV/atom.

For some structures both the US-LDA and PAW-GGA calculations are presented. To avoid confusion, we specify the type of calculation in brackets: "(us-lda)" or "(paw-gga)". *In addition, all the results of the PAW-GGA calculations are described in italics.*

**Symmetries of the pure elements.** Both the US-LDA and PAW-GGA calculations reproduce the correct experimental crystal structures of the pure elements at room temperature. The only exception is Sodium. In the two formalisms, Na-hcp is very slightly favored over Na-bcc and Na-fcc, in agreement with other first principle calculations [26–30]. At room temperature Sodium has the bcc structure, and undergoes a martensitic transformation below 35K, to a closed packed structure [31–38]. Therefore our results, Na-hcp stable and the very small energy differences with Na-bcc and Na-fcc, are consistent with the behavior at low temperature only.

**High-throughput computing.** To perform the high number of calculations, we have implemented a set of automatic tools to prepare initial data, perform calculations and analyze results.

*Preparation of input files.* All input files are prepared by starting from the templates based on the prototype chemistry. The volume of the unit cells is determined as a linear combination of atomic volumes of pure elements with Vegard’s law [39]. The internal position of the atoms have been taken from geometrical configurations (for fcc, bcc, hcp superstructures) or have been extracted from the CRYSTMET and the Pauling File databases [11,10].

*Ab initio Calculations.* The calculations are performed by a high-throughput tool, called AFLOW (automatic flow), which searches inside the library for potential input files and performs the proper *ab initio* calculations. AFLOW is able to balance the CPU loads in a multi-processor and cluster environment, maximizing the total throughput of the process [15]. AFLOW extracts the energy and initiates further relaxations with the atomic positions and unit cell geometries obtained from VASP. Therefore, all the structures are relaxed at least twice, and many ( $\sim 10\%$  of the total) are relaxed three or more times, until proper geometrical and energetic convergence is obtained. To conclude, for a library of 176 crystal structures in 80 binary alloys, with a total of 14080 structures, AFLOW performed 32,402 VASP calculations. The total computing time used for this project was  $\sim 9.05 \cdot 10^8$  CPU seconds ( $\sim 28.7$  CPU years), which was spread over a large set of computers [40]. Given the different types of CPUs used, we can only *estimate* the total amount of computation for the project at roughly  $\sim 1.2 \cdot 10^6$  TER-AFLOP.

*Collection and error check of the results.* Once each structure has been calculated, space group symmetry, bond distances, coordination numbers and unit volumes are compared for all the structures of that alloy with the same concentration in the library. Frequently, several structures, starting from different prototypes, relax to the same final structure with the same energy. Therefore, to identify the correct stable phase, it is mandatory to be able to determine the final relaxed structure with the highest possible reliability. Details of the high-throughput error checking tool can be found in reference [15]. A few stable structures remain unidentified. For those we report the unit cell and atomic positions in Appendix XI. Such prototypes might be new phases to be checked experimentally.

*Calculation of the formation energies and the convex hull.* The formation energy for each structure is determined with respect to the most stable structure of the pure elements. To determine the ground states of a system one needs to find, as a function of composition, the ordered compounds that have an energy lower than any

other structure or any linear combination of structures that gives the proper composition. This set of ground state structures forms a *convex hull*, as all other structures have an energy that falls above the set of tie lines that connects the energy of the ground states. In thermodynamical terms, the *convex hull* represents the Gibbs free energy of the alloy at zero temperature.

**Comparison with experiments.** To compare the *ab initio* results to experimental information, we relied on the information and references in the Binary Alloy Phase Diagrams (Massalski [9]) and in the Pauling File [10]. Though in some cases references not included in these were also used, no systematic approach to go beyond information in the Pauling File or Binary Alloy Phase Diagrams was used.

#### IV. DISCUSSION AND SUMMARY OF RESULTS

In comparing the stable structures predicted by the *ab initio* computations with available experimental information, we have attempted to classify the results in a few distinct categories. Table 5 gives the compounds where the *ab initio* result and experiments are in unambiguous agreement. The fact that there are a large number of compounds (89) in Table 5 is a positive statement about the accuracy of LDA/GGA in capturing the close energetic competition between the 176 structures in our library. For one of the systems in Table 5 (PdTi<sub>3</sub>) we took the liberty of modifying the experimental result [9] which shows the A15 structure (stoichiometry AB<sub>3</sub>) as a line compound at composition PdTi<sub>4</sub>. While off-stoichiometric compounds are obviously possible, this usually goes together with significant width of the single-phase field. Hence, we concluded (maybe erroneously) that the placement of A15 at composition PdTi<sub>4</sub> in reference [9] is likely a typographical error.

Table 6 shows compositions which are experimentally known to form compounds, but lack a complete identification of the structure type. Hence, the *ab initio* prediction should be seen as a likely crystal structure for the compound. In most cases, the *ab initio* structure is consistent with the conditions imposed by the limited experimental data (e.g. bcc-ordering is seen for Ag-Cd, and we predict B19; or C37 is speculated for Au-Sc, in agreement with what we predict). Hence, it is likely that with further experimental characterization, many of these systems would move to Table 5.

Table 7a-b contains compositions which are experimentally characterized as solid solutions, high-temperature two-phase regions, or have not been studied at all in a particular composition range. Because of the lack of low-temperature information in these systems, an unambiguous statement about the accuracy of the LDA/GGA prediction cannot be made. For some systems, the *ab initio*

result is very consistent with the experimentally observed behavior. For example, in Ag-Au we find many fcc ordered superstructures with low formation energies, indicating a weak ordering interaction. So it is likely that the *ab initio* predicted structures are stable at low temperature, but disorder into a solid solution at elevated temperature, a rather common occurrence for noble-metal alloys. For other systems in this table the comparison between experiments and *ab initio* is more troubling. For example, while Mo-Ti is experimentally described as a two-phase system with no known compounds down to 400°C, we find very strong compound formation. While it is possible that these compounds disappear through peritectoid reactions below 400°C, the large negative formation energies make this unlikely. It is more likely that either the experimental characterization of this system, or the *ab initio* result is significantly in error. A system such as Mo-Nb, on the other hand, is not at all studied experimentally, and no statement about the accuracy of our prediction in this system can be made.

Table 8 contains the compounds whose crystal structure is not present in the library, and hence, it is not possible to make a comparison with the *ab initio* data. In some cases (e.g. Au<sub>10</sub>Zr<sub>7</sub>), this is because the crystal structure is uncommon and has a large unit cell, making it less worthwhile to include it in the library. In other cases (e.g. Rh<sub>5</sub>Ti) the structure is simply unknown. Table 8 also includes structures that are only stable at off-stoichiometric compositions (e.g. B19 in Au-Ti), as we did not include disorder in the library prototypes.

Finally, Table 9 contains the compositions for which there seems to be a clear disagreement between the experimental data in references [9,10] and the *ab initio* results. Because these systems can point at either experimental errors, or shortcomings of the *ab initio* method, we discuss them here in more detail. Note that *ab initio* errors are most likely due to the LDA or GGA approximations or the pseudopotentials being used. In general, one should consider that our calculations only produce the zero-K energy, whereas all the experimental results are at non-zero temperature. Given that entropic differences between structures can be of the order  $0.1 \sim 1.0k_B$  per atom [381], very small energy differences between the experimentally observed structure and our *ab initio* results, could be reversed at elevated temperature. In particular, AuNb<sub>3</sub>-A15, NbRh<sub>3</sub>-L1<sub>2</sub>, NbRu<sub>3</sub>-L1<sub>2</sub> and NbRu'-L1<sub>0</sub> may be in this category. This phenomenon is quite common. As an example, Wolverton and Ozilins have shown that, in the case of the aluminum-copper system, the vibrational entropy difference is responsible for stabilizing the  $\theta$  phase Al<sub>2</sub>Cu (tetragonal C16) over the competing Al<sub>2</sub>Cu- $\theta'$  phase (distortion of  $\theta_c$ -C1, the cubic fluorite phase with CaF<sub>2</sub> prototype), which has the lowest energy, and, therefore, is the stable struc-

ture at zero Kelvin [382]. At temperatures higher than  $T \sim 150 - 200^\circ\text{C}$ , Al<sub>2</sub>Cu- $\theta$  is more favorable.

### A. Discussion of disagreement between experimental and *ab initio* results

**AuNb<sub>3</sub>.** The structure AuNb<sub>3</sub>-A15 has been reported a number of times [9,10,127–141]. In particular, Röschel *et al.* [132] observed the A15 structure to grow in quenched samples. Ball-milling samples of the material to form disordered bcc, revert upon heat treatment in an exothermic reaction to A15, suggesting that A15 could be the ground state for this composition at low temperature. The relatively small energy difference between A15 and the AuNb<sub>2</sub>↔Nb tie-line in our calculation could lead to finite temperature stability of A15. Alternatively, the  $\sim 7\text{meV/atom}$  energy difference (US-LDA and PAW-GGA) could simply be an error of the *ab initio* approach.

**AuY.** While we predict the B33 structure to be stable by  $26\text{meV/atom}$  below the B2 structure, this system is experimentally listed as having a B2 structure. This experimental classification is based on a paper by Chao *et al.* [170,10]. Chao's work mentioned that they only see B2 when performing a rapid quench. Further work by Kusma [172] and Dwight [158] did not observe the B2 structure. The experimental results in this system are therefore somewhat suspect. It is possible that B2 is a high temperature structure while B33 is the low temperature form. However, it should also be pointed out that the mixing energies in this system are very large ( $\sim 1\text{eV}$ ), and that the potential error of  $\sim 25\text{meV/atom}$  (US-LDA and PAW-GGA) is a small fraction of this.

**Cd<sub>3</sub>Nb.** The structure of this compound is one of the more interesting discrepancies between *ab initio* and experiments to emerge from our study. Based on experimental work of Von Holleck [178], a single L1<sub>2</sub> compound is claimed to be stable in this system. Computationally, no compounds are stable at all, and we find this system to be immiscible. The compound with lowest energy is a bcc superstructure at composition CdNb, and energy  $\sim 55\text{meV/atom}$  above the Cd↔Nb tie-line ( $\sim 62\text{meV/atom}$  with PAW-GGA). The Cd<sub>3</sub>Nb-L1<sub>2</sub> is  $70\text{meV/atom}$  above that same tie-line ( $> 100\text{meV/atom}$  with PAW-GGA). It is not common for LDA/GGA to make such large and qualitative errors in metals, and further investigation of this system is suggested, as it will likely lead to a reconsideration of the experimental classification, or to some novel understanding of the errors that *ab initio* methods can produce in metals.

**CdPt<sub>3</sub>.** Experimentally this compound is claimed to form in the L1<sub>2</sub> structure, while we predict it to form in a new structure for which no prototype yet exists

( $\text{CdPt}_3^{proto}$  in Appendix VIII). We believe the experimental assignment to be uncertain. It is based on a single paper by Nowotny [181] which actually does not observe the  $L1_2$  structure in this system, but assigns it by chemical similarity with the  $\text{Pt}_3\text{Zn}$  system.

**NbRh<sub>3</sub>.** This compound is characterized as an  $L1_2$  structure, whereas our *ab initio* results find the  $\text{Al}_3\text{Pu}$  prototype to be 8meV/atom lower in energy (5.3meV/atom with PAW-GGA). This small energy difference could very well be an LDA/GGA error, or could be reversed at elevated temperature by entropic effects.

**NbRu<sub>3</sub>.**  $\text{NbRu}_3$  is similar to the discrepancy of compound  $\text{NbRh}_3$ . Experimentally it is found to be an  $L1_2$  structure, whereas we find a  $\text{D0}_{24}$  structure that is 8meV/atom below the  $L1_2$ . With PAW pseudopotentials and the GGA exchange correlation corrections the  $\text{D0}_{24}$ - $L1_2$  energy difference reduces to 2.5meV/atom. Because this number is so small, extremely large  $\mathbf{k}$ -points sets and high energy cutoff were used to converge it. The results indicate that  $L1_2$  and  $\text{D0}_{24}$  are all but degenerate in this system. Since  $\text{D0}_{24}$  and  $L1_2$  are very similar ( $\text{D0}_{24}$  is a periodically anti-phased version of  $L1_2$ ) subtle entropic effects can easily reverse the stability between these two.

**NbRu.** Experimentally this system is classified to have the  $L1_0$  structure, whereas the *ab initio* results indicate an unusual two-phase region between  $\text{Nb}_3\text{Ru}$  ( $\text{D0}_3$ ) and  $\text{NbRu}_2$  (C37) covering this composition [9,10,233,237]. The most recent experimental result is based on the assignment by Chen [237] who observes a disordered bcc solution at high temperature and a transformation to a tetragonal structure near 1000°C. Between 720~920°C they see a further symmetry reduction to an orthorhombic phase. Hence, even if the tetragonal structure below 1000°C would be  $L1_0$  (which is only speculated by Chen) its further transformation to an orthorhombic structure indicates that  $L1_0$  is not the ground state structure. Based on a diffusion couple study, Hurley [235] believes that a two-phase region exists near 50% Ru, though the results seem to be irreproducible. Besides the difficulty with interpreting the experimental data, significant problems also exists on the *ab initio* side with this compound. The PAW-GGA result is substantially different from the US-LDA result. GGA gives  $L1_0$  only 4meV/atom above the tie-line (versus 20meV/atom in LDA), whereas B19 seems to be >100meV/atom above the tie-line (versus 13meV/atom with LDA).

**PtY.** Experimental assignment of the structure of this compound as B27 is based on two papers [277,316]. The *ab initio* work finds B33 to be lowest in energy with B27 higher by 50meV/atom (60meV/atom with PAW-GGA). Given that the experimental results seem sound, this is probably a true *ab initio* error.

**Pt<sub>3</sub>Zr<sub>5</sub>.** The work of Schubert *et al.* [323] establishes  $\text{Pt}_3\text{Zr}_5$  as a  $\text{D8}_8$  structure, whereas our *ab initio* (LDA)

results put the  $\text{D8}_8$  structure 36meV/atom above the tie-line formed by  $\text{PtZr}_2$ -C16 and  $\text{PtZr}$ -B33. The GGA result is 26meV/atom above the tie-line. In each case the  $\text{W}_5\text{Si}_3$  structure is lower in energy than the  $\text{D8}_8$ . Given the large mixing energies in this system (of the order of 1 eV/atom), these *ab initio* errors seem plausible.

## V. CONCLUSIONS

Overall, the comparison between experimental data and *ab initio* results is encouraging. A large number of the ground states are predicted correctly, even though significant competition exists between various structures, indicating that relative energy differences are well reproduced by LDA/GGA. In many cases, the direct comparison between *ab initio* and experiments is difficult, as systems have often not been studied completely, or have not been studied to low enough temperature to make a reliable statement about the ground state structures. For only a small number of cases, there is a clear discrepancy between *ab initio* and experiments (Table 9). On further investigations, we find that some of the experimental assignments are poorly justified (e.g.  $\text{CdPt}_3$ ). In a few of the "error systems", the energy difference between the observed structure and the *ab initio* structure is small, which makes it fall within the uncertainty one would expect from LDA/GGA or from a lack of entropic considerations.

A few systems display, in our opinion, such a significant discrepancy between available experimental data and *ab initio* results as to make them worthwhile for further study. These include  $\text{Cd}_3\text{Nb}$  ( $L1_2$  observed, but no compounds from *ab initio*), Nb-Ru and  $\text{Pt}_3\text{Zr}_5$  (respectively  $L1_0$  and  $\text{D8}_8$  observed, but no stable compounds at that composition in *ab initio*),  $\text{PtY}$  (significant error between B33 and B27) and the complete Mo-Ti system (which from experiments appears to be a miscibility gap, but in the *ab initio* results display a number of novel and strongly stabilized compounds). These systems should be investigated further, either to find experimental errors, or to shed new light on *ab initio* problems.

Our findings are summarized in Table 3. By comparing all the available *ab initio* calculations with the experimental results [9,10], we obtain 284 potential structure comparisons. A subset of these, (48), are not available due by the lack of the proper prototype or the unknown experimental compound. The rest of the structure comparisons, (236), can be divided in 89 *agreements* in ordered systems ( $N_{ac}$ ), 21 *agreements* in immiscible systems ( $N_{ai}$ ), 9 *disagreements* ( $N_d$ ), 21 *good predictions* ( $N_{gp}$ ), and 96 *possible predictions* ( $N_{pp}$ ). This division is summarized in the following table.

Total Experiments comparisons: 284				
Available comparisons: 236				
	Experimental	<i>Ab initio</i>	#	Table
Agreements	Compound	Compound	$N_{ac}$ 89	5
Agreements	Immiscibility	Immiscibility	$N_{ai}$ 21	3
Disagreements	Comp./ Immisc.	Incorrect	$N_d$ 9	9
Good predictions	Comp. unknown, uncertain, guessed	Compound prediction	$N_{gp}$ 21	6
Possible predictions	not-studied, solid-solution, two-phase region	Possible compound	$N_{pp}$ 96	7a-b
Unavailable comparisons: 48				
Reason			#	Table
unavailable <i>ab initio</i> prototype			21	8
unknown experimental compound			27	8

TABLE 3. Summary of the 284 structure comparisons between experimental and *ab initio* calculations. When available, we use the PAW-GGA calculations, otherwise we use the US-LDA ones. If only US-LDA calculations were used, we would obtain  $N_{ac}^{LDA}=84$  agreements and  $N_d^{LDA}=14$  disagreements.

The reliability of our *ab initio* method can be defined as the fraction of correct compounds (agreements) over the number of accessible compounds (agreements and disagreements):

$$\eta_c \equiv \frac{N_{ac}}{N_{ac} + N_d} \approx 90.8\%. \quad (2)$$

Such quantity,  $\eta_c$ , contains the reliability of the experimental results, which can be removed by considering only the *true unambiguous disagreements* of Table 9 ( $N_d^* = 3$ ). Hence the reliability of the method becomes:

$$\eta_c^* \equiv \frac{N_{ac}}{N_{ac} + N_d^*} \approx 96.7\%. \quad (3)$$

Such quantities,  $\eta_c$  and  $\eta_c^*$ , can be considered as the probabilities that the most stable *ab initio* compounds reproduce the correct experimental compound. The quantity  $\eta_c^*$  should be used if the experimental compound is certain.

If we extend the argument to the agreements with experimental compounds and immiscible systems, then the reliabilities become:

$$\eta \equiv \frac{N_{ac} + N_{ai}}{N_{ac} + N_{ai} + N_d} \approx 92.4\%, \quad (4)$$

$$\eta^* \equiv \frac{N_{ac} + N_{ai}}{N_{ac} + N_{ai} + N_d^*} \approx 97.3\% \quad (5)$$

where the quantity  $\eta_c^*$  should be used if the experimental compound or immiscibility is certain. Such quantities,  $\eta$  and  $\eta^*$ , can be considered as the probabilities that *ab initio* results reproduce the correct experimental compounds or immiscibilities.

Given the large number of calculations of this project, we believe  $\eta$ ,  $\eta^*$ ,  $\eta_c$ , and  $\eta_c^*$  to be good estimations of state of the art pseudopotential *ab initio* accuracies in phase stability prediction.

## VI. ALLOYS WITHOUT AB INITIO COMPOUNDS

Table 4 gives the alloys for which we find no compounds with negative formation energy, and the structure with lowest formation energy in the system. All of these agree with experiments except for the ones described below.

System	Structure with lowest $E_f$	$E_f$ (us-lda) meV/atom	References [9–11] and
Ag-Mo	AgMo <sub>3</sub> -BCC proto. #72 in [16]	208	[81,82]
Ag-Nb	AgNb <sub>3</sub> -BCC proto. #72 in [16]	62	[86,87]
Ag-Rh	AgRh <sub>3</sub> -FCC $_{AB_3}^{[111]}$	116	[50,94–96]
Ag-Ru	AgRu <sub>3</sub> -HEX proto. #127 in [16]	199	[41,43,96–98]
Ag-Tc	AgTc-HEX proto. #126 in [16]	147	[99]
Au-Mo	AuMo <sub>3</sub> -D0 <sub>19</sub>	75	[41,46,118–122]
Au-Pt	Au <sub>2</sub> Pt-FCC $_{AB_2}^{[111]}$	9	[41,117,119,146–148]
Au-Rh	AuRh <sub>3</sub> -FCC $_{AB_3}^{[001]}$	91	[116,119,149,150]
Au-Ru	AuRu <sub>3</sub> -HEX proto. #125 in [16]	165	[116,119,151,152]
Au-Tc	AuTc-HEX proto. #126 in [16]	74	[116,159]
Cd-Mo	Cd <sub>5</sub> Mo-HEX proto. #128 in [16]	173	[9]
Cd-Nb	CdNb-BCC proto. #71 in [16]	55 (us-lda) 58 ( <i>paw-gga</i> )	[178] see note “Cd-Nb”
Cd-Ru	CdRu-FCC $_{A_2B_2}^{[001]}$	88	see note “Cd-Ru”
Cd-Tc	CdTc-B11	92	[182]
Cr-Mg	CrMg-B11	251	[45,191]
Mo-Tc	Mo <sub>5</sub> Tc-A15	53	[44,217] see note “Mo-Tc”
Mo-Y	Mo <sub>2</sub> Y-C15	40	[222,223]
Nb-Y	Nb <sub>2</sub> Y-C49	132	[244–248]
Nb-Zr	NbZr <sub>2</sub> -HEX proto. #129 in [16]	22	[249–253,90] [238–240,254–258]
Pd-Rh	PdRh <sub>3</sub> -FCC $_{AB_3}^{[111]}$	35	[13,263–270]
Pd-Ru	PdRu-HEX proto. #126 in [16]	44	[271–274]
Ti-Zr	Ti <sub>2</sub> Zr-B8 <sub>2</sub>	18	[48,49,371–374]
Y-Zr	YZr <sub>5</sub> -HEX proto. #141 in [16]	35	[49,375–380]

TABLE 4. Systems without intermetallic compounds. The second and third columns give, for each system, the structure with the lowest formation energy  $E_f$  (US-LDA calculations). The table contains 23 entries. 21 of these are in agreement with experiments. References include both experimental and *ab initio* studies.

**Cd-Nb.** One compound, Cd<sub>3</sub>Nb-L1<sub>2</sub>, has been reported for the system Cd-Nb [9,178]. However, we did not find any stable phase (Cd<sub>3</sub>Nb-L1<sub>2</sub> has formation energy of  $\sim 70$ meV/atom). The disagreement of compound Cd<sub>3</sub>Nb-L1<sub>2</sub> is further discussed in the Section (IV).

**Cd-Ru.** The authors are not aware of any experimental result for the Cd-Ru system.

**Mo-Tc.** Two compounds have been suggested based on thermodynamic models:  $\beta$ Mo<sub>2</sub>Tc<sub>3</sub>-A15 and  $\sigma$ Mo<sub>3</sub>Tc<sub>7</sub>-D8<sub>b</sub> [9,44]. However, we did not find any stable phase for the system, nor can we check the suggested compounds, since our library does not have the  $\sigma$  phase or the off-stoichiometry A15.



## VII. ALLOYS WITH AB INITIO COMPOUNDS

**Ag-Au (Silver - Gold).** The system Ag-Au has not been studied in great detail at low temperatures, and no intermetallic compounds have been reported [9,10,52–55,119]. The solid is reported to be short-range ordered fcc, though it is suggested that long-order might exist at low temperature. At low temperature we find several stable compounds:  $\text{Ag}_4\text{Au}$ ,  $\text{Ag}_3\text{Au}$ ,  $\text{Ag}_2\text{Au}$ ,  $\text{AgAu-L1}_0$ ,  $\text{AgAu}_2$  and  $\text{AgAu}_3$ . In our electronic structure approach, the ground states are degenerate for  $\text{Ag}_3\text{Au}$ ,  $\text{Ag}_2\text{Au}$ ,  $\text{AgAu}_2$  and  $\text{AgAu}_3$ . Our best candidates are  $L1_2$ ,  $D0_{23}$ ,  $\text{Al}_3\text{Pu}$ ,  $\text{NbPd}_3$ ,  $D0_{22}$  and  $D0_{24}$  for  $\text{Ag}_3\text{Au}$ ,  $C37$  and  $\text{MoPt}_2$  for  $\text{Ag}_2\text{Au}$  and  $\text{AgAu}_2$ , and  $L1_2$ ,  $D0_{22}$  and  $D0_{23}$  for  $\text{AgAu}_3$ , as shown in figure (1). The considerable degeneracy of the ground states indicates that only very small effective interactions exist between Ag and Au, consistent with the experimentally observed complete solid solubility. For composition  $\text{Ag}_4\text{Au}$ , the structure  $D1_a$  is degenerate with the tie-line of the two-phase region  $\text{Ag} \leftrightarrow \text{Ag}_3\text{Au}$ . We conclude that further experimental and theoretical investigations are necessary to determine the behavior of AgAu. *To address the degenerate structures, we further investigate  $\text{Ag}_3\text{Au}$ ,  $\text{Ag}_2\text{Au}$ ,  $\text{AgAu}_2$  and  $\text{AgAu}_3$  with PAW-GGA potentials, as described in Section (III). With PAW, for composition  $\text{Ag}_3\text{Au}$ ,  $L1_2$  is the most stable compound and  $D0_{22}$ ,  $D0_{23}$ ,  $\text{Al}_3\text{Pu}$ ,  $\text{NbPd}_3$ ,  $D0_{24}$  are higher by 0.9, 1.6, 2.2, 2.4, and 3.0 meV/atom, respectively. For both composition  $\text{Ag}_2\text{Au}$  and  $\text{AgAu}_2$ ,  $C37$  is the most stable compound and  $\text{MoPt}_2$  is higher by 1.9 meV/atom and 4.3 meV/atom, respectively. For composition  $\text{AgAu}_3$ ,  $L1_2$  is the most stable compound and  $D0_{23}$  and  $D0_{22}$  are higher by 3.4 meV/atom and 3.9 meV/atom, respectively.*

Other *ab initio* studies, relevant for this system, can be found in references [56–66].

Ag-Au system		
Low Temperature Phases comparison chart		
Composition % Au	Experimental (Massalski [9])	<i>Ab initio</i> result
20	short-range order $\gtrsim 950^\circ\text{C}$	$\text{Ag}_4\text{Au-D1}_a$ /tie-line
25	short-range order $\gtrsim 950^\circ\text{C}$	$\text{Ag}_3\text{Au}$ $L1_2/D0_{23}/\text{Al}_3\text{Pu}$ (us-lda) $\text{NbPd}_3/D0_{22}/D0_{24}$ (us-lda) $L1_2$ stable (paw-gga) $D0_{22} \sim 0.9\text{meV/at.}$ $D0_{23} \sim 1.6\text{meV/at.}$ $\text{Al}_3\text{Pu} \sim 2.2\text{meV/at.}$ $\text{NbPd}_3 \sim 2.4\text{meV/at.}$ $D0_{24} \sim 3.0\text{meV/at.}$ <i>above <math>L1_2</math> (paw-gga).</i>
33.3	short-range order $\gtrsim 950^\circ\text{C}$	$\text{Ag}_2\text{Au-C37}/\text{MoPt}_2$ (us-lda) $C37$ stable (paw-gga) $\text{MoPt}_2 \sim 1.9\text{meV/at.}$ <i>above <math>C37</math> (paw-gga).</i>
50	short-range order $\gtrsim 950^\circ\text{C}$	$\text{AgAu-L1}_0$
66.6	short-range order $\gtrsim 950^\circ\text{C}$	$\text{AgAu}_2\text{-C37}/\text{MoPt}_2$ (us-lda) $C37$ stable (paw-gga) $\text{MoPt}_2 \sim 4.3\text{meV/at.}$ <i>above <math>C37</math> (paw-gga).</i>
75.0	short-range order $\gtrsim 950^\circ\text{C}$	$\text{AgAu}_3$ $L1_2/D0_{22}/D0_{23}$ (us-lda) $L1_2$ stable (paw-gga) $D0_{23} \sim 3.4\text{meV/at.}$ $D0_{22} \sim 3.9\text{meV/at.}$ <i>above <math>L1_2</math> (paw-gga).</i>

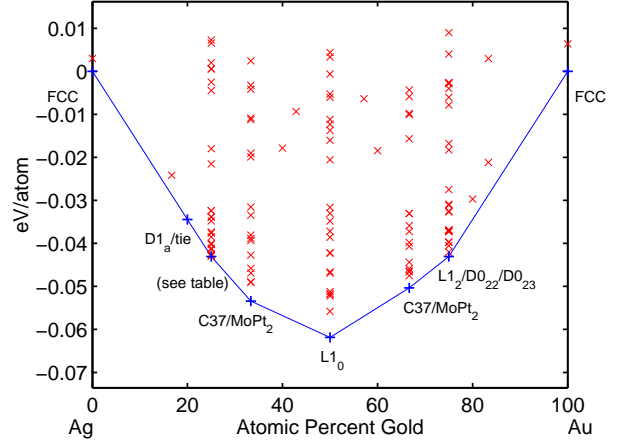


FIG. 1. AgAu (Silver - Gold) ground state convex hull.

**Ag-Cd (Silver - Cadmium).** At composition  $\text{AgCd}_3$  we find  $D0_{19}$  stable, while only disordered hcp solid solution has been reported at this composition. Hence,  $D0_{19}$ , an ordered hcp superstructure, probably is stable at low temperature in this system. At composition  $\text{AgCd}_2$  we find a previously unknown compound  $\text{AgCd}_2\text{-ZrSi}_2$ . The low temperature  $\beta'$ , near  $\text{AgCd}$  stoichiometry, is reported to be ordered bcc in Massalski [9]. In particular, the Pauling File reports  $\text{AgCd-B2}$  [10,67–70]. We find B2, B19 and B27 to have degenerate energies (B19 is quite common for Cd alloys). The experimental phase diagram only displays solid solution on the Ag-rich side [9,10]. We find C37 at  $\text{Ag}_2\text{Cd}$  and a stable phase with stoichiometry  $\text{Ag}_3\text{Cd}$ . The ground state of  $\text{Ag}_3\text{Cd}$  is degenerate: three distinct structure ( $D0_{19}$ ,  $D0_{22}$ ,  $D0_{24}$ ) have similar energy. *To address the degenerate structures, we further investigate  $\text{AgCd}$  and  $\text{Ag}_3\text{Cd}$  with PAW-GGA potentials, as described in Section (III). With PAW, for compound  $\text{AgCd}$ , B19 is the most stable structure, and B27 and B2 are higher by 2.8meV/atom and 3.4meV/atom, respectively. For compound  $\text{Ag}_3\text{Cd}$ ,  $D0_{22}$  and  $D0_{24}$  are still degenerate ground states and  $D0_{19}$  is higher by only 2.2meV/atom. It is possible that these compounds have not yet been observed, or that they have low ordering temperatures.*

Ag-Cd system		
Low Temperature Phases comparison chart		
Composition % Cd	Experimental (Massalski [9])	Ab initio result
25.0	fcc solid solution	$\text{Ag}_3\text{Cd}$ $D0_{19}/D0_{22}/D0_{24}$ (us-lda) $D0_{22}/D0_{24}$ (paw-gga) $D0_{19} \sim 2.2\text{meV/at.}$ above $D0_{22}/D0_{24}$ (paw-gga)
33.3	fcc solid solution	$\text{Ag}_2\text{Cd-C37}$
48.5 to 50	$\beta'$ -bcc B2 [10]	$\text{AgCd-B2/B19/B27}$ (us-lda). B19 stable (paw-gga) $B27 \sim 2.8\text{meV/at.}$ $B2 \sim 3.4\text{meV/at.}$ above B19 (paw-gga).
66.6	none	$\text{AgCd}_2\text{-ZrSi}_2$ .
64.5 to 81	hcp solid solution	$\text{AgCd}_3\text{-D0}_{19}$

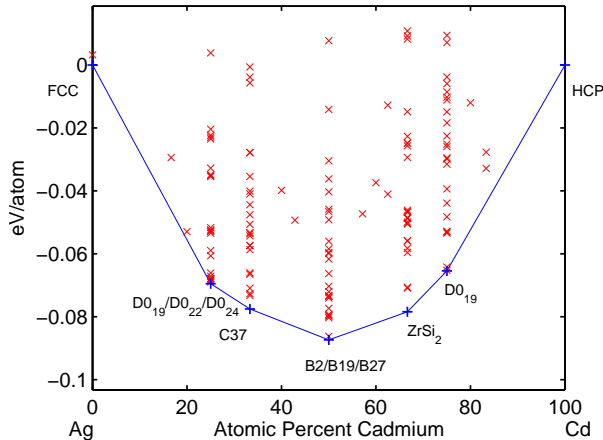


FIG. 2.  $\text{AgCd}$  (Silver - Cadmium) ground state convex hull.

**Ag-Mg (Silver - Magnesium).** The phase diagram of the system  $\text{Ag-Mg}$  is known with reasonable accuracy [9,10,71,72,75,77]. Our *ab initio* method confirms the stability of  $\text{AgMg-B2}$ . In the Ag-rich side of the phase diagram, at stoichiometry  $\text{Ag}_3\text{Mg}$ , we find  $D0_{23}$  and  $D0_{24}$  to be degenerate. While Massalski [9] indicates  $\text{Ag}_3\text{Mg}$  to be  $L1_2$ , it is known from detailed High Resolution Electronic Microscopy (HREM) that  $\text{Ag}_3\text{Mg}$  forms Long Period Superstructure (LPS) modulations of  $L1_2$  [73,74] ( $LPS D0_{23}$  is present in our library). For a detailed discussion of this system see Kulik *et-al.* [76].  $L1_2$  is 15.2meV/atom above  $D0_{23}/D0_{24}$ . On the Mg-rich side, our library does not have prototypes at 80% Mg concentration, so we are not able to find any hexagonal  $\text{AgMg}_4$  (with unknown prototype [75,77]). However we find a stable compound  $\text{AgMg}_3$ . Two phases,  $\text{AgMg}_3\text{-D0}_a$  and  $\text{AgMg}_3\text{-D0}_{19}$ , have degenerate energies. This is important, since experiments suggest that  $\text{AgMg}_4$  was probably identified as hexagonal  $\text{AgMg}_3$  in early studies. Unfortunately, we cannot determine the correct *ab initio* solution since we lack the hexagonal  $\text{AgMg}_4$  prototypes in our library. *To address the degenerate structures, we further investigate  $\text{Ag}_3\text{Mg}$  and  $\text{AgMg}_3$  with PAW-GGA potentials, as described in Section (III). For compound  $\text{Ag}_3\text{Mg}$ , with PAW,  $D0_{23}$  is the most stable compound (in agreement with [73,74,76]),  $D0_{24}$  and  $L1_2$  are 1.1meV/atom and 11.3meV/atom higher than  $D0_{23}$ , respectively. In addition, for compound  $\text{AgMg}_3$ ,  $D0_{19}$  is the most stable structure and  $D0_a$  is  $\sim 6.8\text{meV/atom}$  higher than  $D0_{19}$ .*

Other *ab initio* studies, relevant for this system, can be found in references [78–80].

Ag-Mg system		
Low Temperature Phases comparison chart		
Composition % Mg	Experimental (Massalski [9])	Ab initio result
25.0	$L1_2$ $D0_{23}$ [73,74,76]	$\text{Ag}_3\text{Mg-D0}_{23}/D0_{24}$ (us-lda) $L1_2 \sim 15\text{meV/atom}$ above. $D0_{23}$ stable (paw-gga) $D0_{24} \sim 1.1\text{meV/at.}$ $L1_2 \sim 11.3\text{meV/at.}$ above $D0_{23}$ (paw-gga)
35.5 to 65.4	B2	$\text{AgMg-B2}$
75.8 to 78.2	cF* (unknown)	$\text{AgMg}_3$ $D0_{19}$ (hP8)/ $D0_a$ (oP8) (us) $D0_{19}$ stable (paw-gga) $D0_a \sim 6.8\text{meV/at.}$ above $D0_{19}$ (paw-gga)
80.0	hP* (unknown)	unavailable (see text)

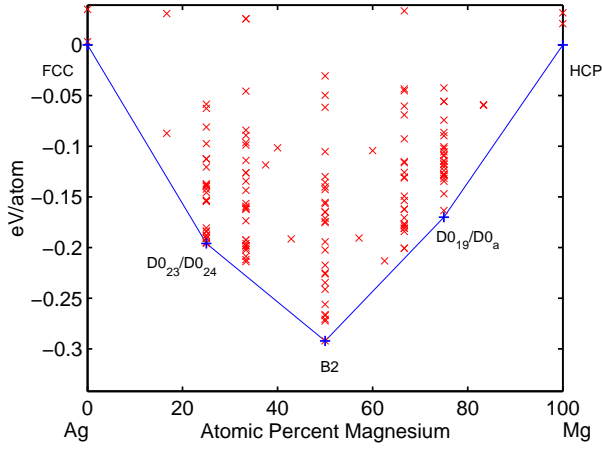


FIG. 3. AgMg (Silver - Magnesium) ground state convex hull.

**Ag-Na (Silver - Sodium).** The phase diagram of the system Ag-Na is known with reasonable accuracy and has only one intermetallic compound [9,10,83–85]. We confirm the stability of  $\text{Ag}_2\text{Na-C15}$  and find almost all the other compounds to have positive formation energies. Both with US-LDA and PAW-GGA, Na-hcp is very slightly favored over Na-bcc and Na-fcc, in agreement with other first principle calculations [26–30]. At room temperature Sodium has the bcc structure, and undergoes a martensitic transformation below 35K, to a closed packed structure [31–38]. Therefore our results, Na-hcp stable and the very small energy differences with Na-bcc and Na-fcc, are consistent with the behaviour at low temperature.

Ag-Na system		
Low Temperature Phases comparison chart		
Composition % Na	Experimental (Massalski [9])	<i>Ab initio</i> result
33.0	C15	$\text{Ag}_2\text{Na-C15}$

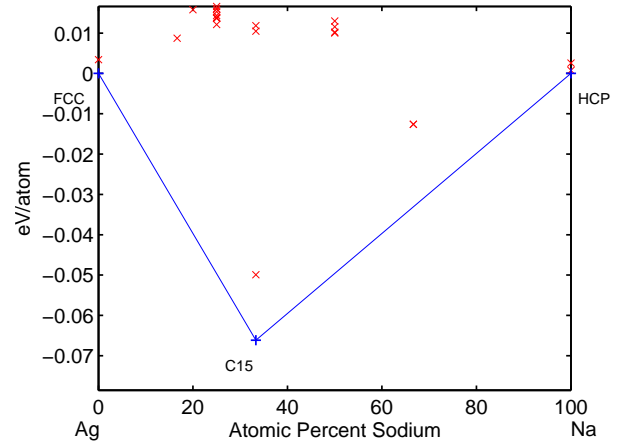


FIG. 4. AgNa (Silver - Sodium) ground state convex hull.

**Ag-Pd (Silver - Palladium).** The system Ag-Pd has not been studied in great detail and no intermetallic compounds have been reported [9,10,41,88]. The solid is reported to be disordered fcc. At low temperature we find three stable compounds: AgPd-L1<sub>1</sub>, Ag<sub>2</sub>Pd and Ag<sub>3</sub>Pd. In our computations, for Ag<sub>2</sub>Pd and Ag<sub>3</sub>Pd, the ground states are degenerate: our best candidates are C49 or C37 for Ag<sub>2</sub>Pd, and L1<sub>2</sub> or D0<sub>22</sub> for Ag<sub>3</sub>Pd, as shown in figure (5). *To address the degenerate structures, we further investigate Ag<sub>2</sub>Pd and Ag<sub>3</sub>Pd with PAW-GGA potentials, as described in Section (III). With PAW, for composition Ag<sub>2</sub>Pd, C37 is the most stable compound and C49 is higher by 4meV/atom. For composition Ag<sub>3</sub>Pd, L1<sub>2</sub> and D0<sub>22</sub> remain degenerate. In fact, D0<sub>22</sub> has an energy 0.4meV/atom greater than L1<sub>2</sub>, too small compared to the numerical accuracy of the ab initio calculation.*

Other *ab initio* studies, relevant for this system, can be found in references [89–93].

Ag-Pd system		
Low Temperature Phases comparison chart		
Composition % Ag	Experimental (Massalski [9])	<i>Ab initio</i> result
50	solid solution > 900°C	AgPd-L1 <sub>1</sub>
66.6	solid solution > 900°C	Ag <sub>2</sub> Pd C37/C49 (us-lda) C37 stable ( <i>paw-gga</i> ) C49~4meV/at. above C37 ( <i>paw-gga</i> )
75.0	solid solution > 900°C	Ag <sub>3</sub> Pd L1 <sub>2</sub> /D0 <sub>22</sub> (us & <i>paw-gga</i> )

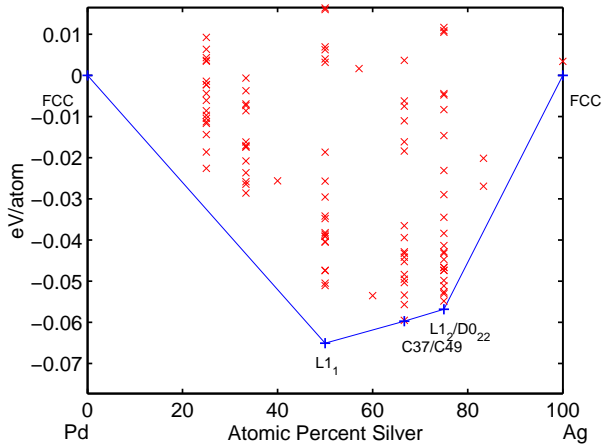


FIG. 5. AgPd (Silver - Palladium) ground state convex hull.

**Ag-Ti (Silver - Titanium).** The stability of AgTi<sub>2</sub>-C11<sub>b</sub> and AgTi-B11 is confirmed [9,10,100,101], and no other stable phases are found computationally. Hence, we conclude that the low temperature part of the phase diagram of AgTi is probably accurate.

Ag-Ti system		
Low Temperature Phases comparison chart		
Composition % Ag	Experimental (Massalski [9])	<i>Ab initio</i> result
33.3	C11 <sub>b</sub>	AgTi <sub>2</sub> -C11 <sub>b</sub>
50	B11	AgTi-B11 ( $\gamma$ CuTi)

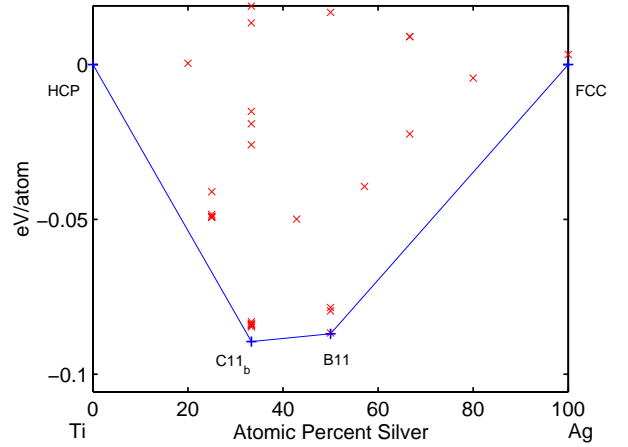


FIG. 6. AgTi (Silver - Titanium) ground state convex hull.

**Ag-Y (Silver - Yttrium).** The stability of AgY-B2 and Ag<sub>2</sub>Y-C11<sub>b</sub> is confirmed [9,10,102]. In the Ag-rich region, we do not determine the stability of Ag<sub>51</sub>Y<sub>14</sub>, since we do not have the prototype in our library [103,104]. Instead, we find Ag<sub>3</sub>Y with D0<sub>a</sub> structure stable with an energy  $\sim 22\text{meV}/\text{atom}$  below the energy of a two-phase region Ag $\leftrightarrow$ Ag<sub>2</sub>Y. In the real system, the presence of Ag<sub>51</sub>Y<sub>14</sub> probably makes structure D0<sub>a</sub> metastable. In the Y-rich region we find AgY<sub>2</sub>-C37 degenerate with the two-phase region Y $\leftrightarrow$ AgY (within  $\sim 1.7\text{meV}/\text{atom}$ ) as shown in figure (7).

Ag-Y system		
Low Temperature Phases comparison chart		
Composition % Ag	Experimental (Massalski [9])	<i>Ab initio</i> result
33.3	two-phase region above 200°C	AgY <sub>2</sub> -C37/tie-line
50	B2	AgY-B2
66.6	C11 <sub>b</sub>	Ag <sub>2</sub> Y-C11 <sub>b</sub>
75	two-phase region above 200°C	Ag <sub>3</sub> Y-D0 <sub>a</sub> (uncertain)
78.5	Ag <sub>51</sub> Gd <sub>14</sub>	unavailable

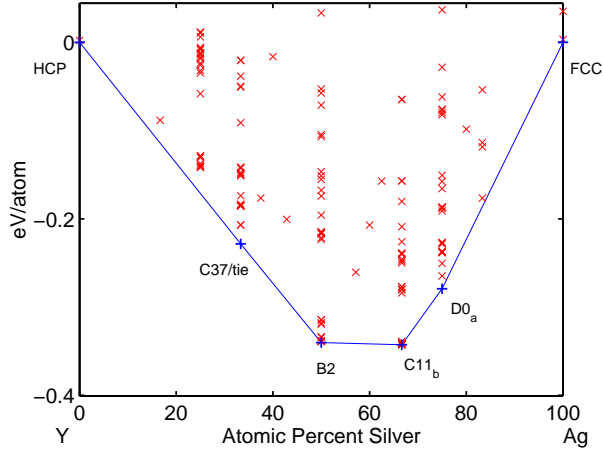


FIG. 7. AgY (Silver - Yttrium) ground state convex hull.

**Ag-Zr (Silver - Zirconium).** The phase diagram of Ag-Zr is known partially, and it has been estimated from thermodynamic properties [9,10,105,106]. The stability of the two known phases AgZr-B11 ( $\gamma$ -CuTi prototype) and AgZr<sub>2</sub>-C11<sub>b</sub> is confirmed by our calculation. In addition to the known intermetallic compounds, we find a stable phase Ag<sub>2</sub>Zr, which is not present in Massalski [9]: the C6 and C32 structures are degenerate. To conclude, we find AgZr<sub>3</sub>-FCC<sub>AB3</sub><sup>[001]</sup> degenerate with the two-phase region Zr $\leftrightarrow$ AgZr<sub>2</sub> (within  $\sim 1.3\text{meV}/\text{atom}$ ). To address the degenerate structures, we further investigate Ag<sub>2</sub>Zr with PAW-GGA potentials, as described in Section (III). With PAW, C32 is the most stable compound and C6 is 2meV/atom above C32.

Ag-Zr system		
Low Temperature Phases comparison chart		
Composition % Ag	Experimental (Massalski [9])	<i>Ab initio</i> result
25.0	two-phase region estimated above 700°C	AgZr <sub>3</sub> FCC <sub>AB3</sub> <sup>[001]</sup> /tie-line
33.3	C11 <sub>b</sub>	AgZr <sub>2</sub> -C11 <sub>b</sub>
50	B11	AgZr-B11 ( $\gamma$ -CuTi)
66.6	two-phase region estimated above 700°C	Ag <sub>2</sub> Zr C6/C32 (us-lda) C32 stable (paw-gga) C6 $\sim 2\text{meV}/\text{at.}$ above C32 (paw-gga)

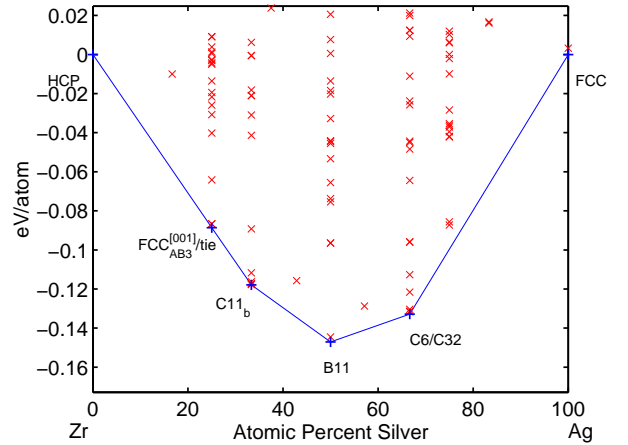


FIG. 8. AgZr (Silver - Zirconium) ground state convex hull.

**Al-Sc (Aluminum - Scandium).** The experimental phase diagram has compounds at compositions:  $\text{Al}_3\text{Sc}$ ,  $\text{Al}_2\text{Sc}$ ,  $\text{AlSc}$ , and  $\text{AlSc}_2$  [9,10,107–109]. The *ab initio* technique confirms the stability of  $\text{Al}_3\text{Sc-L1}_2$ ,  $\text{Al}_2\text{Sc-C15}$ ,  $\text{AlSc-B2}$ , and  $\text{AlSc}_2\text{-B8}_2$ . In the Sc-rich region of the phase diagram, we find a new hexagonal stable phase  $\text{AlSc}_3\text{-D0}_{19}$ , which is not present in Massalski [9]. Only very limited experimental data is available for this side of the phase diagram.

Other *ab initio* studies, relevant for this system, can be found in references [110–115].

Al-Sc system		
Low Temperature Phases comparison chart		
Composition % Al	Experimental (Massalski [9])	<i>Ab initio</i> result
25.0	two-phase region above 0°C	$\text{AlSc}_3\text{-D0}_{19}$
33.3	$\text{B8}_2$	$\text{AlSc}_2\text{-B8}_2$
50	$\text{B2}$	$\text{AlSc-B2}$
66.6	$\text{C15}$	$\text{Al}_2\text{Sc-C15}$
75	$\text{L1}_2$	$\text{Al}_3\text{Sc-L1}_2$

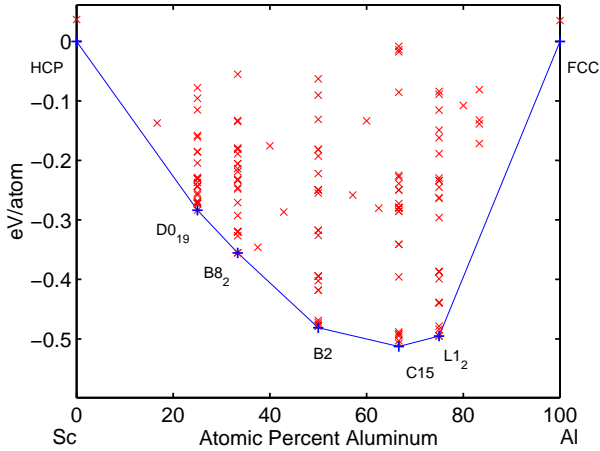


FIG. 9. AlSc (Aluminum - Scandium) ground state convex hull.

**Au-Cd (Gold - Cadmium).** Several compounds have been reported for the system Au-Cd, and the phase diagram is known with reasonable accuracy [9,10,41,117,119,123–126]. We confirm  $\beta'$ -AuCd-B19 and the high-temperature phase  $\beta$ -AuCd-B2 (with energy  $\sim 6\text{meV/atom}$  higher than B19). At 25% Cd composition, we do not find the compound  $\alpha_1\text{Au}_3\text{Cd-Ag}_3\text{Mg}$  because we do not have the proper prototype in our library. Instead, we find structures  $\text{D0}_{24}$ ,  $\text{D0}_{19}$ , and  $\text{Al}_3\text{Pu}$  ( $\text{Co}_3\text{V}$ ) with degenerate energies. Such structures have hexagonal lattices and they are candidates for the phase field  $\alpha_2$  which has been reported to be a long-period superstructure with hP lattice [9]. At 33% Cd composition, we find three phases  $\text{Au}_2\text{Cd-C37}$ ,  $\text{Au}_2\text{Cd-MoPt}_2$ , and  $\text{Au}_2\text{Cd-C49}$  with energies  $4\text{meV/atom}$ ,  $14\text{meV/atom}$  and  $16\text{meV/atom}$  above the tie-line  $\text{Au}_3\text{Cd} \leftrightarrow \text{AuCd}$ , respectively. At 50% Cd composition, the prototype of the phase  $\beta''$ -AuCd is not known, but it is reported to have a hexagonal structure. For  $\beta''$ , we suggest two candidates:  $\text{AuCd-L1}_0$  and  $\text{AuCd-FCC}_{A2B2}^{[201]}$  (CH “40” in reference [262]), which have energies higher by  $5.4\text{meV/atom}$  and  $5.5\text{meV/atom}$  with respect to B19. None of these structures has hexagonal lattice type, and all our hexagonal prototypes have much higher energies.

Au-Cd system		
Low Temperature Phases comparison chart		
Composition % Cd	Experimental (Massalski [9])	<i>Ab initio</i> result
$\sim 25$	$\alpha_1\text{-Ag}_3\text{Mg}$	unavailable
$\sim 25.5$ to $35.5$	$\alpha_2\text{-hP?}$ (unknown)	$\text{Au}_3\text{Cd}$ $\text{D0}_{24}/\text{D0}_{19}/\text{Al}_3\text{Pu}$ hP candidates for $\alpha_2$
33.3	two-phase region	$\text{Au}_3\text{Cd} \leftrightarrow \text{AuCd}$ $\text{Au}_2\text{Cd-C37}$ , $\text{MoPt}_2$ , $\text{C49}$ above tie-line
$\sim 47.5$ $\sim 50$ 43 to 57	$\beta'$ -B19 $\beta''$ unknown $\beta$ -B2 (high T)	$\text{AuCd-B19}$ $\text{L1}_0/\text{FCC}_{A2B2}^{[201]}$ $\sim 5\text{meV/at.}$ $\text{B2} \sim 6\text{meV/at.}$ above B19
61.6 to 62.1	$\text{Au}_3\text{Cd}_5\text{-D8}_m$	unavailable
72 to 76	$\epsilon'$ -unknown tentative phase field	$\text{AuCd}_3\text{-L6}_0$
$\sim 82$	$\eta'$ -unknown tentative phase field	nothing stable at 83.3%

At concentration  $\sim 75\%$  Cd, a stable phase  $\epsilon'$ , with unknown structure, is believed to exist [9]. We confirm the existence of a stable compound and our best prediction is  $\text{AuCd}_3\text{-L6}_0$ . At concentration  $\sim 82\%$  Cd another stable phase  $\eta'$  is believed to exist. We are not able to confirm  $\eta'$ . In fact at 83.3% Cd, the phase with lowest energy is  $\sim 60\text{meV/atom}$  higher than the two tie-line  $\text{AuCd}_3 \leftrightarrow \text{Cd}$ . To address the degenerate structures, we further investigate  $\text{Au}_3\text{Cd}$  with PAW-GGA potentials, as described in Section (III). Also with PAW,  $\text{D0}_{24}$ ,  $\text{Al}_3\text{Pu}$  and  $\text{D0}_{19}$  remain degenerate.

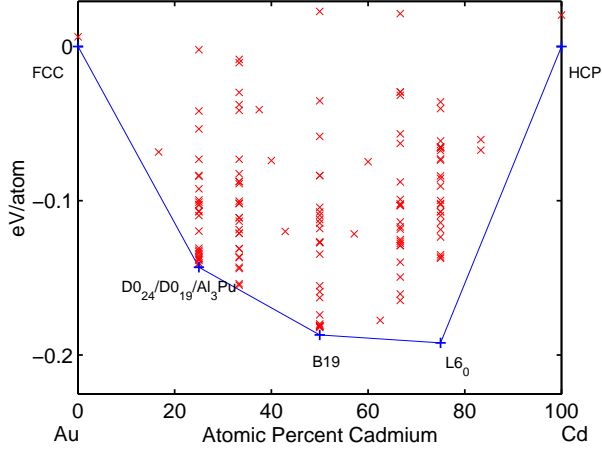


FIG. 10. AuCd (Gold - Cadmium) ground state convex hull.

**Au-Nb (Gold - Niobium).** The phase diagram of the system Au-Nb is based on three known compounds ( $\text{Au}_2\text{Nb}$ ,  $\text{Au}_2\text{Nb}_3$ ,  $\text{AuNb}_3$ ) [9,10,47,117,119,127–141]. We do not confirm the stability of phase  $\text{Au}_2\text{Nb}$ -C32 [9,10,47]. Instead of C32, we find a stable compound  $\text{Au}_2\text{Nb}$ -C6 and C32 with energy higher by  $\sim 12\text{meV}/\text{atom}$  with respect to C6. We can not conclude anything about stability of  $\text{Au}_2\text{Nb}_3$  since our library does not contain any  $\text{A}_2\text{B}_3$  prototype. The Nb-rich side of the experimental phase diagram is drawn with the assumption that  $\text{AuNb}_3$ -A15 is stable at low temperature ( $\sim 500^\circ\text{C}$ ) [9]. Our calculations suggest that  $\text{AuNb}_3$ -A15 might not be stable at low-temperature as it is  $\sim 7\text{meV}/\text{atom}$  above the two phase field  $\text{AuNb}_2 \leftrightarrow \text{Nb}$ . In addition, we find a stable phase  $\text{AuNb}_2$  at 66.6% Nb composition, with bcc parent lattice, and space group Fmmm #69. The compound, labeled as  $\text{BCC}_{AB2}^{[011]}$ , has AB2 stacking along [011] direction. If the prototype  $\text{BCC}_{AB2}^{[011]}$  were not included in the calculation, the phase  $\text{AuNb}_3$ -A15 would be stable, as shown in figure (11). To conclude, we think it might be worthwhile to reconsider the thermodynamic modeling of the Nb-rich side of the phase diagram with the inclusion of  $\text{AuNb}_2$ - $\text{BCC}_{AB2}^{[011]}$ , to obtain the proper temperature and concentration ranges of phase A15. *To address the disagreements with the experimental results, we further investigate  $\text{Au}_2\text{Nb}$  and  $\text{AuNb}_3$  with PAW-GGA potentials, as described in Section (III). For the compound  $\text{Au}_2\text{Nb}$  C32 is the most stable compound and C6 is higher by  $3.2\text{meV}/\text{atom}$ . For composition  $\text{AuNb}_3$ , A15 is still unstable, being  $\sim 6.5\text{meV}/\text{atom}$  above the tie-line  $\text{AuNb}_2 \leftrightarrow \text{Nb}$ . The disagreement at composition  $\text{AuNb}_3$  is further discussed in Section (IV).*

Au-Nb system		
Low Temperature Phases comparison chart		
Composition % Nb	Experimental (Massalski [9])	<i>Ab initio</i> result
33.3	C32	$\text{Au}_2\text{Nb}$ -C6 (us-lda). C32 $\sim 12\text{meV}/\text{at}$ . above C6 (us-lda). C32 stable (paw-gga) C6 $\sim 3.2\text{meV}/\text{at}$ . above C32 (paw-gga).
60	$\text{Au}_2\text{Nb}_3$ (unknown) tI10 I4/mmm	unavailable
66.6	two-phase region (calculated)	$\text{AuNb}_2$ - $\text{BCC}_{AB2}^{[011]}$
73 to 83	A15	two-phase region $\text{AuNb}_2 \leftrightarrow \text{Nb}$ . $\text{AuNb}_3$ -A15 is $\sim 7\text{meV}/\text{at}$ . above tie-line (us-lda). A15 is $\sim 6.5\text{meV}/\text{at}$ . above tie-line (paw-gga). See Section (IV).

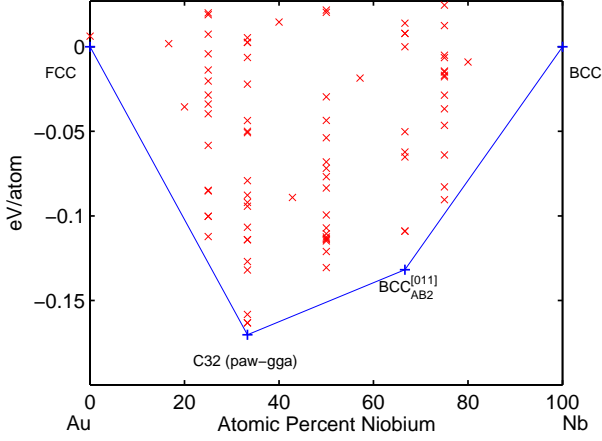


FIG. 11. AuPd (Gold - Niobium) ground state convex hull.

**Au-Pd (Gold - Palladium).** Two ordered compounds have been suggested for the system Au-Pd in the fcc solid solution (Au,Pd):  $\text{Au}_3\text{Pd}$  and  $\text{AuPd}_3$  [142–145]. The low-temperature part of the phase diagram has been constructed with the addition of a phase field AuPd that is believed to exist below  $\sim 100^\circ\text{C}$  [9,10,117,119]. In the Au-rich part of the phase diagram, we confirm the stability of a compound  $\text{Au}_3\text{Pd}$ , but we find three structures,  $\text{D0}_{23}$ ,  $\text{D0}_{22}$  and  $\text{L1}_2$ , with degenerate energy. At composition  $\text{Au}_4\text{Pd}$ , we find the structure  $\text{D1}_a$  to be degenerate with the tie-line  $\text{Au} \leftrightarrow \text{Au}_3\text{Pd}$ . At composition 33.3% Pd, we find a stable compound  $\text{Au}_2\text{Pd}$ , but again, two structures  $\text{C49}$  and  $\text{C37}$  are degenerate. At composition 50%, we confirm the existence of a stable phase AuPd. The prototype is not known. Our best guess is  $\text{AuPd-FCC}_{A_2B_2}^{[201]}$  (CH “40” in reference [262]), and  $\text{L1}_0$  with an energy higher by 8meV/atom with respect to  $\text{FCC}_{A_2B_2}^{[201]}$ . Finally, in the Pd-rich part of the phase diagram, we find a compound  $\text{AuPd}_3$  to be degenerate with the tie-line of the two-phase region  $\text{AuPd} \leftrightarrow \text{Pd}$ . For this compound, three structures,  $\text{D0}_{23}$ ,  $\text{D0}_{22}$  and  $\text{L1}_2$ , have degenerate energies. The considerable degeneracy of the ground states is indicative of weak effective interactions and consistent with the significant miscibility of the two elements inside each other. The near degeneracy of structures such as  $\text{D0}_{23}$ ,  $\text{D0}_{22}$  and  $\text{L1}_2$ , which are related to each other by periodic antiphase boundaries, indicates that more complicated Long Period Superstructures (LPS) might be present. *To address the small energy differences between structures, we further investigate  $\text{Au}_3\text{Pd}$ ,  $\text{Au}_2\text{Pd}$ ,  $\text{AuPd}$ , and  $\text{AuPd}_3$  with PAW-GGA potentials, as described in Section (III). For the compound  $\text{Au}_3\text{Pd}$ ,  $\text{D0}_{23}$  is the most stable compound and  $\text{D0}_{22}$  and  $\text{L1}_2$  are higher by 9.4meV/atom and 12.7meV/atom, respectively. For the compound  $\text{AuPd}_3$ ,  $\text{D0}_{23}$  is the most stable compound and  $\text{L1}_2$  and  $\text{D0}_{22}$  are higher by 1.8meV/atom and 4.8meV/atom, respectively. Also with PAW, for the compound  $\text{Au}_2\text{Pd}$ ,  $\text{C37}$  and  $\text{C49}$  remain degenerate. For the compound  $\text{AuPd}$ ,  $\text{FCC}_{A_2B_2}^{[201]}$  is the most stable compound and  $\text{L1}_0$  is higher by 10.8meV/atom.*

Another *ab initio* study, relevant for this system, can be found in reference [60].



Au-Pd system		
Low Temperature Phases comparison chart		
Composition % Pd	Experimental (Massalski [9])	<i>Ab initio</i> result
12 to 32	Au <sub>3</sub> Pd-L1 <sub>2</sub> (guessed)	Au <sub>3</sub> Pd D0 <sub>23</sub> /D0 <sub>22</sub> /L1 <sub>2</sub> (us-lda) D0 <sub>23</sub> stable ( <i>paw-gga</i> ) D0 <sub>22</sub> ~ 9.4 meV/at. L1 <sub>2</sub> ~ 12.7 meV/at. above D0 <sub>23</sub> ( <i>paw-gga</i> ) Au <sub>4</sub> Pd-D1 <sub>a</sub> /tie-line (us-lda)
20	solid solution	Au <sub>2</sub> Pd C49/C37 (us-lda/ <i>paw-gga</i> )
50	AuPd (guessed) unknown prototype	AuPd-FCC <sup>[201]</sup> <sub>A2B2</sub> (us-lda) L1 <sub>0</sub> ~ 8 meV/at. above FCC <sup>[201]</sup> <sub>A2B2</sub> (us-lda) FCC <sup>[201]</sup> <sub>A2B2</sub> stable ( <i>paw-gga</i> ) L1 <sub>0</sub> ~ 10.8 meV/at. above FCC <sup>[201]</sup> <sub>A2B2</sub> ( <i>paw-gga</i> ).
68 to 90	L1 <sub>2</sub> (guessed)	AuPd <sub>3</sub> -D0 <sub>23</sub> /D0 <sub>22</sub> / /L1 <sub>2</sub> /tie-line (us-lda) D0 <sub>23</sub> stable ( <i>paw-gga</i> ) L1 <sub>2</sub> ~ 1.8 meV/at. D0 <sub>22</sub> ~ 4.8 meV/at. above D0 <sub>23</sub> ( <i>paw-gga</i> )

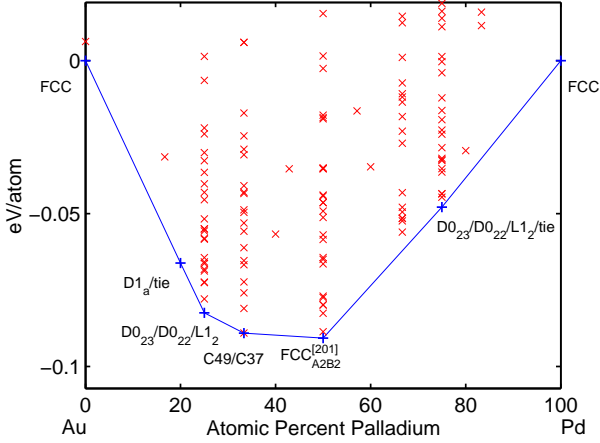


FIG. 12. AuPd (Gold - Palladium) ground state convex hull.

**Au-Sc (Gold - Scandium).** The phase diagram of the system Au-Sc is known only in the Au-rich region, and a total of three intermetallic compounds have been reported: Au<sub>4</sub>Sc, Au<sub>3</sub>Sc, and AuSc [9,10,119,153–158]. At 20% Sc, we confirm Au<sub>4</sub>Sc-D1<sub>a</sub>. At 25% Sc, we find a two-phase region, in agreement with experiments. In fact, Au<sub>3</sub>Sc-D0<sub>a</sub>, the structure with lowest energy, is higher by ~7meV/atom with respect to the tie-line Au<sub>4</sub>Sc-D1<sub>a</sub> ↔ Au<sub>2</sub>Sc-C11<sub>b</sub>. At 33% and at 50% concentrations of Sc, we find two stable phases Au<sub>2</sub>Sc and AuSc, but in both cases two structures are degenerate C11<sub>b</sub> and MoPt<sub>2</sub> for Au<sub>2</sub>Sc, and B2 and B19 for AuSc. The experimental results indicate Au<sub>2</sub>Sc-C11<sub>b</sub> and AuSc-B2. The AuSc<sub>2</sub>-C37 (Co<sub>2</sub>Si prototype) compound has been speculated to exist by similarity with other Au-(Rare Earth)<sub>2</sub> systems [153]. Our *ab initio* method confirms AuSc<sub>2</sub>-C37. To address the degenerate structures, we further investigate Au<sub>2</sub>Sc and AuSc with PAW-GGA potentials, as described in Section (III). For compound Au<sub>2</sub>Sc, with PAW, Au<sub>2</sub>Sc-C11<sub>b</sub> is the most stable compound and Au<sub>2</sub>Sc-MoPt<sub>2</sub> is higher by 1.0meV/atom. In addition, for compound AuSc, Au<sub>2</sub>Sc-B2 is the most stable compound and Au<sub>2</sub>Sc-B19 is higher by 2.2meV/atom. While these energy differences are very small, both calculations are in agreement with experiments.

Au-Sc system		
Low Temperature Phases comparison chart		
Composition % Sc	Experimental (Massalski [9])	<i>Ab initio</i> result
20	D1 <sub>a</sub>	Au <sub>4</sub> Sc-D1 <sub>a</sub>
25	two-phase region	two-phase region Au <sub>3</sub> Sc-D0 <sub>a</sub> ~ 7meV/at. above Au <sub>4</sub> Sc ↔ Au <sub>2</sub> Sc.
33.3	C11 <sub>b</sub>	Au <sub>2</sub> Sc-C11 <sub>b</sub> /MoPt <sub>2</sub> (us-lda) C11 <sub>b</sub> stable ( <i>paw-gga</i> ) MoPt <sub>2</sub> ~ 1.0meV/at. above C11 <sub>b</sub> ( <i>paw-gga</i> ).
50	B2	AuSc-B2/B19 (us-lda) B2 stable ( <i>paw-gga</i> ) B19 ~ 2.2meV/at. above B2 ( <i>paw-gga</i> ).
66.6	C37 (Co <sub>2</sub> Si) (guessed)	AuSc <sub>2</sub> -C37

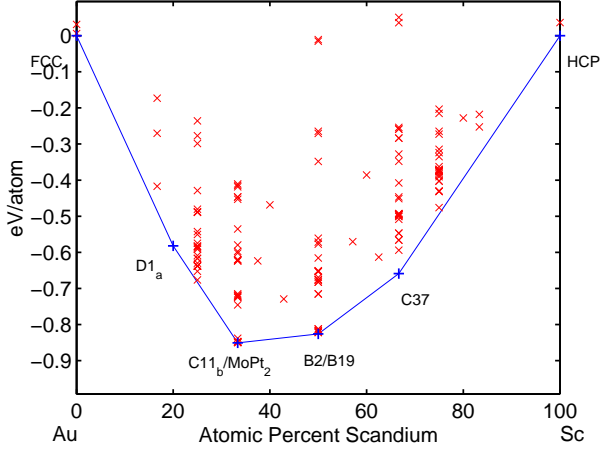


FIG. 13. AuSc (Gold - Scandium) ground state convex hull.

**Au-Ti (Gold - Titanium).** Five ordered compounds have been reported for the system Au-Ti at low temperature:  $\text{Au}_4\text{Ti}$ ,  $\text{Au}_2\text{Ti}$ ,  $\alpha\text{AuTi}$ ,  $\beta\text{AuTi}$ , and  $\text{AuTi}_3$  [9,10,48,101,160–169,311,283,321,298]. We confirm the stability of  $\alpha\text{AuTi}$ -B11,  $\text{Au}_4\text{Ti}$ -D1<sub>a</sub> and  $\text{AuTi}_3$ -A15. At 25% Ti, we find a two-phase region, in agreement with experiments. In fact,  $\text{Au}_3\text{Ti}$ -D0<sub>a</sub>, the structure with lowest energy, is higher by  $\sim 11\text{meV}/\text{atom}$  with respect to the tie-line  $\text{Au}_4\text{Ti} \leftrightarrow \text{Au}_2\text{Ti}$ . For compound  $\text{Au}_2\text{Ti}$ , the experimental phase is C11<sub>b</sub>. At such composition we find two structures with degenerate energies:  $\text{Au}_2\text{Ti}$ -C11<sub>b</sub> and  $\text{Au}_2\text{Ti}$ -MoPt<sub>2</sub>. We do not confirm an off-stoichiometry stable phase  $\beta\text{AuTi}$ -B19, because we do not have such prototype in our library. The stoichiometric B19 has an energy  $\sim 50\text{meV}/\text{atom}$  above  $\alpha\text{AuTi}$ -B11. At 42.8% concentration of Ti, we find a previously unknown compound  $\text{Au}_4\text{Ti}_3$ -Cu<sub>4</sub>Ti<sub>3</sub>. This compound is degenerate with the tie-line of the two-phase field  $\text{Au}_2\text{Ti} \leftrightarrow \text{AuTi}$ , therefore its existence is uncertain. *To address the degenerate structures  $\text{Au}_2\text{Ti}$ -C11<sub>b</sub>/MoPt<sub>2</sub> and the energy difference between  $\alpha\text{AuTi}$ -B11 and  $\beta\text{AuTi}$ -B19 phases, we further investigate  $\text{Au}_2\text{Ti}$  and  $\text{AuTi}$  with PAW-GGA potentials, as described in Section (III). With PAW,  $\text{Au}_2\text{Ti}$ -C11<sub>b</sub> is the most stable compound and  $\text{Au}_2\text{Ti}$ -MoPt<sub>2</sub> is higher by  $3.7\text{meV}/\text{atom}$ . For phase  $\text{AuTi}$ ,  $\text{AuTi}$ -B11 is the most stable compound (as in the ultrasoft pseudopotential case), and  $\text{AuTi}$ -B19 is higher by  $53.6\text{meV}/\text{atom}$ .*

Au-Ti system		
Low Temperature Phases comparison chart		
Composition % Ti	Experimental (Massalski [9])	<i>Ab initio</i> result
18-21	D1 <sub>a</sub>	$\text{Au}_4\text{Ti}$ -D1 <sub>a</sub>
25	two-phase region above 500°C	two-phase region $\text{Au}_3\text{Ti}$ -D0 <sub>a</sub> $\sim 11\text{meV}/\text{at}$ . above $\text{Au}_4\text{Ti} \leftrightarrow \text{Au}_2\text{Ti}$ .
33.3	C11 <sub>b</sub>	$\text{Au}_2\text{Ti}$ C11 <sub>b</sub> /MoPt <sub>2</sub> (us-lda) C11 <sub>b</sub> stable (paw-gga) MoPt <sub>2</sub> $\sim 3.7\text{meV}/\text{at}$ . above C11 <sub>b</sub> (paw-gga).
42.8	two-phase region above 500°C	$\text{Au}_4\text{Ti}_3$ Cu <sub>4</sub> Ti <sub>3</sub> /tie
50 50-51	$\alpha\text{AuTi}$ -B11 $\beta\text{AuTi}$ -B19	$\text{AuTi}$ -B11 B19 $\sim 50\text{meV}/\text{at}$ . B19 $\sim 53.6\text{meV}/\text{at}$ . (us-lda) above B11 (paw-gga).
38-52	$\gamma\text{AuTi}$ -B2 high-temperature	B2 $\sim 135\text{meV}/\text{at}$ . above B11 (us-lda).
75	A15	$\text{AuTi}_3$ -A15

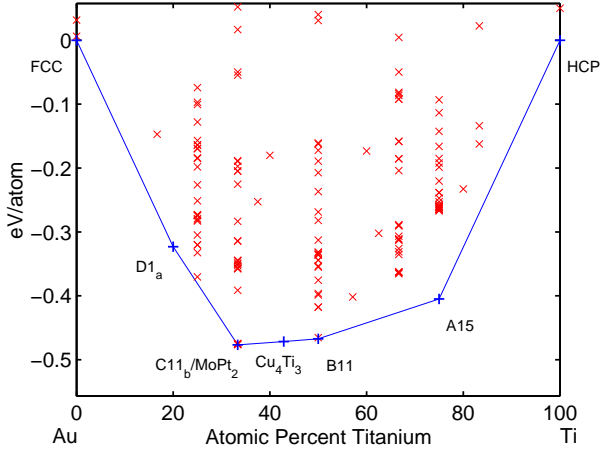


FIG. 14. AuTi (Gold - Titanium) ground state convex hull.

**Au-Y (Gold - Yttrium).** Four intermetallic compounds have been reported for the system Au-Y:  $\text{Au}_3\text{Y}$ ,  $\text{Au}_2\text{Y}$ ,  $\text{AuY}$ , and  $\text{AuY}_3$  [9,10,119,155–158,170–173]. With our *ab initio* method, we confirm stability of  $\text{Au}_3\text{Y}$ - $\text{D0}_a$  and  $\text{Au}_2\text{Y}$ - $\text{C11}_b$ . At equal composition,  $\text{AuY}$ , we do not confirm B2: we find a stable B33 and phase B2 higher by  $\sim 26\text{meV}/\text{atom}$ . No experimental compound is reported for composition  $\text{AuY}_2$ , though we obtain  $\text{AuY}_2$ - $\text{C37}$ . At 75% composition of Y, we do not find a stable  $\text{AuY}_3$  compound reported experimentally [10,156]: the structure with lowest energy is  $\text{AuY}_3$ - $\text{D0}_{11}$  with an energy higher by  $\sim 30\text{meV}/\text{atom}$  with respect to the tie-line. We further investigate  $\text{AuY}$  with PAW-GGA potentials, as described in Section (III). With PAW, B33 is the most stable compound and B2 is  $\sim 25\text{meV}/\text{atom}$  higher than B33. The disagreement at composition  $\text{AuY}$  is further discussed in Section (IV).

Au-Y system		
Low Temperature Phases comparison chart		
Composition % Y	Experimental (Massalski [9])	<i>Ab initio</i> result
25	$\text{D0}_a$	$\text{Au}_3\text{Y}$ - $\text{D0}_a$
33.3	$\text{C11}_b$	$\text{Au}_2\text{Y}$ - $\text{C11}_b$
50	B2	$\text{AuY}$ -B33 (us-lda) B2 $\sim 26\text{meV}/\text{at}$ . above B33 (us-lda). B33 stable (paw-gga) B2 $\sim 25\text{meV}/\text{at}$ . above B33 (paw-gga). See Section (IV).
66.6	not studied	$\text{AuY}_2$ - $\text{C37}$
75	hyp (uncertain prototype)	nothing stable $\text{D0}_{11}$ $\sim 30\text{meV}/\text{at}$ . above tie-line

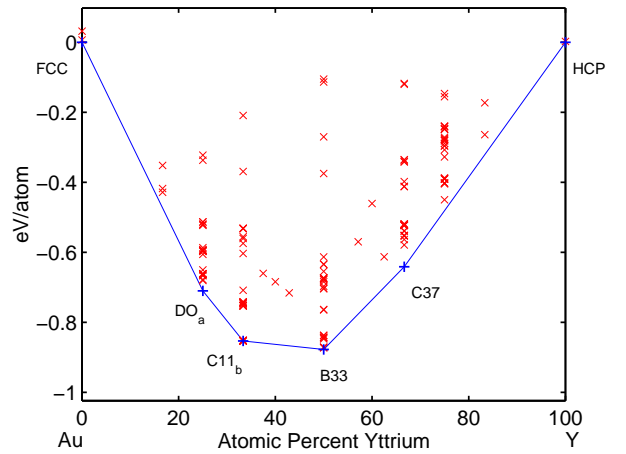


FIG. 15. AuY (Gold - Yttrium) ground state convex hull.

**Au-Zr (Gold - Zirconium).** Several ordered compounds have been reported for the system Au-Zr: Au<sub>4</sub>Zr, Au<sub>3</sub>Zr, Au<sub>2</sub>Zr, Au<sub>10</sub>Zr<sub>7</sub>, Au<sub>4</sub>Zr<sub>5</sub>, AuZr<sub>2</sub>, and AuZr<sub>3</sub> [9,10,163,174–177]. Our *ab initio* method confirms the stability of Au<sub>3</sub>Zr-D0<sub>a</sub>, Au<sub>2</sub>Zr-C11<sub>b</sub> and AuZr<sub>3</sub>-A15. At composition AuZr<sub>2</sub>, Massalski and the Pauling file report C11<sub>b</sub> and CuZr<sub>2</sub> type compounds, respectively [9,10]. C11<sub>b</sub> (MoSi<sub>2</sub> prototype) and CuZr<sub>2</sub> are very similar structures, both tetragonal (tI6) and with the same space group #139. C11<sub>b</sub> belongs to the bcc superstructure family while CuZr<sub>2</sub>, a slightly distorted version of C11<sub>b</sub>, is a closed packed structure [10], therefore, within the formalism of the atomic environments, they represents two different prototypes [10]. Our library contains both prototypes. However, in our calculations, AuZr<sub>2</sub>-C11<sub>b</sub> and AuZr<sub>2</sub>-CuZr<sub>2</sub> are both unstable with degenerate energies higher by  $\sim 20\text{meV}/\text{atom}$  with respect to the tie-line AuZr $\leftrightarrow$ AuZr<sub>3</sub>. We can not say anything about Au<sub>4</sub>Zr, Au<sub>10</sub>Zr<sub>7</sub> and Au<sub>4</sub>Zr<sub>5</sub>, because our library lacks prototypes at the proper concentrations. At AuZr composition we find two structures with degenerate energies: B11 and FCC<sup>[001]<sub>A2B2</sub></sup>. This prediction is unreliable because such compounds appear in the two-phase region Au<sub>10</sub>Zr<sub>7</sub> $\leftrightarrow$ Au<sub>4</sub>Zr<sub>5</sub>, that we are not able to describe properly. At 42.8% concentration of Zr, we find Au<sub>4</sub>Zr<sub>3</sub>-Cu<sub>4</sub>Ti<sub>3</sub>. As before, this prediction is unreliable because it appears in the two-phase region Au<sub>2</sub>Zr $\leftrightarrow$ Au<sub>10</sub>Zr<sub>7</sub>, that we are not able to describe. To conclude, the inclusion of prototypes of Au<sub>10</sub>Zr<sub>7</sub> and Au<sub>4</sub>Zr<sub>5</sub> in our calculations, might change the stability of the predicted AuZr and Au<sub>4</sub>Zr<sub>3</sub> phases. *To address the degenerate structures, we further investigate AuZr<sub>2</sub> with PAW-GGA potentials, as described in Section (III). With PAW, AuZr<sub>2</sub>-CuZr<sub>2</sub> and AuZr<sub>2</sub>-C11<sub>b</sub> are still degenerate, but become stable with an energy 6.6meV/atom lower than the tie-line AuZr $\leftrightarrow$ AuZr<sub>3</sub>.*

Au-Zr system		
Low Temperature Phases comparison chart		
Composition % Zr	Experimental (Massalski [9])	<i>Ab initio</i> result
20	Au <sub>4</sub> Zr oP20 - Pnma	unavailable
25	D0 <sub>a</sub>	Au <sub>3</sub> Zr-D0 <sub>a</sub>
33.3	C11 <sub>b</sub>	Au <sub>2</sub> Zr-C11 <sub>b</sub>
42.8	two-phase region Au <sub>2</sub> Zr $\leftrightarrow$ Au <sub>10</sub> Zr <sub>7</sub>	Au <sub>4</sub> Zr <sub>3</sub> -Cu <sub>4</sub> Ti <sub>3</sub> unreliable, see text.
45	Au <sub>10</sub> Zr <sub>7</sub> tI34	unavailable
50	two-phase region Au <sub>10</sub> Zr <sub>7</sub> $\leftrightarrow$ Au <sub>4</sub> Zr <sub>5</sub>	AuZr-B11/FCC <sup>[001]<sub>A2B2</sub></sup> unreliable, see text.
55.5	Au <sub>4</sub> Zr <sub>5</sub> unknown prototype	unavailable
66.6	C11 <sub>b</sub> [9] CuZr <sub>2</sub> [10]	two-phase region (us-lda) AuZr <sub>2</sub> -CuZr <sub>2</sub> /C11 <sub>b</sub> $\sim 20\text{meV}/\text{at.}$ above tie-line AuZr $\leftrightarrow$ AuZr <sub>3</sub> (us-lda). CuZr <sub>2</sub> /C11 <sub>b</sub> stable $\sim 6.6\text{meV}/\text{at.}$ below AuZr $\leftrightarrow$ AuZr <sub>3</sub> ( <i>paw-gga</i> ).
75	A15	AuZr <sub>3</sub> -A15

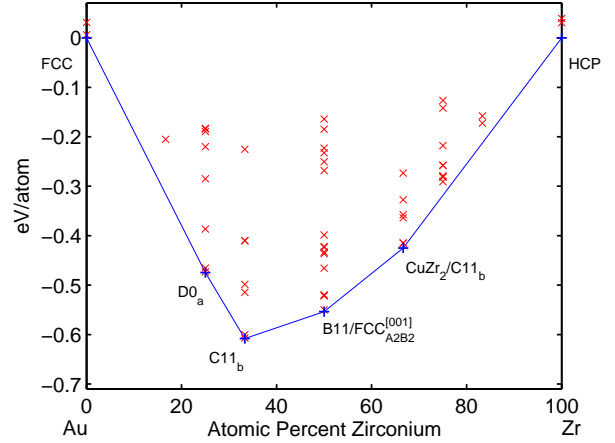


FIG. 16. AuZr (Gold - Zirconium) ground state convex hull.

**Cd-Nb (Cadmium - Niobium).** The phase diagram for the system Cd-Nb is not known [9]. It has been reported that  $\text{Cd}_3\text{Nb}$  has  $L1_2$  prototype [178]. However, we are not able to find any stable compound, so we propose that the system is not compound-forming, but will display low-temperature immiscibility. In our calculations,  $\text{Cd}_3\text{Nb-L1}_2$  is  $\sim 70\text{meV/atom}$  higher in energy than the phase separation of  $\text{Cd}\leftrightarrow\text{Nb}$ . In addition, the structure with the lowest formation energy is a bcc superstructure at composition  $\text{CdNb}$  and energy  $\sim 55\text{meV/atom}$  higher than  $\text{Cd}\leftrightarrow\text{Nb}$ . *To address the disagreement with the experimental result, we further investigate the relevant compounds with PAW-GGA potentials, as described in Section (III). With PAW,  $\text{Cd}_3\text{Nb-L1}_2$  is  $>100\text{meV/atom}$  higher in energy than the tie-line  $\text{Cd}\leftrightarrow\text{Nb}$ . The structure with the lowest formation energy is a bcc superstructure at composition  $\text{CdNb}_3$ , and energy  $\sim 58\text{meV/atom}$  above  $\text{Cd}\leftrightarrow\text{Nb}$ . It is unlikely that the *ab initio* calculations have such a large errors. The disagreement at composition  $\text{Cd}_3\text{Nb}$  is further discussed in Section (IV).*

Cd-Nb system		
Low Temperature Phases comparison chart		
Composition % Nb	Experimental (Massalski [9])	<i>Ab initio</i> result
25	$\text{Cd}_3\text{Nb-L1}_2$	immiscible See Section (IV).

**Cd-Pd (Cadmium - Palladium).** Four Cd-Pd compounds have been identified experimentally at low-temperature ( $\gamma$ ,  $\gamma_1$ ,  $\gamma'$  and  $\beta_1$  [179,180,9]). However, the phase boundaries are unknown. We confirm  $\beta_1$ -CdPd- $L1_0$ . In the Cd-rich part of the phase diagram, we find  $\text{Cd}_3\text{Pd}$  (near  $\gamma'$  at 74%Cd). We are not able to determine the exact structure of  $\text{Cd}_3\text{Pd}$  but our best candidates are  $D0_{19}$ ,  $D0_{24}$ ,  $\text{NbPd}_3$ -type, and  $\text{Al}_3\text{Pu}$ -type ( $\text{Co}_3\text{V}$ ). In the Pd-rich part of the phase diagram, we find a stable phase  $\text{CdPd}_3$ . As before, we cannot determine its structure, precisely. Our guesses are  $D0_{22}$  and  $\text{NbPd}_3$ -type, which have degenerate energies. At concentration 33.3% Cd, we find a new compound  $\text{CdPd}_2$ -C37 which is not present in Massalski [9]. *To address the degenerate structures, we further investigate  $\text{CdPd}_3$  and  $\text{Cd}_3\text{Pd}$  with PAW-GGA potentials, as described in Section (III). Compounds  $\text{CdPd}_3$ - $D0_{22}$  and  $\text{CdPd}_3$ - $\text{NbPd}_3$  remain degenerate with PAW (the energy difference is  $1.1\text{meV/atom}$ ). In addition, for  $\text{Cd}_3\text{Pd}$  composition,  $\text{NbPd}_3/\text{Al}_3\text{Pu}$  remain degenerate compounds, and  $D0_{22}$ ,  $D0_{19}$ ,  $D0_{24}$  are higher by  $4.7\text{meV/atom}$ ,  $5.6\text{meV/atom}$ ,  $6.7\text{meV/atom}$ , respectively.*

Cd-Pd system		
Low Temperature Phases comparison chart		
Composition % Cd	Experimental (Massalski [9])	<i>Ab initio</i> result
25	Pd phase above $100^\circ\text{C}$	$\text{CdPd}_3$ $D0_{22}/\text{NbPd}_3$ (us-lda) $D0_{22}/\text{NbPd}_3$ (paw-gga)
33.3	two-phase region above $100^\circ\text{C}$ , between $\beta_1$ -Pd	$\text{CdPd}_2$ -C37
37-55	$\beta_1$ - $L1_0$	$\text{CdPd-L1}_0$
74	$\gamma'$ -(unknown)	$\text{Cd}_3\text{Pd-D0}_{19}$ or $D0_{24}/\text{NbPd}_3/\text{Al}_3\text{Pu}$ (us-lda) $\text{NbPd}_3/\text{Al}_3\text{Pu}$ stable (paw-gga) $D0_{22} \sim 4.7\text{meV/at.}$ , $D0_{19} \sim 5.6\text{meV/at.}$ , $D0_{24} \sim 6.7\text{meV/at.}$ above $\text{NbPd}_3/\text{Al}_3\text{Pu}$ (paw-gga)
77-80	$\gamma_1$ -(unknown)	unavailable
81-83	$\gamma$ - $D8_3$	unavailable

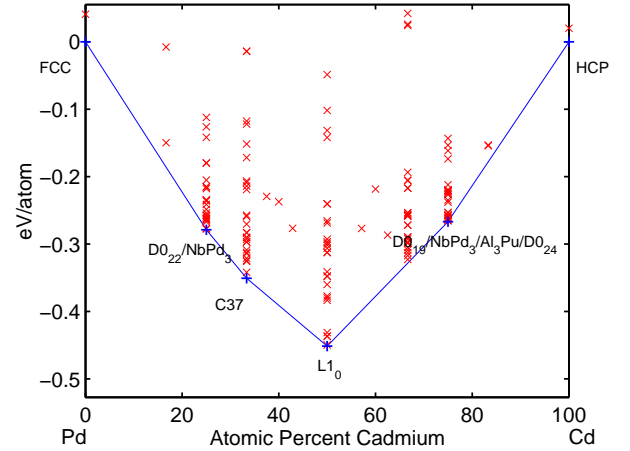


FIG. 17. CdPd (Cadmium - Palladium) ground state convex hull.

**Cd-Pt (Cadmium - Platinum).** The phase diagram of the system Cd-Pt is partially known [181,9], with several compounds of unknown structure. We confirm the stability of phase  $\alpha'_1$ -CdPt-L1<sub>0</sub>. In the Cd-rich part of the phase diagram, the prototypes of Cd<sub>2</sub>Pt and  $\gamma_1$  are unknown. For Cd<sub>2</sub>Pt, our best guess are two degenerate structures, Cd<sub>2</sub>Pt-C37 and Cd<sub>2</sub>Pt-C16, which are also degenerate with the hull. For  $\gamma_1$ , at stoichiometry Cd<sub>3</sub>Pt, we find two degenerate structures D0<sub>11</sub>, D0<sub>a</sub> and D0<sub>22</sub>. In the Pt-rich part of the phase diagram, we do not find a stable compound  $\alpha'$ -CdPt<sub>3</sub>-L1<sub>2</sub>. Instead, we find a stable orthorhombic CdPt<sub>3</sub> with fcc superstructure and Cmmm #65 space group. The prototype, labeled as CdPt<sub>3</sub><sup>prto</sup>, is described in Appendix (XI). In addition, CdPt<sub>3</sub>-L1<sub>2</sub> is found with an energy  $\sim 25$ meV/atom above CdPt<sub>3</sub><sup>prto</sup>. To address the degenerate structures and the disagreement with experimental results for compound CdPt<sub>3</sub>, we further investigate CdPt<sub>3</sub>, Cd<sub>2</sub>Pt and Cd<sub>3</sub>Pt with PAW-GGA potentials, as described in Section (III). With PAW, CdPt<sub>3</sub>-CdPt<sub>3</sub><sup>prto</sup> is the most stable structure and CdPt<sub>3</sub>-L1<sub>2</sub> higher by  $\sim 10.4$ meV/atom. For compound Cd<sub>2</sub>Pt, C16 is the most stable compound and C37 is  $\sim 33$ meV/atom higher than C16. For compound Cd<sub>3</sub>Pt, D0<sub>11</sub> is the most stable compound and D0<sub>a</sub> and D0<sub>22</sub> are higher by  $\sim 52$ meV/atom and  $\sim 60$ meV/atom, respectively. The disagreement at composition CdPt<sub>3</sub> is further discussed in Section (IV).

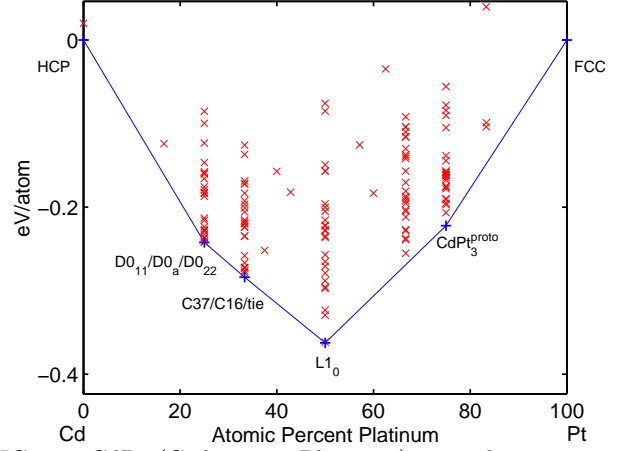


FIG. 18. CdPt (Cadmium - Platinum) ground state convex hull.

Cd-Pt system		
Low Temperature Phases comparison chart		
Composition % Pt	Experimental (Massalski [9])	<i>Ab initio</i> result
$\sim 13$ to 17	$\gamma$ -(unknown)	two-phase region
24 to 26	$\gamma_1$ -(unknown)	Cd <sub>3</sub> Pt D0 <sub>11</sub> /D0 <sub>a</sub> /D0 <sub>22</sub> (us-lda) D0 <sub>11</sub> stable (paw-gga) D0 <sub>a</sub> $\sim 52$ meV/at. D0 <sub>22</sub> $\sim 60$ meV/at. above D0 <sub>11</sub> (paw-gga)
$\sim 26$ to 28	$\gamma_2$ -(unknown)	unavailable
$\sim 31$ to 38	Cd <sub>2</sub> Pt-(unknown)	Cd <sub>2</sub> Pt C37/C16/tie-line (us-lda) C16 stable (paw-gga) C37 $\sim 33$ meV/at. above C16 (paw-gga)
$\sim 49$ to 51	$\alpha'_1$ -L1 <sub>0</sub>	CdPt-L1 <sub>0</sub>
$\sim 75$	$\alpha'$ -L1 <sub>2</sub>	CdPt <sub>3</sub> <sup>prto</sup> Appendix (XI) L1 <sub>2</sub> $\sim 25$ meV/at. above CdPt <sub>3</sub> <sup>prto</sup> . CdPt <sub>3</sub> <sup>prto</sup> stable (paw-gga) L1 <sub>2</sub> $\sim 10.4$ meV/at. above CdPt <sub>3</sub> <sup>prto</sup> (paw-gga). See Section (IV).

**Cd-Rh (Cadmium - Rhodium).** No experimental phase diagram is available [9]. With our *ab initio* technique we find two stable compounds, Cd<sub>2</sub>Rh-C37, and Cd<sub>3</sub>Rh. Our best guesses for Cd<sub>3</sub>Rh are Cd<sub>3</sub>Rh-D0<sub>24</sub> and Cd<sub>3</sub>Rh-Al<sub>3</sub>Pu-type (C<sub>03</sub>V), which have degenerate energies (2meV/atom difference). Interesting metastable phases are Cd<sub>3</sub>Rh-D0<sub>19</sub>, (11 meV/atom above Cd<sub>3</sub>Rh), and Cd<sub>2</sub>Rh-C49 (8meV/atom above Cd<sub>2</sub>Rh-C37). *To address the degenerate structures, we further investigate Cd<sub>3</sub>Rh with PAW-GGA potentials, as described in Section (III). With PAW, Cd<sub>3</sub>Rh-Al<sub>3</sub>Pu is the ground state, and Cd<sub>3</sub>Rh-D0<sub>24</sub> has an energy 5meV/atom higher.*

Cd-Rh system		
Low Temperature Phases comparison chart		
Composition % Cd	Experimental (Massalski [9])	<i>Ab initio</i> result
66.6	not studied	Cd <sub>2</sub> Rh-C37 C49 metastable
75	not studied	Cd <sub>3</sub> Rh D0 <sub>24</sub> /Al <sub>3</sub> Pu (us-lda) D0 <sub>19</sub> ~ 11meV/at. above D0 <sub>24</sub> /Al <sub>3</sub> Pu (us-lda) Al <sub>3</sub> Pu stable (paw-gga) D0 <sub>24</sub> ~ 5meV/at. above Al <sub>3</sub> Pu (paw-gga)

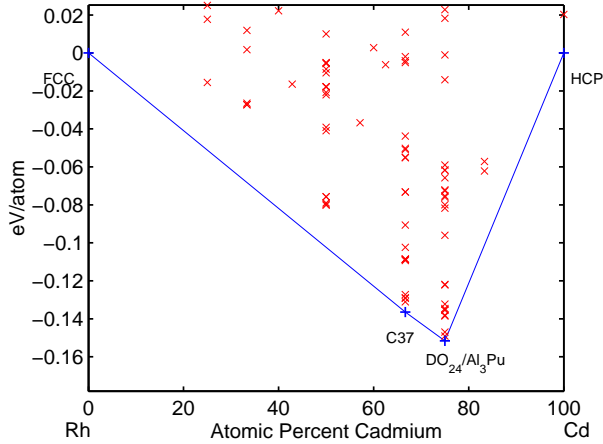


FIG. 19. CdRh (Cadmium - Rhodium) ground state convex hull.

**Cd-Ti (Cadmium - Titanium).** Little is known for the system Cd-Ti at high-temperature [9,10,183,184]. At low temperature only two stable intermetallic compounds have been reported [184]. We confirm the stability of Ti<sub>2</sub>Cd-C11<sub>b</sub>. At composition CdTi, Massalski and the Pauling file, report B11 and CdTi compounds, respectively [9,10]. B11 ( $\gamma$ CuTi prototype) and CdTi are very similar structures, both tetragonal (tP4) and with the same space group #129. B11 belongs to the bcc superstructure family while CdTi, a slightly distorted version of B11, is a closed packed structure [10]. Therefore, within the formalism of the atomic environments, they represents two different prototypes [10]. The *ab initio* calculation is able to relax one structure into the other, easily. For CdTi we confirm the experimental results. In addition, at concentration 42.8%Cd, we find a compound Cd<sub>3</sub>Ti<sub>4</sub>-Cu<sub>4</sub>Ti<sub>3</sub>, degenerate with the tie-line of the two-phase region CdTi<sub>2</sub> $\leftrightarrow$ CdTi. We have not found any other stable or metastable compound: we conclude that the low temperature part of the phase diagram is complete. Note that this system is very similar to Ag-Ti.

Cd-Ti system		
Low Temperature Phases comparison chart		
Composition % Cd	Experimental (Massalski [9])	<i>Ab initio</i> result
33.3	C11 <sub>b</sub>	CdTi <sub>2</sub> -C11 <sub>b</sub>
42.8	two-phase region above 200° C	Cd <sub>3</sub> Ti <sub>4</sub> Cu <sub>4</sub> Ti <sub>3</sub> /tie-line
50	B11 CdTi [10]	CdTi-B11 (CdTi)

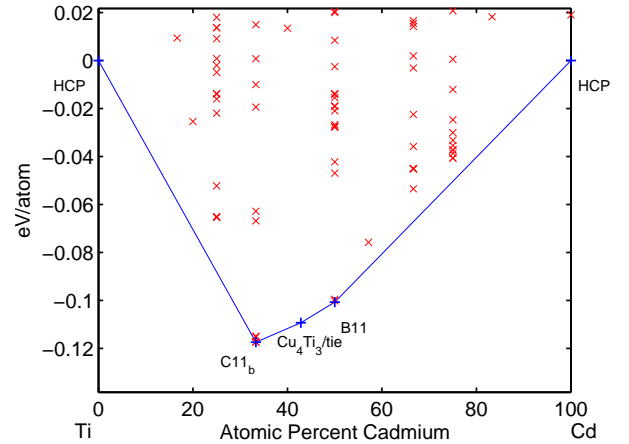


FIG. 20. CdTi (Cadmium - Titanium) ground state convex hull.

**Cd-Y (Cadmium - Yttrium).** The stability of compounds  $YCd$ -B2,  $YCd_2$ -C6 and  $YCd_3$  ( $Cd_3Er$  prototype) [9,10,185–187] is confirmed. The Yttrium-rich side of the phase diagram is poorly known. In that region we find two degenerate phases  $Y_2Cd$ -C49 and  $Y_2Cd$ -C37, both of which are close to the energy of the two phase region  $Y \leftrightarrow CdY$  (figure (21)). We do not find any other stable or metastable phase. *To address the degenerate structures, we further investigate  $Y_2Cd$  with PAW-GGA potentials, as described in Section (III). With PAW, C37 is the most stable compound and C49 is higher by 7.7meV/atom.*

Another *ab initio* study, relevant for this system, can be found in reference [188].

Cd-Y system		
Low Temperature Phases comparison chart		
Composition % Cd	Experimental (Massalski [9])	<i>Ab initio</i> result
33.3	not studied/ two-phase region	$CdY_2$ C37/C49 (us-lda) C37 stable ( <i>paw-gga</i> ) C49 ~ 7.7meV/at. above C37 ( <i>paw-gga</i> )
50	B2	$CdY$ -B2
66.6	C6	$Cd_2Y$ -C6
75	$Cd_3Er$	$Cd_3Y$ - $Cd_3Er$
80.4	$Cd_{45}Y_{11}$ - $Cd_{45}Sm_{11}$	unavailable
81.7	$Cd_{58}Y_{13}$ - $Pu_{13}Zn_{58}$	unavailable
85.7	$Cd_6Y$	unavailable

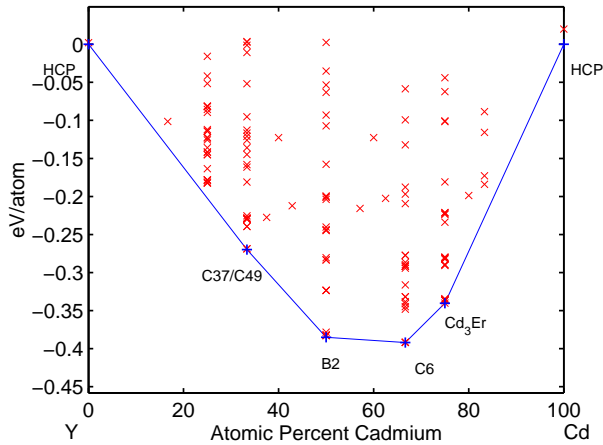


FIG. 21. CdY (Cadmium - Yttrium) ground state convex hull.

**Cd-Zr (Cadmium - Zirconium).** The Cd-Zr system is poorly characterized [49,9,189], and compounds have been identified at four compositions  $Cd_3Zr$ ,  $Cd_2Zr$ ,  $CdZr$ , and  $CdZr_2$ . Massalski [9] reports  $Cd_3Zr$ -L1<sub>0</sub>-AuCu, which we consider a misprint for  $Cd_3Zr$ -L1<sub>2</sub>-AuCu<sub>3</sub>, while CRYSTMET and Pauling File databases [10,11] report  $Cd_3Zr$ -D0<sub>a</sub>- $\beta$ Cu<sub>3</sub>Ti from reference [190]. We confirm the stability of  $Cd_3Zr$ -L1<sub>2</sub> and  $CdZr_2$ -C11<sub>b</sub>. At composition  $CdZr$ , Massalski and the Pauling file, report B11 and  $CdTi$  compounds, respectively [9,10]. B11 ( $\gamma$ CuTi prototype) and  $CdTi$  are very similar structures, both tetragonal (tP4) and with the same space group #129. B11 belongs to the bcc superstructure family while  $CdTi$ , a slightly distorted version of B11, is a closed packed structure [10]. Therefore, within the formalism of the atomic environments, they represents two different prototypes [10]. The *ab initio* calculation is able to relax one structure into the other, easily. For  $CdZr$ , we find  $CdZr$ -L1<sub>0</sub> instead of  $CdZr$ -B11, which has an energy ~18meV/atom higher than L1<sub>0</sub>. The prototype of  $Cd_2Zr$  is not known: our best guess is  $Cd_2Zr$ -C11<sub>b</sub>. In addition, we find a stable compound  $CdZr_3$ -A15 not present in Massalski [9], and a metastable L1<sub>2</sub> which is 8.5meV/atom higher than A15. *To address the disagreement with the experimental results for compound  $CdZr$ , we further investigate L1<sub>0</sub> and B11 with PAW-GGA potentials, as described in Section (III). With PAW,  $CdZr$ -B11 is the most stable compound and  $CdZr$ -L1<sub>0</sub> is higher by 13meV/atom.*

Cd-Zr system		
Low Temperature Phases comparison chart		
Composition % Cd	Experimental (Massalski [9])	<i>Ab initio</i> result
25	two-phase region not studied	$CdZr_3$ -A15 L1 <sub>2</sub> ~ 8.5meV/at. above A15
33.3	C11 <sub>b</sub>	$CdZr_2$ -C11 <sub>b</sub>
50	B11	$CdZr$ -L1 <sub>0</sub> (us-lda) B11 ~ 18meV/at. above L1 <sub>0</sub> (us-lda). B11 stable ( <i>paw-gga</i> ) L1 <sub>0</sub> ~ 13meV/at. above L1 <sub>0</sub> ( <i>paw-gga</i> ).
66.6	cubic (unknown)	$Cd_2Zr$ -C11 <sub>b</sub>
75	L1 <sub>2</sub> [9] D0 <sub>a</sub> [190,10,11]	$Cd_3Zr$ -L1 <sub>2</sub>



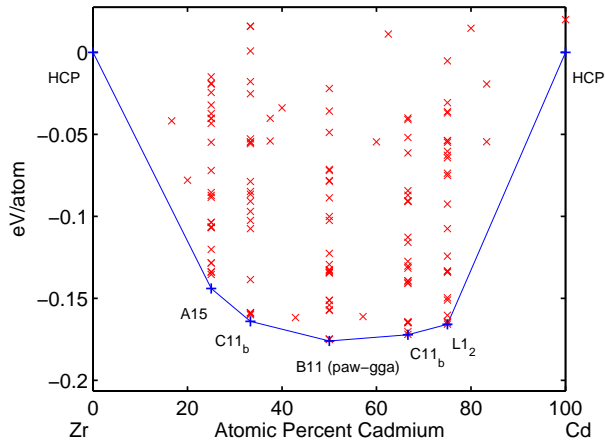


FIG. 22. CdZr (Cadmium - Zirconium) ground state convex hull.

**Mo-Nb (Molybdenum - Niobium).** The system MoNb has not been studied in great detail and no experimental intermetallic compounds have been found [9,10,47,197]. A bcc solid solution is reported from 2400°C up to the melt. We predict four stable compounds at low temperature: MoNb<sub>2</sub>-C11<sub>b</sub>, MoNb-B2, Mo<sub>2</sub>Nb-C11<sub>b</sub>, and Mo<sub>3</sub>Nb-D0<sub>3</sub>, as shown in figure (23).

Other *ab initio* studies, relevant for this system, can be found in references [90,198–200].

Mo-Nb system		
Low Temperature Phases comparison chart		
Composition % Mo	Experimental (Massalski [9])	<i>Ab initio</i> result
33.3	not studied	MoNb <sub>2</sub> -C11 <sub>b</sub>
50	not studied	MoNb-B2
66.6	not studied	Mo <sub>2</sub> Nb-C11 <sub>b</sub>
75	not studied	Mo <sub>3</sub> Nb -D0 <sub>3</sub>

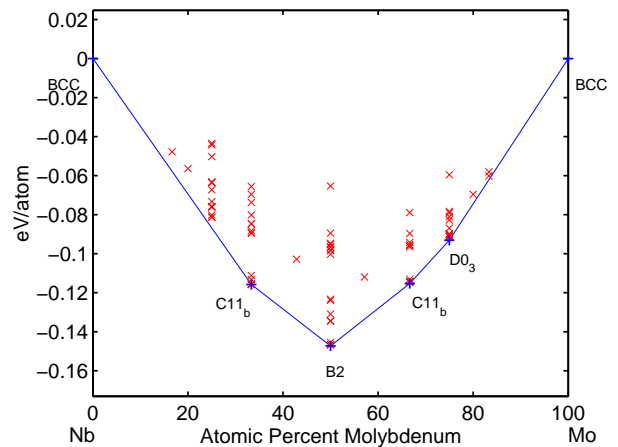


FIG. 23. MoNb (Molybdenum - Niobium) ground state convex hull.

**Mo-Pd (Molybdenum - Palladium).** The phase diagram of this alloy is known from experimental investigations and thermodynamic calculations [9,10,46,51,201]. The only compound is at composition  $\text{MoPd}_2$  and is listed in Massalski as having approximately the  $\text{MoPt}_2$  structure [9,10,201]. Our *ab initio* method finds that the  $\text{MoPt}_2$  structure is 8meV/atom higher than  $\text{MoPd}_2$ - $\text{ZrSi}_2$ . In addition, we find a stable phase  $\text{MoPd}_4$ - $\text{D1}_a$  ( $\text{MoNi}_4$  prototype), previously unknown.

Mo-Pd system		
Low Temperature Phases comparison chart		
Composition % Pd	Experimental (Massalski [9])	<i>Ab initio</i> result
66 to 67	$\sim \text{MoPt}_2$	$\text{MoPd}_2$ - $\text{ZrSi}_2$ $\text{MoPt}_2 \sim 8\text{meV/at.}$ $\text{ZrSi}_2$
80	disorder fcc Pd-A1	$\text{MoPd}_4$ - $\text{D1}_a$

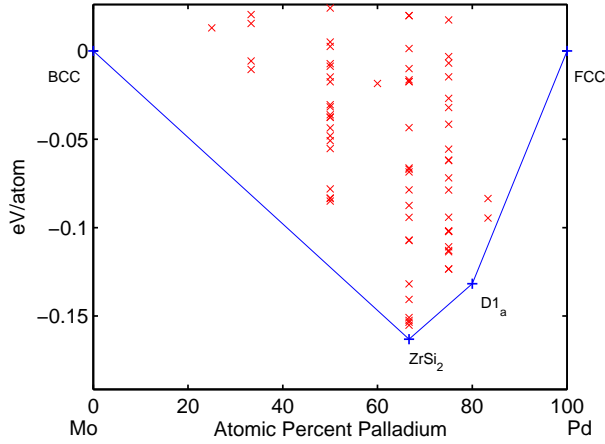


FIG. 24. MoPd (Molybdenum - Palladium) ground state convex hull.

**Mo-Pt (Molybdenum - Platinum).** The phase diagram of this alloy is known from experimental investigations and thermodynamic modeling [9,10,201–210,277]. We confirm the stability of  $\text{MoPt}$ -B19 and  $\text{MoPt}_2$  (with  $\text{MoPt}_2$  prototype). In the Pt-rich part of the phase diagram, we find a compound  $\text{MoPt}_4$ - $\text{D1}_a$  ( $\text{MoNi}_4$  prototype), previously unknown. The observed high-temperature phase A15, reported as  $\text{Mo}_6\text{Pt}$  in Massalski [9] and as  $\text{Mo}_{3.2}\text{Pt}_{0.8}$  in the Pauling File [10], is off-stoichiometry. Our *ab initio* method finds a stoichiometric  $\text{Mo}_3\text{Pt}$ -A15 to be  $\sim 45\text{meV/atom}$  above the two-phase region  $\text{Mo} \leftrightarrow \text{MoPt}$ -B19. For a detailed experimental study of such A15 phase, see reference [210].

Mo-Pt system		
Low Temperature Phases comparison chart		
Composition % Pt	Experimental (Massalski [9])	<i>Ab initio</i> result
18.5 20	$\text{Mo}_6\text{Pt}$ -A15 [9] $\text{Mo}_{3.2}\text{Pt}_{0.8}$ -A15 [10] above $\sim 1200^\circ\text{C}$	$\text{Mo}_3\text{Pt}$ -A15 $\sim 45\text{meV/at.}$ above $\text{Mo} \leftrightarrow \text{MoPt}$ -B19
31.5 to 45	$\epsilon'$ - $\text{D0}_{19}$ above $1000^\circ\text{C}$	unavailable at such composition
50	B19	$\text{MoPt}$ -B19
66.6	$\text{MoPt}_2$	$\text{MoPt}_2$
80	two-phase region $\text{MoPt}_2 \leftrightarrow \text{Pt}$	$\text{MoPt}_4$ - $\text{D1}_a$

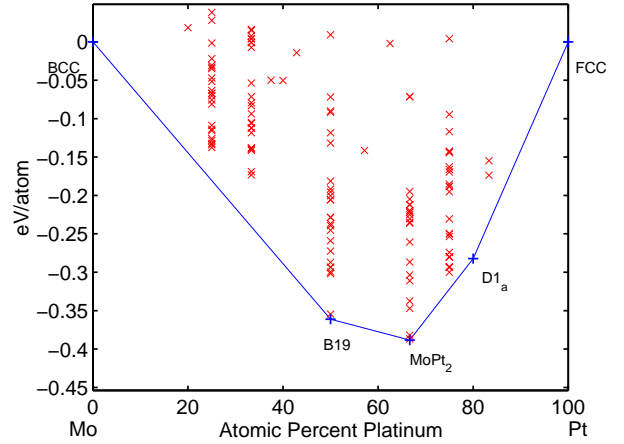


FIG. 25. MoPt (Molybdenum - Platinum) ground state convex hull.

**Mo-Rh (Molybdenum - Rhodium).** The phase diagram of the system Mo-Rh is known above  $\sim 900^\circ\text{C}$  and it is based on thermodynamic calculations and experimental results [9,10,51,211–214]. We confirm the stability of the two known compounds MoRh-B19 [9] and MoRh<sub>3</sub>-CdMg<sub>3</sub> [10,213]. At concentration 66.6% Rh, we find the stable phase MoRh<sub>2</sub>-C37 (prototype Co<sub>2</sub>Si), previously not identified [9].

Mo-Rh system		
Low Temperature Phases comparison chart		
Composition % Rh	Experimental (Massalski [9])	<i>Ab initio</i> result
$\sim 50$	B19	MoRh-B19
66.6	two-phase region above 900°C	Mo <sub>2</sub> Rh-C37
$\sim 75$	CdMg <sub>3</sub> [10,213]	MoRh <sub>3</sub> -CdMg <sub>3</sub>

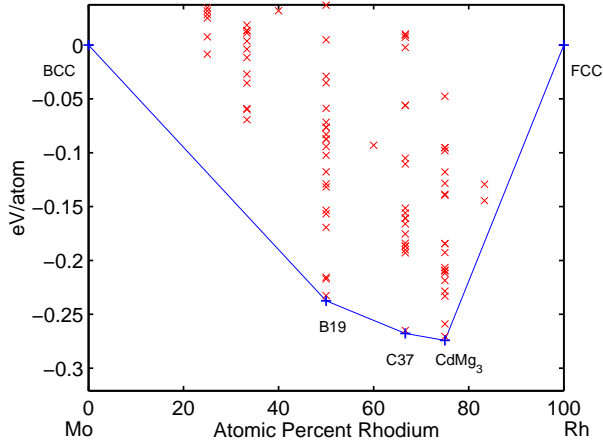


FIG. 26. MoRh (Molybdenum - Rhodium) ground state convex hull.

**Mo-Ru (Molybdenum - Ruthenium).** The phase diagram of this system is known at medium and high-temperature [9,10,215]. There is a  $\sigma$  phase around 38% Ru, which is quite common when bcc (Mo) and hcp (Ru) elements are mixed. We are not able to confirm the  $\sigma$  phase since we do not have the proper prototype in our library. At concentration 75% Ru, we find the stable phase MoRu<sub>3</sub>-D0<sub>19</sub> (formation energy  $\sim 60\text{meV/atom}$ ), not present in Massalski [9], indicating that it might be a low-temperature ordered structure.

Another *ab initio* study, relevant for this system, can be found in reference [216].

Mo-Ru system		
Low Temperature Phases comparison chart		
Composition % Ru	Experimental (Massalski [9])	<i>Ab initio</i> result
75	disorder hcp Ru-A3 above 800°C	MoRu <sub>3</sub> -D0 <sub>19</sub>

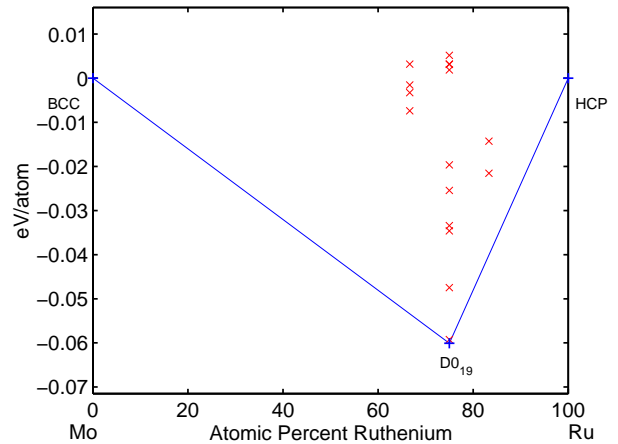


FIG. 27. MoRu (Molybdenum - Ruthenium) ground state convex hull.

**Mo-Ti (Molybdenum - Titanium).** To our knowledge, no intermetallic compounds have been reported for the system Mo-Ti [9,10,48,218–220], and it is considered a non-compound forming system [10,11]. In contrast to the experimental assessment, we find seven stable compounds. Four of these have bcc superstructures: orthorhombic  $\text{MoTi}_3$ , degenerate with the two-phase region  $\text{Ti} \leftrightarrow \text{MoTi}_2$ , with space group  $\text{Immm}$  #71 and prototype  $\text{MoTi}_3^{\text{proto}}$  (Appendix (XI)); orthorhombic  $\text{Mo}_3\text{Ti}$  with space group  $\text{Immm}$  #71 and prototype  $\text{Mo}_3\text{Ti}^{\text{proto}}$  (Appendix (XI)); trigonal  $\text{MoTi}_2\text{-BCC}_{AB2}^{[211]}$ , and orthorhombic  $\text{MoTi}$  with space group  $\text{Imma}$  #74 and prototype  $\text{MoTi}^{\text{proto}}$  (Appendix (XI)). In addition, we find a stable compound  $\text{Mo}_2\text{Ti-C11}_b$ , a compound  $\text{Mo}_4\text{Ti-D1}_a$  degenerate with the tie-line, and finally a monoclinic  $\text{Mo}_5\text{Ti}$  which has space group  $\text{C2/m}$  #12 and prototype  $\text{Mo}_5\text{Ti}^{\text{proto}}$  (Appendix (XII)). Given the relatively large value of the formation energy, the experimental miscibility gap is surprising. This system warrants further study to sort out the apparent discrepancy between experiments and *ab initio* computation.

Another *ab initio* study, relevant for this system, can be found in reference [221].

Mo-Ti system		
Low Temperature Phases comparison chart		
Composition % Mo	Experimental (Massalski [9])	<i>Ab initio</i> result
25	two-phase region, $(\beta\text{Ti},\text{Mo})\text{-A2} \leftrightarrow (\alpha\text{Ti})\text{-A3}$ , above $400^\circ\text{C}$	$\text{MoTi}_3^{\text{proto}}$ /tie-line Appendix (XI)
33.3	same as above	$\text{MoTi}_2\text{-BCC}_{AB2}^{[211]}$
50	same as above	$\text{MoTi}^{\text{proto}}$ Appendix (XI)
66.6	same as above	$\text{Mo}_2\text{Ti-C11}_b$
75	same as above	$\text{Mo}_3\text{Ti}^{\text{proto}}$ Appendix (XI)
80	same as above	$\text{Mo}_4\text{Ti-D1}_a$ /tie-line
83.3	same as above	$\text{Mo}_5\text{Ti}^{\text{proto}}$ Appendix (XII)

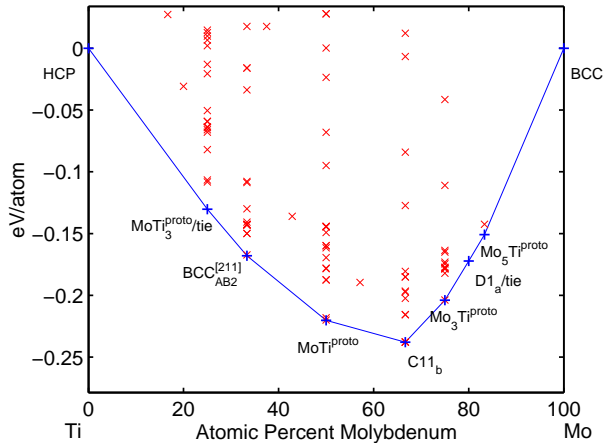


FIG. 28. MoTi (Molybdenum - Titanium) ground state convex hull.

**Mo-Zr (Molybdenum - Zirconium).** Not much is known of the system Mo-Zr to produce a reliable phase diagram [9,10,49]. We confirm the stability of the only known compound  $\text{Mo}_2\text{Zr-C15}$ . Experimentally, the Zr-rich side of the phase diagram has not been explored in detail at low temperature, and it is reported to have a two-phase region  $\text{Mo}_2\text{Zr-C15} \leftrightarrow (\alpha\text{Zr})\text{-A3}$  above  $400^\circ\text{C}$ . However, we find two possible new compounds: the orthorhombic phase  $\text{MoZr}_3$  with space group  $\text{Imma}$  #74, prototype  $\text{MoZr}_3^{\text{proto}}$  (Appendix (XII)), and the monoclinic compound  $\text{MoZr}_5\text{-Mo}_5\text{Ti}^{\text{proto}}$  with space group  $\text{C2/m}$  #12, and prototype  $\text{Mo}_5\text{Ti}^{\text{proto}}$  (Appendix (XII)). Both compounds  $\text{MoZr}_3^{\text{proto}}$  and  $\text{MoZr}_5\text{-Mo}_5\text{Ti}^{\text{proto}}$  are quasi-degenerate with respect to the two-phase region  $\text{Mo}_2\text{Zr} \leftrightarrow (\alpha\text{Zr})$ . Hence, the existence of  $\text{MoZr}_3^{\text{proto}}$  and  $\text{MoZr}_5\text{-Mo}_5\text{Ti}^{\text{proto}}$  is uncertain. It is useful mentioning that we find a metastable orthorhombic phase  $\text{MoZr}$  with space group  $\text{Imma}$  #74 and prototype similar to  $\text{MoTi}^{\text{proto}}$  (Appendix (XI)) only  $\sim 2\text{meV/atom}$  above the tie-line  $\text{Mo}_2\text{Zr} \leftrightarrow (\alpha\text{Zr})$ .

Another *ab initio* study, relevant for this system, can be found in reference [110].

Mo-Zr system		
Low Temperature Phases comparison chart		
Composition % Mo	Experimental (Massalski [9])	<i>Ab initio</i> result
16.6	two-phase region above $400^\circ\text{C}$	$\text{MoZr}_5\text{-Mo}_5\text{Ti}^{\text{proto}}$ /tie-line Appendix (XII)
25	same as above	$\text{MoZr}_3^{\text{proto}}$ /tie-line Appendix (XII)
50	same as above	$\sim \text{MoTi}^{\text{proto}} \sim 2\text{meV/at.}$ above $\text{Mo}_2\text{Zr} \leftrightarrow (\alpha\text{Zr})$
60-67	C15	$\text{Mo}_2\text{Zr-C15}$

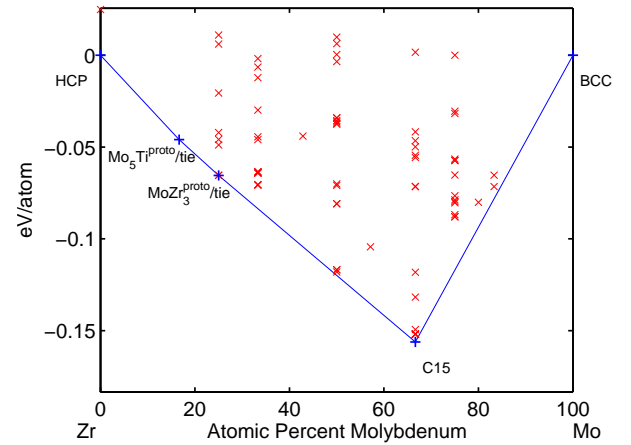


FIG. 29. MoZr (Molybdenum - Zirconium) ground state convex hull.

**Nb-Pd (Niobium - Palladium).** The Pd-Nb phase diagram is known with reasonable accuracy in the Pd-rich region [9,10,47,259]. The stability of the experimental phase  $\text{NbPd}_2\text{-MoPt}_2$  and  $\alpha\text{NbPd}_3\text{-D0}_{22}$  is confirmed. In the Nb-rich region, at concentration 33% Nb, we find an orthorhombic compound  $\text{Nb}_2\text{Pd-BCC}_{AB2}^{[011]}$ , not present in Massalski [9]. The energy of this phase is  $\sim 11\text{meV/atom}$  below the tie-line of the two-phase region  $\text{Nb}\leftrightarrow\text{NbPd}_2$ .

Another *ab initio* study, relevant for this system, can be found in reference [224].

Nb-Pd system		
Low Temperature Phases comparison chart		
Composition % Pd	Experimental (Massalski [9])	<i>Ab initio</i> result
33.3	two-phase region above 700°C	$\text{Nb}_2\text{Pd-BCC}_{AB2}^{[011]}$ $\sim 11\text{meV/at.}$ below $\text{Nb}\leftrightarrow\text{NbPd}_2$
66.6	$\text{MoPt}_2$	$\text{NbPd}_2\text{-MoPt}_2$
75	$\alpha\text{-D0}_{22}$	$\text{NbPd}_3\text{-D0}_{22}$

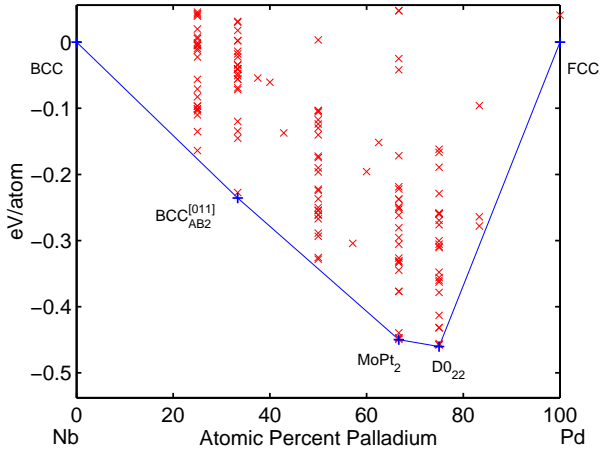


FIG. 30. NbPd (Niobium - Palladium) ground state convex hull.

**Nb-Pt (Niobium - Platinum).** Several intermetallic compounds have been reported for the system Nb-Pt [9,10,47,225–229]. We confirm the experimental phases  $\text{Nb}_3\text{Pt-A15}$  and  $\alpha\text{NbPt}_3\text{-D0}_a$  ( $\beta\text{Cu}_3\text{Ti}$  prototype). The prototype of  $\text{NbPt}_2$  is not reported in Massalski [9] (orthorhombic oI6, with space group Immm). We find  $\text{NbPt}_2\text{-MoPt}_2$ , in agreement with references [10,227,228]. At 50% concentration we do not confirm the stability of  $\text{NbPt-B19}$ . Instead of B19 we find  $\text{NbPt-L1}_0$ , and B19 to be higher by  $\sim 11\text{meV/atom}$  above  $\text{L1}_0$ . It is possible that  $\text{L1}_0$  is a ground state and B19 a high-temperature state. We can not say anything about the  $\sigma$ -phase  $\text{D8}_b$  since we do not have such prototype in our library. *We further investigated NbPt-L10 and NbPt-B19 with PAW-GGA potentials, as described in Section (III). With PAW, L10 is the most stable compound and B19 is  $\sim 18.5\text{meV/atom}$  higher than L10.*

Nb-Pt system		
Low Temperature Phases comparison chart		
Composition % Pt	Experimental (Massalski [9])	<i>Ab initio</i> result
19 to 28	A15	$\text{Nb}_3\text{Pt-A15}$
31 to 38	$\text{D8}_b$	unavailable $\sigma$ -phase
$\sim 50$	$\text{Nb}_{1-x}\text{Pt}_{1+x}\text{-B19}$	$\text{NbPt-L1}_0$ B19 $\sim 11\text{meV/at.}$ above $\text{L1}_0$ (us-lda) $\text{L1}_0$ stable (paw-gga) B19 $\sim 18.5\text{meV/at.}$ above $\text{L1}_0$ (paw-gga)
$\sim 67$	$\text{MoPt}_2$ [10,227,228]	$\text{NbPt}_2\text{-MoPt}_2$
$\sim 76$	$\text{D0}_a$	$\text{NbPt}_3\text{-D0}_a$

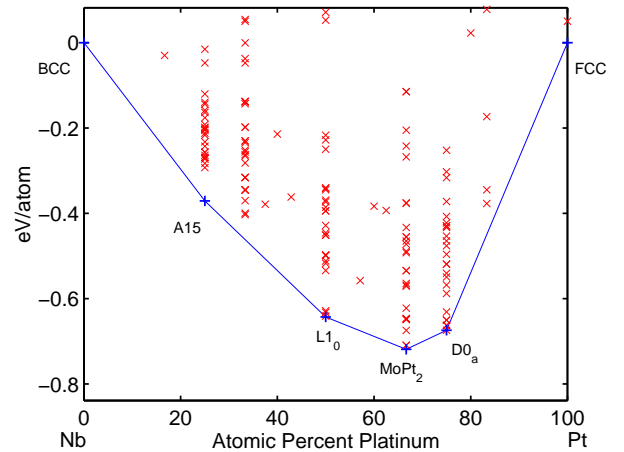


FIG. 31. NbPt (Niobium - Platinum) ground state convex hull.

**Nb-Rh (Niobium - Rhodium).** The system Nb-Rh is poorly characterized in the range of concentration 50~80% Rh [9,10,47,226,230,231,51]. We confirm the stability of Nb<sub>3</sub>Rh-A15, NbRh-L1<sub>0</sub>. NbRh-B19, which is observed as a high-temperature state, is ~27meV/atom above L1<sub>0</sub>, and it is possibly stabilized by entropic effects. Note: in Massalski and in the Pauling File [9,10] there is no phase at 50% composition, and Nb<sub>0.96</sub>Rh<sub>1.04</sub>-L1<sub>0</sub> appears off-stoichiometry. At concentration 75% Rh, we find the stable phase  $\eta$ -Al<sub>3</sub>Pu (Co<sub>3</sub>V) and  $\kappa$ NbRh<sub>3</sub>-L1<sub>2</sub> to be higher by 8meV/atom. Hence, we think that  $\eta$  prevails at low-temperature over  $\kappa$ , in contrast with the sketched phase diagram of reference [9]. We can not say anything about D8<sub>b</sub> and  $\xi$ (Nb<sub>2</sub>Rh<sub>3</sub>) since we do not have the  $\sigma$ -phase D8<sub>b</sub> and any A<sub>2</sub>B<sub>3</sub> prototypes in our library. *To address the structures with similar energy, we further investigate NbRh<sub>3</sub> with PAW-GGA potentials, as described in Section (III). With PAW, NbRh<sub>3</sub>-Al<sub>3</sub>Pu is the most stable compound and NbRh<sub>3</sub>-L1<sub>2</sub> is higher by 5.3meV/atom. The disagreement at composition NbRh<sub>3</sub> is further discussed in Section (IV).*

Another *ab initio* study, relevant for this system, can be found in reference [232].

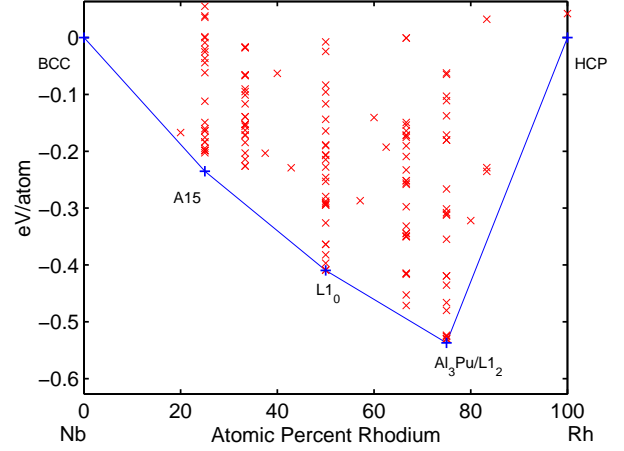


FIG. 32. NbRh (Niobium - Rhodium) ground state convex hull.

Nb-Rh system		
Low Temperature Phases comparison chart		
Composition % Rh	Experimental (Massalski [9])	<i>Ab initio</i> result
25	$\alpha'$ (Nb <sub>3</sub> Rh)-A15	Nb <sub>3</sub> Rh-A15
28.5 to 39.5	$\sigma$ (Nb <sub>13</sub> Rh <sub>7</sub> )-D8 <sub>b</sub>	unavailable
~51.5 to 52	Nb <sub>0.96</sub> Rh <sub>1.04</sub> -L1 <sub>0</sub> ( $\lesssim 1337^\circ\text{C}$ )	NbRh-L1 <sub>0</sub>
~56 to 62	$\epsilon$ (Nb <sub>2</sub> Rh <sub>3</sub> )-B19 (high-temperature $\gtrsim 1330^\circ\text{C}$ )	NbRh-B19 ~27meV/at. above L1 <sub>0</sub> (us-lda)
59 to ~64	$\xi$ (Nb <sub>2</sub> Rh <sub>3</sub> )-Nb <sub>2</sub> Rh <sub>3</sub>	unavailable
~67 to 70	$\eta$ (Nb <sub>13</sub> Rh <sub>27</sub> )-Al <sub>3</sub> Pu ( $\equiv$ Co <sub>3</sub> V in [9])	see below for Al <sub>3</sub> Pu
~71 to 79	$\kappa$ (NbRh <sub>3</sub> )-L1 <sub>2</sub>	NbRh <sub>3</sub> -Al <sub>3</sub> Pu (us-lda) L1 <sub>2</sub> ~8meV/at. above Al <sub>3</sub> Pu (us-lda) <i>Al<sub>3</sub>Pu stable (paw-gga)</i> L1 <sub>2</sub> ~5.3meV/at. <i>above Al<sub>3</sub>Pu (paw-gga)</i> See Section (IV).

**Nb-Ru (Niobium - Ruthenium).** Very little is known for the alloy Nb-Ru, especially at low-temperature [9,10,47,233–237]. We do not confirm the stability of any low-temperature compound at composition NbRu, but instead find a two-phase field between Nb<sub>3</sub>Ru and NbRu<sub>2</sub>, even though a high and low-temperature phase of NbRu has been observed [233,237]. In the Ru-rich side of the phase diagram, we find NbRu<sub>3</sub>-D0<sub>24</sub> to be 8meV/atom lower than L1<sub>2</sub> which is suggested experimentally. At 66% Ru we find NbRu<sub>2</sub>-C37 (with oP12-Co<sub>2</sub>Si prototype). With respect to the two-phase field Nb<sub>3</sub>Ru↔NbRu<sub>2</sub>, the structures closest to the tie-line at NbRu composition are B19 (~13meV/atom), L1<sub>0</sub> (~20meV/atom), B27 (~23meV/atom), B33 (~39meV/atom), and B2 (~45meV/atom). Experiments have not found any other stable compound. However, in the Nb-rich side of the phase diagram, we find Nb<sub>3</sub>Ru-D0<sub>3</sub> and a monoclinic Nb<sub>5</sub>Ru with C2/m #12 space group and prototype Mo<sub>5</sub>Ti<sup>proto</sup>. The structure Nb<sub>5</sub>Ru-Mo<sub>5</sub>Ti<sup>proto</sup> is described in Appendix (XII). *To address the disagreements at compositions NbRu and NbRu<sub>3</sub> we further investigate the relevant compounds with PAW-GGA potentials, as described in Section (III). For composition NbRu, the PAW-GGA result is substantially different from the US-LDA result. GGA gives L1<sub>0</sub> only 4meV/atom above the tie-line (versus 20meV/atom in LDA), whereas B19 was difficult to converge numerically, and seems to be >100meV/atom above the tie-line. For composition NbRu<sub>3</sub>, also with PAW, D0<sub>24</sub> is the most stable compound and L1<sub>2</sub> is higher by 2.5meV/atom. Because this number is so small, extremely large  $\mathbf{k}$ -points sets and high energy cutoff were used to converge it. The disagreements at compositions NbRu and NbRu<sub>3</sub> are further discussed in Section (IV).*

Other *ab initio* studies, relevant for this system, can be found in references [238–240].

Nb-Ru system		
Low Temperature Phases comparison chart		
Composition % Ru	Experimental (Massalski [9])	<i>Ab initio</i> result
16.6	disorder Nb-A2	Nb <sub>5</sub> Ru-Mo <sub>5</sub> Ti <sup>proto</sup> Appendix (XII)
25	disorder Nb-A2	Nb <sub>3</sub> Ru-D0 <sub>3</sub>
~50	NbRu'-L1 <sub>0</sub> (room-temperature)	two-phase region Nb <sub>3</sub> Ru↔NbRu <sub>2</sub> . L1 <sub>0</sub> ~4meV/at. ( <i>paw-gga</i> ) B19 >100meV/at. above tie-line ( <i>paw-gga</i> ).
~50	NbRu-B2 (high-temperature)	B19~13meV/at. (us-lda) L1 <sub>0</sub> ~20meV/at. B2 ~45meV/at. above the tie-line See Section (IV).
66.6	two-phase region above ~700°C	NbRu <sub>2</sub> -C37
75	L1 <sub>2</sub>	NbRu <sub>3</sub> -D0 <sub>24</sub> (us-lda) L1 <sub>2</sub> ~8meV/at. above D0 <sub>24</sub> (us-lda) D0 <sub>24</sub> stable ( <i>paw-gga</i> ) L1 <sub>2</sub> ~2.5meV/at. above D0 <sub>24</sub> ( <i>paw-gga</i> ) See Section (IV).

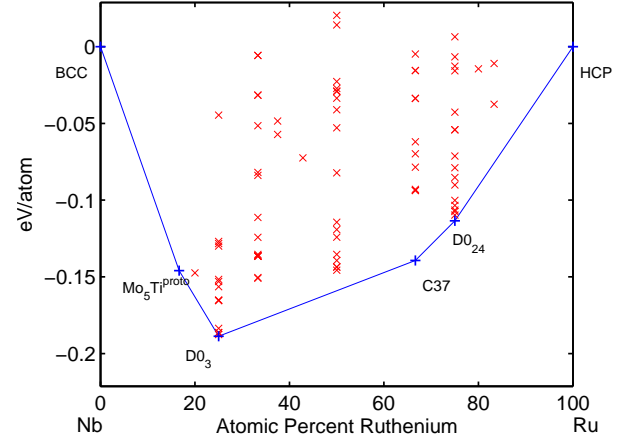


FIG. 33. NbRu (Niobium - Ruthenium) ground state convex hull.

**Nb-Tc (Niobium - Technetium).** The phase diagram of the system Nb-Tc is not known and only one intermetallic compound, NbTc<sub>3</sub> (metallic and superconductor) has been reported with  $\alpha$ Mn structure [9,10,47,241–243,365]. The compound NbTc<sub>3</sub> is classified as phase Nb<sub>0.15</sub>Tc<sub>0.85</sub> in the Pauling File [10]. We do not have  $\alpha$ Mn in our library of prototypes, and, at such stoichiometry, we do not find any stable compound. In the Tc-rich side of the phase diagram, we find a two-phase field NbTc $\leftrightarrow$ Tc, as shown in figure (34). At 50% concentration, we obtain NbTc-B2, and in the Nb-rich side of the diagram, we find Nb<sub>2</sub>Tc-C11<sub>b</sub> and an orthorhombic phase Nb<sub>3</sub>Tc with space group Immm #71, bcc superstructure, and prototype Nb<sub>3</sub>Tc<sup>proto</sup> described in Appendix (XI). Trends of Tc alloys are further discussed in Section (VIII).

Nb-Tc system		
Low Temperature Phases comparison chart		
Composition % Tc	Experimental (Massalski [9])	<i>Ab initio</i> result
25	not studied, unknown	Nb <sub>3</sub> Tc <sup>proto</sup> Appendix (XI)
33.3	same as above	Nb <sub>2</sub> Tc-C11 <sub>b</sub>
50	same as above	NbTc-B2
75	NbTc <sub>3</sub> - $\alpha$ Mn [9]	nothing stable
85	Nb <sub>0.15</sub> Tc <sub>0.85</sub> - $\alpha$ Mn [10]	

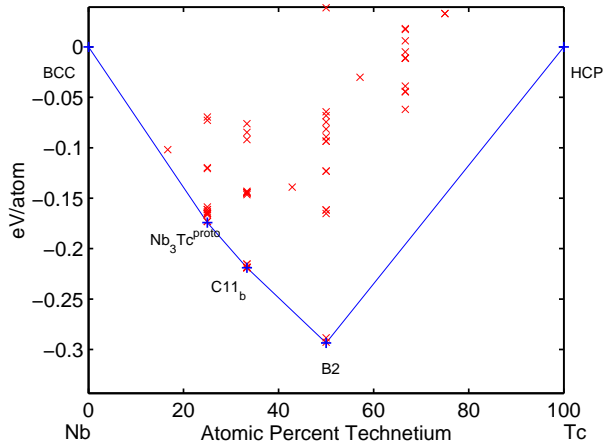


FIG. 34. NbTc (Niobium - Technetium) ground state convex hull.

**Pd-Pt (Palladium - Platinum).** The low temperature part of the phase diagram is believed to have a miscibility gap at a temperature of about 770°C. This miscibility gap is predicted on the basis of the difference of melting points between Pd and Pt [9,10,43,260,261]. Instead of such gap, we find three unknown stable compounds with fcc superstructures (Pd and Pt are both fcc). We find PdPt-L1<sub>1</sub>, and two orthorhombic phases, Pd<sub>3</sub>Pt and PdPt<sub>3</sub>, with space group Cmmm #65 and prototypes described in Appendix (XI). The prototypes are labeled as Pd<sub>3</sub>Pt<sup>proto</sup> and PdPt<sub>3</sub><sup>proto</sup>. The compound Pd<sub>3</sub>Pt is degenerate with respect to the two-phase fields Pd-A1 $\leftrightarrow$ PdPt-L1<sub>1</sub>, therefore its existence is uncertain. As shown in figure (35), all the stable phases have small formation energy (< 50meV/atom) making them difficult to determine experimentally. However, we believe the experimental phase diagram to be in error. We further investigate PdPt with PAW-GGA potentials, as described in Section (III). With PAW, PdPt-L1<sub>1</sub> is the most stable compound and PdPt-L1<sub>0</sub> is higher by 5.5meV/atom. Our results are in disagreement with previous FLAPW-LDA calculations, where L1<sub>0</sub> is found to be the most stable compound [262].

Other *ab initio* studies, relevant for this system, can be found in references [13,62].

Pd-Pt system		
Low Temperature Phases comparison chart		
Composition % Pt	Experimental (Massalski [9])	<i>Ab initio</i> result
25	predicted two-phase region Pd-A1 $\leftrightarrow$ Pt-A1	Pd <sub>3</sub> Pt <sup>proto</sup> /tie-line (uncertain) Appendix (XI)
50	same as above	PdPt-L1 <sub>1</sub> L1 <sub>0</sub> ~11meV/at. higher than L1 <sub>1</sub> (us-lda) L1 <sub>1</sub> stable L1 <sub>0</sub> ~5.5meV/at. higher than L1 <sub>1</sub> (paw-gga)
75	same as above	PdPt <sub>3</sub> <sup>proto</sup> Appendix (XI)

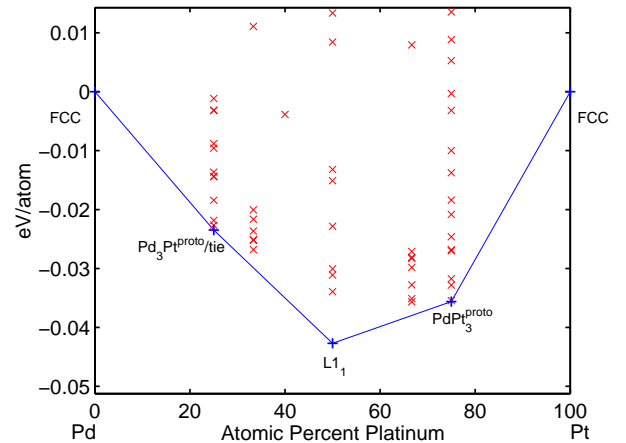


FIG. 35. PdPt (Palladium - Platinum) ground state convex hull.



**Pd-Tc (Palladium - Technetium).** The phase diagram for the system Pd-Tc is sketched based on the solid solubility data [9,10,43,365,368,275,346]. Experimental results report two solid solutions (fcc Pd-rich) and (hcp Tc-rich) with a two-phase region in between. No intermetallic compounds have been reported [9,10]. However, we find one stable phases PdTc<sub>3</sub>-D0<sub>19</sub>. In addition, at 50% concentration, we find a hcp superstructure (trigonal lattice, hP4, space group P $\bar{3}$ m1) which has an energy  $\sim 3\text{meV}/\text{atom}$  higher than the tie-line of the two-phase region PdTc<sub>3</sub> $\leftrightarrow$ Pd. Trends of Tc alloys are further discussed in Section (VIII).

Pd-Tc system		
Low Temperature Phases comparison chart		
Composition % Pd	Experimental (Massalski [9])	<i>Ab initio</i> result
25	two-phase region above $\sim 1000^\circ\text{C}$ Pd-A1 $\leftrightarrow$ Tc-A3	PdTc <sub>3</sub> -D0 <sub>19</sub>
50	two-phase region above $\sim 1000^\circ\text{C}$ Pd-A1 $\leftrightarrow$ Tc-A3	two-phase region PdTc <sub>3</sub> $\leftrightarrow$ Pd hcp superstr. $\sim 3\text{meV}/\text{at.}$ above tie-line

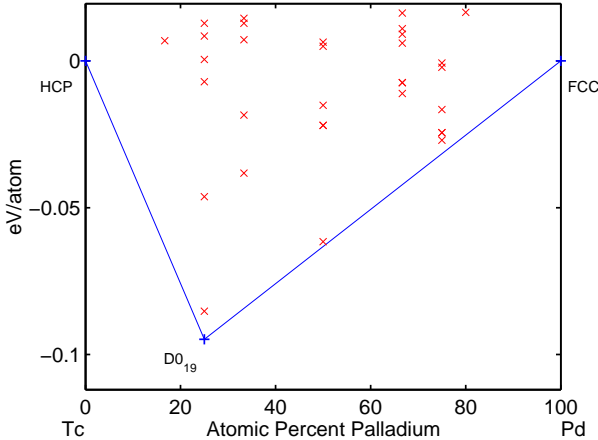


FIG. 36. PdTc (Palladium - Technetium) ground state convex hull.

**Pd-Ti (Palladium - Titanium).** This system has been subject of conflicting results for several years [9,10,169,276–291]. Our *ab initio* method confirms the stability of the compounds PdTi<sub>2</sub>-C11<sub>b</sub>, PdTi<sub>3</sub>-A15, and Pd<sub>3</sub>Ti-D0<sub>24</sub>. Near 80% Pd, Long Period Superstructures (LPS) modulations of L1<sub>2</sub> are observed [279]. While we do not have such off-stoichiometric LPS, we find L1<sub>2</sub> to be only 6meV/atom above D0<sub>24</sub> at Pd<sub>3</sub>Ti composition. The low energy difference between L1<sub>2</sub> and D0<sub>24</sub> indicates that it may be easy to form antiphase boundaries and LPS near this composition. We find Pd<sub>2</sub>Ti-MoPt<sub>2</sub> which is an orthorhombic distortion of C11<sub>b</sub> (MoPt<sub>2</sub> is orthorhombic, while C11<sub>b</sub> is tetragonal). We find Pd<sub>2</sub>Ti-C49 and Pd<sub>2</sub>Ti-C11<sub>b</sub> to be higher by 3meV/atom and 14meV/atom above MoPt<sub>2</sub>, respectively. At low temperature, at concentration 50%, we find a stable compound  $\alpha$ TiPd, but two prototypes are degenerate: L1<sub>0</sub> and B19 (which is reported experimentally). We can not find the reported phase PdTi<sub>4</sub>-A15 (off-stoichiometry) [9], which we think should appear inside the two-phase region of Ti  $\sim$  PdTi<sub>3</sub>, or at composition PdTi<sub>3</sub>. While off-stoichiometric compounds are obviously possible, this usually goes together with significant width of the single-phase field. Hence, we concluded (maybe erroneously) that the placement of A15 at composition PdTi<sub>4</sub> in reference [9] is likely a typographical error. *To address the degenerate structures, we further investigate  $\alpha$ TiPd with PAW-GGA potentials, as described in Section (III). With PAW, PdTi-B19 is the most stable compound and PdTi-L1<sub>0</sub> is higher by 10meV/atom.*

Another *ab initio* study, relevant for this system, can be found in reference [292].

Pd-Ti system		
Low Temperature Phases comparison chart		
Composition % Pd	Experimental (Massalski [9])	<i>Ab initio</i> result
20 and 25	A15 at 20%	PdTi <sub>3</sub> -A15 at 25%
33.3	C11 <sub>b</sub>	PdTi <sub>2</sub> -C11 <sub>b</sub>
47 to 53	$\alpha$ (TiPd)-B19	PdTi-B19/L1 <sub>0</sub> (us-lda) B19 stable (paw-gga) L1 <sub>0</sub> $\sim 10\text{meV}/\text{at.}$ above B19 (paw-gga)
60	Pd <sub>3</sub> Ti <sub>2</sub> $\sim$ Au <sub>2</sub> V	unavailable
62.5	Pd <sub>5</sub> Ti <sub>3</sub> $\sim$ C11 <sub>b</sub>	unavailable
66.6	orthorhombic distortion of C11 <sub>b</sub>	Pd <sub>2</sub> Ti-MoPt <sub>2</sub> (distortion of C11 <sub>b</sub> ) C49 $\sim 3\text{meV}/\text{at.}$ C11 <sub>b</sub> $\sim 14\text{meV}/\text{at.}$ above MoPt <sub>2</sub>
75	D0 <sub>24</sub>	Pd <sub>3</sub> Ti-D0 <sub>24</sub> L1 <sub>2</sub> $\sim 6\text{meV}/\text{at.}$ above D0 <sub>24</sub>
80	L1 <sub>2</sub>	L1 <sub>2</sub> metastable at 75% (see text)

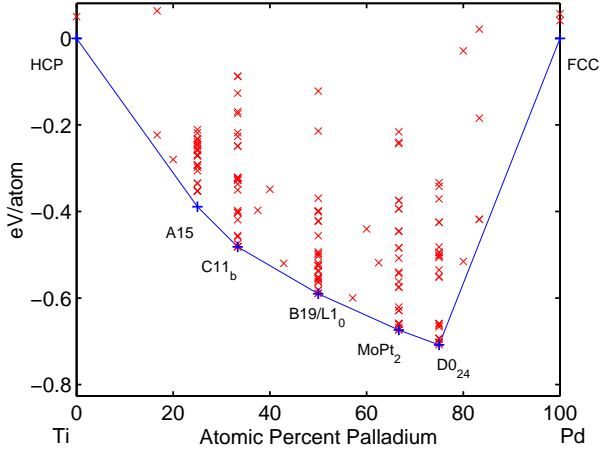


FIG. 37. PdTi (Palladium - Titanium) ground state convex hull.

**Pd-Y (Palladium - Yttrium).** The phase diagram for the system Pd-Y is known with reasonable accuracy. Several intermetallic compounds have been reported, but not all the structures have been determined experimentally [9,10,293–296]. We confirm the stability of the compounds Pd<sub>3</sub>Y-L1<sub>2</sub> and PdY<sub>3</sub>-D0<sub>11</sub>. The prototype of  $\alpha$ PdY is not known [293]. Our best guesses are PdY-B27 and PdY-B33 (CrB), which are degenerate in the calculation. We also find PdY<sub>2</sub>-C37, which occurs in a concentration between two known compounds Pd<sub>2</sub>Y<sub>3</sub> and Pd<sub>2</sub>Y<sub>5</sub> and is very close to the tie-line of the two-phase field PdY<sub>3</sub> $\leftrightarrow$ PdY (5meV/atom) Hence, if Pd<sub>2</sub>Y<sub>3</sub> and Pd<sub>2</sub>Y<sub>5</sub> were to be included, C37 would likely not be stable. We cannot check this prediction since we do not have Pd<sub>2</sub>Y<sub>3</sub> and Pd<sub>2</sub>Y<sub>5</sub> prototypes in the set of calculations. *To address the degenerate structures, we further investigate PdY with PAW-GGA potentials, as described in Section (III). With PAW, PdY-B27 is the most stable compound and PdY-B33 is higher by 3.1meV/atom.*

Pd-Y system		
Low Temperature Phases comparison chart		
Composition % Pd	Experimental (Massalski [9])	<i>Ab initio</i> result
25	D0 <sub>11</sub>	PdY <sub>3</sub> -D0 <sub>11</sub>
28.6	Pd <sub>2</sub> Y <sub>5</sub> unknown	unavailable
33.3	two-phase region	PdY <sub>2</sub> -C37 (uncertain)
40	Pd <sub>2</sub> Y <sub>3</sub> -hR15 unknown	unavailable
50	$\alpha$ PdY unknown	PdY-B27/B33 (us-lda) B27 stable ( <i>paw-gga</i> ) B33~3.1meV/at. above B27 ( <i>paw-gga</i> )
57.1	Pd <sub>4</sub> Y <sub>3</sub> -hR14 unknown	unavailable
60	$\alpha$ Pd <sub>3</sub> Y <sub>2</sub> unknown	unavailable
66.6	unknown	two phase region
79.5 to 75	L1 <sub>2</sub>	Pd <sub>3</sub> Y-L1 <sub>2</sub>
87.5	unknown	unavailable

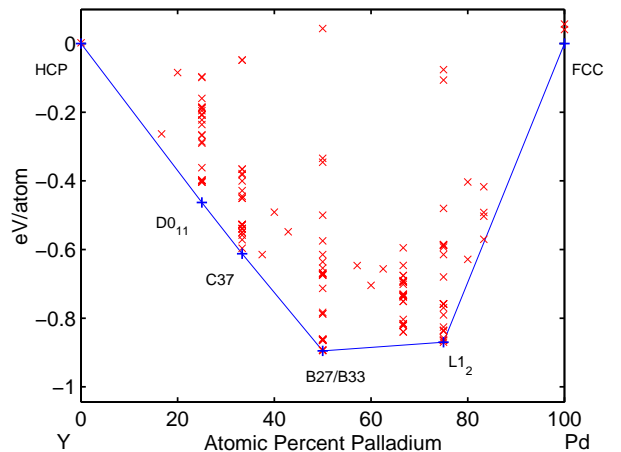


FIG. 38. PdY (Palladium - Yttrium) ground state convex hull.

**Pd-Zr (Palladium - Zirconium).** The experimental phase diagram for the system Pd-Zr is based on limited information [9,10,297–299,282,300–304]. We are able to confirm stability of  $\text{Pd}_3\text{Zr-D0}_{24}$  and  $\text{PdZr}_2\text{-C11}_b$ . The stable phase of PdZr is reported to be CrB (B33) [10,304]. At that composition, we find two degenerate structures: PdZr-B27 or PdZr-B33 (CrB). In the Zr-rich side of the phase diagram, we find  $\text{PdZr}_3\text{-FCC}_{AB3}^{[001]}$ . However, the energy difference between  $\text{PdZr}_3\text{-FCC}_{AB3}^{[001]}$  and the two-phase region  $\text{Zr}\leftrightarrow\text{PdZr}_2\text{-C11}_b$ , is very small ( $\sim 6\text{meV/atom}$ ). Hence, the existence of compound  $\text{PdZr}_3\text{-FCC}_{AB3}^{[001]}$  remains uncertain. At low-temperature, instead of a stable phase with stoichiometry  $\text{Pd}_2\text{Zr}$ , we find the two-phase field  $\text{PdZr}\leftrightarrow\text{Pd}_3\text{Zr-D0}_{24}$ . The least unstable phases are  $\text{Pd}_2\text{Zr-C49}$ ,  $\text{Pd}_2\text{Zr-MoPt}_2$ ,  $\text{Pd}_2\text{Zr-C11}_b$ , with energies  $\sim 18\text{meV/atom}$ ,  $\sim 24\text{meV/atom}$ ,  $\sim 26\text{meV/atom}$  above the tie-line of the two-phase region, respectively. *To address the degenerate structures and the erroneous two phase region  $\text{PdZr}\leftrightarrow\text{Pd}_3\text{Zr}$ , we further investigate PdZr and  $\text{Pd}_2\text{Zr}$  with PAW-GGA potentials, as described in Section (III). With PAW, PdZr-B33 is the most stable compound and PdZr-B27 is higher by  $3.2\text{meV/atom}$ . In addition,  $\text{Pd}_2\text{Zr-C11}_b$  is degenerate with the tie line  $\text{PdZr}\leftrightarrow\text{Pd}_3\text{Zr}$ , and  $\text{MoPt}_2$  and  $\text{C49}$  are higher by  $\sim 1.3\text{meV/atom}$  and  $\sim 7.1\text{meV/atom}$  with respect to  $\text{C11}_b$  (also the tie-line  $\text{PdZr}\leftrightarrow\text{Pd}_3\text{Zr}$  has been recalculated with PAW-GGA potentials).*

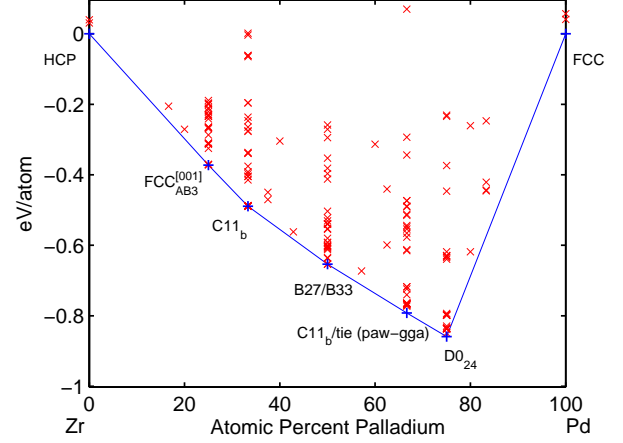


FIG. 39. Pd-Zr (Palladium - Zirconium) ground state convex hull.

Pd-Zr system		
Low Temperature Phases comparison chart		
Composition % Pd	Experimental (Massalski [9])	<i>Ab initio</i> result
25	two-phase region	$\text{PdZr}_3\text{-FCC}_{AB3}^{[001]}$ (uncertain)
33.3	$\text{C11}_b$	$\text{PdZr}_2\text{-C11}_b$
50	disorder fcc [9] CrB(B33-TII) [10,304]	PdZr- B27/B33 (us-lda) <i>B33 stable (paw-gga)</i> <i>B27~3.2meV/at.</i> <i>above B33 (paw-gga)</i>
66.6	$\text{C11}_b$	two-phase region (us-lda). C49~18meV/at. MoPt <sub>2</sub> ~24meV/at. C11 <sub>b</sub> ~26meV/at. above the tie-line (us-lda). <i>C11<sub>b</sub>/tie-line (paw-gga).</i> <i>MoPt<sub>2</sub>~1.3meV/at.,</i> <i>C49~7.1meV/at.</i> <i>above tie-line (paw-gga).</i>
75	$\text{D0}_{24}$	$\text{Pd}_3\text{Zr-D0}_{24}$

**Pt-Rh (Platinum - Rhodium).** The experimental phase diagram of the system Pt-Rh is similar the system Pd-Pt. The low-temperature part of the phase diagram is believed to have a miscibility gap at a temperature of about 760°C [9,10,43,263,305]. Instead of the gap, we find several stable phases, all with fcc superstructure (Pt and Rh are both fcc), similar to previous FLAPW-LDA calculations [262]. We find Pt<sub>4</sub>Rh-D1<sub>a</sub>, Pt<sub>3</sub>Rh-D0<sub>22</sub>, PtRh<sub>2</sub>-C49, PtRh<sub>3</sub>-D0<sub>22</sub>, PtRh<sub>4</sub>-D1<sub>a</sub>, and, at 50% concentration, PtRh-FCC<sub>A<sub>2</sub>B<sub>2</sub></sub><sup>[201]</sup> (CH “40” in reference [262]). As shown in figure (40), all the stable phases have very small formation energy (< 30meV/atom) indicating that they may disorder at relatively low temperature.

Another *ab initio* study, relevant for this system, can be found in reference [62].

Pt-Rh system		
Low Temperature Phases comparison chart		
Composition % Rh	Experimental (Massalski [9]) Theoretical ([262])	<i>Ab initio</i> result
20	two-phase region [9] D1 <sub>a</sub> [262]	Pt <sub>4</sub> Rh-D1 <sub>a</sub>
25	two-phase region [9] two-phase region [262]	Pt <sub>3</sub> Rh-D0 <sub>22</sub>
50	two-phase region [9] FCC <sub>A<sub>2</sub>B<sub>2</sub></sub> <sup>[201]</sup> [262]	PtRh-FCC <sub>A<sub>2</sub>B<sub>2</sub></sub> <sup>[201]</sup>
66.6	two-phase region [9]	PtRh <sub>2</sub> -C49
71.4	two-phase region [9] X2 [262]	unavailable
75	two-phase region [9] D0 <sub>22</sub> [262]	PtRh <sub>3</sub> -D0 <sub>22</sub>
80	two-phase region [9] D1 <sub>a</sub> [262]	PtRh <sub>4</sub> -D1 <sub>a</sub>

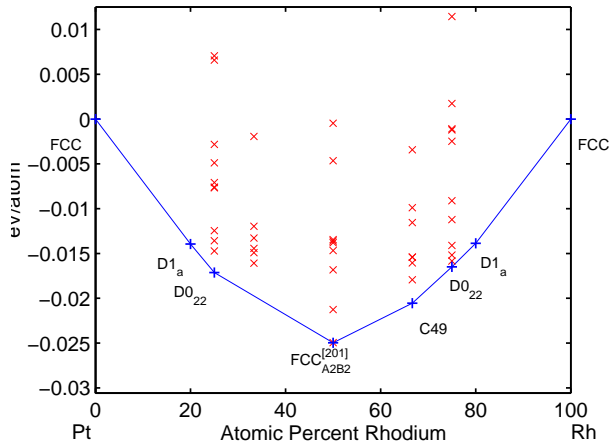


FIG. 40. PtRh (Platinum - Rhodium) ground state convex hull.

**Pt-Ru (Platinum - Ruthenium).** Only one compound has been found for the system Pt-Ru [9,10,306,307]. At low-temperature, the phase diagram reported in Massalski [9] has Platinum-rich and Ruthenium-rich solid solution with large solubilities of the other element, and a two-phase region for concentration between ~70% to ~80% of Ruthenium. However, recent X-ray diffraction experimental work reported the existence of a fcc phase at 50% composition, with unknown prototype [307]. For PtRu, our prediction is PtRu-FCC<sub>A<sub>2</sub>B<sub>2</sub></sub><sup>[001]</sup>. At 25% Ru composition, we find a stable phase Pt<sub>3</sub>Ru-FCC<sub>AB<sub>3</sub></sub><sup>[001]</sup>, degenerate with the two-phase field Pt↔PtRu. Hence, the existence of compound Pt<sub>3</sub>Ru-FCC<sub>AB<sub>3</sub></sub><sup>[001]</sup> remains uncertain. To our knowledge, PtRu is the first known system where the prototype structure FCC<sub>A<sub>2</sub>B<sub>2</sub></sub><sup>[001]</sup> would be stable.

Pt-Ru system		
Low Temperature Phases comparison chart		
Composition % Ru	Experimental (Massalski [9])	<i>Ab initio</i> result
25	disorder Pt-A1 [9]	Pt <sub>3</sub> Ru FCC <sub>AB<sub>3</sub></sub> <sup>[001]</sup> /tie-line (uncertain)
50	disorder Pt-A1 [9] PtRu-fcc [307]	PtRu-FCC <sub>A<sub>2</sub>B<sub>2</sub></sub> <sup>[001]</sup>

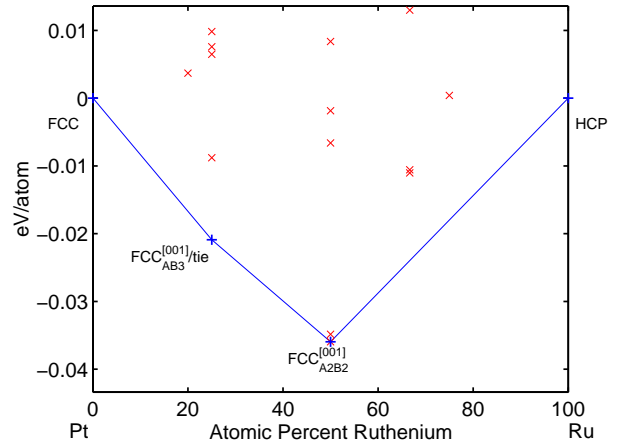


FIG. 41. PtRu (Platinum - Ruthenium) ground state convex hull.

**Pt-Tc (Platinum - Technetium).** The phase diagram for the system Pt-Tc has been determined from experimental solid solubility data [9,10,43,365,368]. No intermetallic compounds have been reported [9]. However, we find two stable phases:  $\text{Pt}_3\text{Tc-FCC}_{AB_3}^{[001]}$  and  $\text{PtTc}_3\text{-D0}_{19}$ .  $\text{PtTc}_3\text{-D0}_{19}$  appears in the composition range of a two-phase region Pt-A1 and Tc-A3, that is present at temperatures higher than  $\sim 1000^\circ\text{C}$ . Trends of Tc alloys are further discussed in Section (VIII).

Pt-Tc system		
Low Temperature Phases comparison chart		
Composition % Tc	Experimental (Massalski [9])	<i>Ab initio</i> result
25	disorder Pt-A1	$\text{Pt}_3\text{Tc-FCC}_{AB_3}^{[001]}$
75	two-phase region above $\sim 1000^\circ\text{C}$ Pt-A1 $\leftrightarrow$ Tc-A3	$\text{PtTc}_3\text{-D0}_{19}$

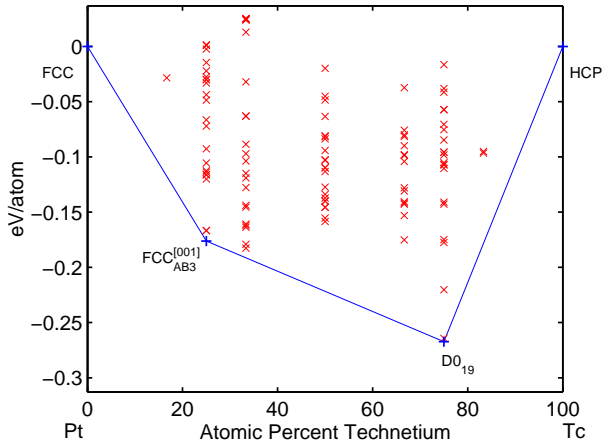


FIG. 42. PtTc (Platinum - Technetium) ground state convex hull.

**Pt-Ti (Platinum - Titanium).** Not much is known of Pt-Ti system to produce a precise phase diagram [9,10,48,285,290,308-311,283,312]. Some intermetallic compounds are reported [308-311,283,312,288]. We confirm the stability of phases  $\text{PtTi}_3\text{-A15}$ ,  $\alpha\text{PtTi-B19}$ ,  $\text{Pt}_3\text{Ti-D0}_{24}$ . B19 is stable at 50% composition, and  $\text{L1}_0$  and B33 are higher by  $\sim 20\text{meV/atom}$  and  $\sim 30\text{meV/atom}$ , respectively. At concentration 25%Ti, we confirm the existence of  $\gamma\text{-L1}_2$ , which has an energy that is  $\sim 5\text{meV/atom}$  higher than  $\text{Pt}_3\text{Ti-D0}_{24}$ . However,  $\text{L1}_2$  has been reported to be stable away from stoichiometry  $< 25\%$  Ti [9]. At composition 33% Ti,  $\text{Pt}_2\text{Ti}$ , Massalski reports a two-phase region above  $600^\circ\text{C}$  [9,10]. Instead of the two-phase field, we find a stable compound  $\text{Pt}_2\text{Ti}$ : two structures, C49 and C37, are degenerate. We cannot say anything about  $\text{Pt}_8\text{Ti-D1}_a$ , because our library does not contain off-stoichiometry  $\text{D1}_a$ . To address the degenerate structures, we further investigate  $\text{Pt}_2\text{Ti}$  with PAW-GGA potentials, as described in Section (III). With PAW,  $\text{Pt}_2\text{Ti-C49}$  is the most stable compound and  $\text{Pt}_2\text{Ti-C37}$  is higher by  $1.9\text{meV/atom}$ .

Another *ab initio* study, relevant for this system, can be found in reference [292].

Pt-Ti system		
Low Temperature Phases comparison chart		
Composition % Ti	Experimental (Massalski [9])	<i>Ab initio</i> result
1 to 12	$\text{Pt}_8\text{Ti-D1}_a$	unavailable
20 to 27	$\text{D0}_{24}$ ( $>25\%$ Ti) $\gamma\text{-L1}_2$ ( $<25\%$ Ti)	$\text{Pt}_3\text{Ti-D0}_{24}$ $\text{L1}_2 \sim 5\text{meV/at.}$ above $\text{D0}_{24}$
33.3	two-phase region above $600^\circ\text{C}$ [9]	$\text{Pt}_2\text{Ti-C49/C37}$ (us-lda) C49 stable C37 $\sim 1.9\text{meV/at.}$ above C49 (paw-gga)
46 to 54	$\alpha\text{PtTi-B19}$	$\text{PtTi-B19}$ $\text{L1}_0 \sim 20\text{meV/at.}$ above B19
71 to 78	A15	$\text{PtTi}_3\text{-A15}$

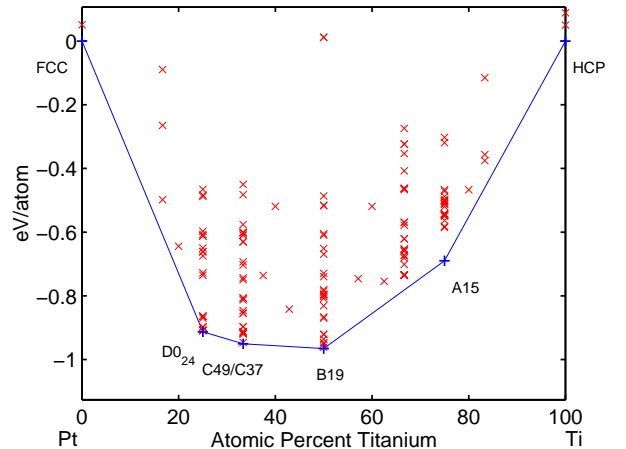


FIG. 43. PtTi (Platinum - Titanium) ground state convex hull.

**Pt-Y (Platinum - Yttrium).** The experimental phase diagram of the system Pt-Y has been sketched by analogy with other Rare Earth-Platinum diagrams [9]. Several intermetallic compounds have been reported [9,10,43,156,277,285,313–320,324]. The stability of the compounds  $\text{Pt}_3\text{Y-L1}_2$ ,  $\text{Pt}_2\text{Y-C15}$ , and  $\text{PtY}_3\text{-D0}_{11}$  is confirmed. At 50% concentration, we do not find any stable PtY-B27. Instead of B27, we find PtY-B33 (CrB prototype) to have lowest energy with B2 and B27 having energies  $\sim 50\text{meV/atom}$  above B33. At 66.6% Y concentration, we find  $\text{PtY}_2\text{-C37}$  which is the prototype of  $\text{Co}_2\text{Si}$  and  $\text{Ni}_2\text{Si}$ . Hence our calculations confirm the correct experimental structure. At concentration 62.5% Y, we do not find  $\text{Pt}_3\text{Y}_5\text{-D8}_8$ , but the two-phase field  $\text{PtY} \leftrightarrow \text{PtY}_2$ .  $\text{D8}_8$  and  $\text{W}_5\text{Si}_3$  are higher by  $\sim 24\text{meV/atom}$  and  $\sim 80\text{meV/atom}$  with respect to the tie-line  $\text{PtY} \leftrightarrow \text{PtY}_2$  (this problem is solved with PAW-GGA potentials). As shown in figure (44), at concentration 16.6% Y, we find a two-phase region instead of the reported stable compound  $\text{Pt}_5\text{Y}$  with unknown structure [9]. Our best guess is  $\text{Pt}_5\text{Y-D2}_d$  which is the least-metastable structure we have at such composition ( $\sim 18\text{meV/atom}$  above the tie-line  $\text{Pt} \leftrightarrow \text{Pt}_3\text{Y}$ ). We conclude that further experimental and theoretical investigations are necessary to determine the behavior of PtY. *To address the disagreement with the experimental results for compounds PtY and  $\text{Pt}_3\text{Y}_5$ , we further investigate the relevant structures with PAW-GGA potentials, as described in Section (III). With PAW, PtY-B33 is stable and PtY-B27 is higher by  $60\text{meV/atom}$ . For compound  $\text{Pt}_3\text{Y}_5$ ,  $\text{D8}_8$  is stable with an energy  $6.9\text{meV/atom}$  lower than the tie-line  $\text{PtY} \leftrightarrow \text{PtY}_2$ , which has also been recalculated with PAW-GGA potentials. The disagreement at composition PtY is further discussed in Section (IV).*

Pt-Y system		
Low Temperature Phases comparison chart		
Composition % Y	Experimental (Massalski [9])	<i>Ab initio</i> result
16.6	unknown	$\text{Pt}_5\text{Y-D2}_d$ metastable. $\text{D2}_d \sim 18\text{meV/at.}$ above the tie-line
25	$\text{L1}_2$	$\text{Pt}_3\text{Y-L1}_2$
33.3	C15	$\text{Pt}_2\text{Y-C15}$
42.9	$\text{Pt}_4\text{Y}_3\text{-Pd}_4\text{Pu}_3$	unavailable
50	B27	$\text{PtY-B33}$ B2/B27 $\sim 50\text{meV/at.}$ above B33 B33 stable ( <i>paw-gga</i> ) B27 $\sim 60\text{meV/at.}$ above B33. ( <i>paw-gga</i> ) See Section (IV).
55.6	$\text{Pt}_4\text{Y}_5\text{-Pu}_5\text{Rh}_4$	unavailable
62.5	$\text{Pt}_3\text{Y}_5\text{-D8}_8$	two-phase region $\text{PtY} \leftrightarrow \text{PtY}_2$ . ( <i>us-lda</i> ) $\text{D8}_8 \sim 24\text{meV/at.}$ above the tie-line ( <i>us-lda</i> ) $\text{D8}_8$ stable ( <i>paw-gga</i> ). $\sim 6.9\text{meV/at.}$ below $\text{PtY} \leftrightarrow \text{PtY}_2$ ( <i>paw-gga</i> ).
66.6	$\text{PtY}_2\text{-Ni}_2\text{Si}$ [9] ( $\text{Co}_2\text{Si}$ )	$\text{PtY}_2\text{-C37}$ ( $\text{Co}_2\text{Si}$ )
70	$\text{Pt}_3\text{Y}_7\text{-D10}_2$	unavailable
75	$\text{D0}_{11}$	$\text{PtY}_3\text{-D0}_{11}$

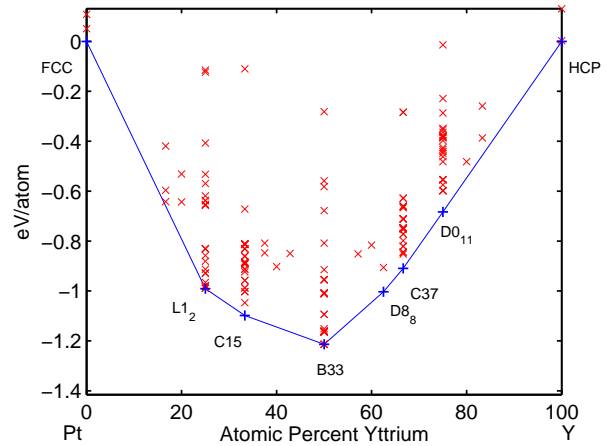


FIG. 44. PtY (Platinum - Yttrium) ground state convex hull.

**Pt-Zr (Platinum - Zirconium).** The system Pt-Zr is quite interesting. Our *ab initio* method confirms the stability of  $\alpha$ PtZr-B33 (CrB prototype). Two crystal structures have been reported for Pt<sub>3</sub>Zr: D0<sub>24</sub> and L1<sub>2</sub> [9,10,321,323,322,324,285,302]. We confirm the stability of Pt<sub>3</sub>Zr-D0<sub>24</sub> and we find L1<sub>2</sub> to be higher by 10meV/atom with respect to D0<sub>24</sub>. In the Zr-rich part of the phase diagram, we find two stable phases PtZr<sub>2</sub>-C16 and PtZr<sub>3</sub>-A15. At concentration 62.5% Zr, we do not find Pt<sub>3</sub>Zr<sub>5</sub>-D8<sub>8</sub>, but the two-phase field PtZr $\leftrightarrow$ PtZr<sub>2</sub>. W<sub>5</sub>Si<sub>3</sub> and D8<sub>8</sub> are higher by  $\sim$ 26meV/atom and  $\sim$ 36meV/atom with respect to the tie-line PtZr $\leftrightarrow$ PtZr<sub>2</sub>. To address the phase instability at composition Pt<sub>3</sub>Zr<sub>5</sub>, we further investigate the relevant compounds with PAW-GGA potentials, as described in Section (III). With PAW, at concentration Pt<sub>3</sub>Zr<sub>5</sub>, there is a two-phase region PtZr $\leftrightarrow$ PtZr<sub>2</sub>. In addition, Pt<sub>3</sub>Zr<sub>5</sub>-W<sub>5</sub>Si<sub>3</sub> and Pt<sub>3</sub>Zr<sub>5</sub>-D8<sub>8</sub> have energies higher by 23meV/atom and 26meV/atoms with respect to the tie-line PtZr $\leftrightarrow$ PtZr<sub>2</sub>, respectively. The disagreement at composition Pt<sub>3</sub>Zr<sub>5</sub> is further discussed in Section (IV).

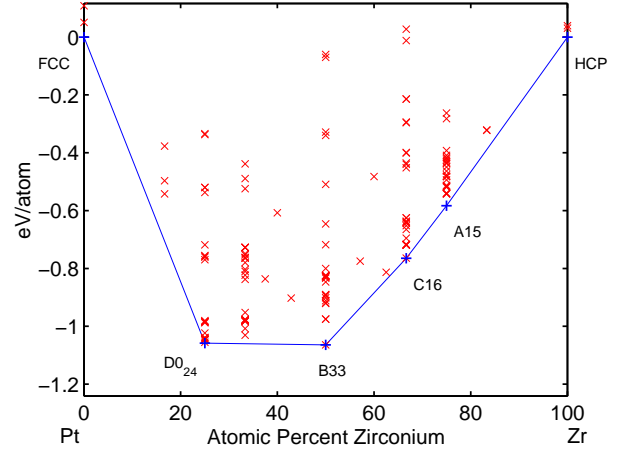


FIG. 45. PtZr (Platinum - Zirconium) ground state convex hull.

Pt-Zr system		
Low Temperature Phases comparison chart		
Composition % Zr	Experimental (Massalski [9])	<i>Ab initio</i> result
25	D0 <sub>24</sub> in [322,302,324,285] L1 <sub>2</sub> in [323]	Pt <sub>3</sub> Zr-D0 <sub>24</sub> L1 <sub>2</sub> $\sim$ 10meV/at. above D0 <sub>24</sub>
50	$\alpha$ PtZr-B33 (CrB)	PtZr-B33
62.5	Pt <sub>3</sub> Zr <sub>5</sub> -D8 <sub>8</sub>	two-phase region (us-lda) W <sub>5</sub> Si <sub>3</sub> $\sim$ 26meV/at. D8 <sub>8</sub> $\sim$ 36meV/at. above tie-line (us-lda). <i>two-phase region (paw-gga)</i> W <sub>5</sub> Si <sub>3</sub> $\sim$ 23meV/at. D8 <sub>8</sub> $\sim$ 26meV/at. above tie-line (paw-gga). See Section (IV).
66.6	two-phase region above 600°C	PtZr <sub>2</sub> -C16 (uncertain)
75	two-phase region above 600°C	PtZr <sub>3</sub> -A15 (uncertain)

**Rh-Ru (Rhodium - Ruthenium).** The phase diagram for the system Rh-Ru is based on the solid solubility data [9,10,43,326]. Experimental results report two solid solutions (fcc Rh-rich) and (hcp Ru-rich) with a two-phase region in between (from 34.5% to 40% atomic percent Ruthenium). No intermetallic compounds have been reported [325–327] and the system is considered to be no compound forming [10]. However, we find two stable phases: an orthorhombic oC12  $\text{RhRu}_2^{\text{proto}}$ , with hcp superstructure and Cmcm #63 space group, and a trigonal hP4  $\text{RhRu}^{\text{proto}}$ , with hcp superstructure and  $P\bar{3}m1$  #164 space group. Both prototypes are described in Appendix (XI). As shown in figure (46), all the stable phases have small formation energy ( $< 10\text{meV}/\text{atom}$ ) making them difficult to determine experimentally. *To better describe the stability of this system, we further investigate all the structures with negative formation energies with PAW-GGA potentials, as described in Section (III). Also with PAW,  $\text{RhRu}_2^{\text{proto}}$  and  $\text{RhRu}^{\text{proto}}$  are the most stable structures, with formation energies of  $-8.3\text{meV}/\text{atom}$  and  $-8.8\text{meV}/\text{atom}$ , respectively.*

Rh-Ru system		
Low Temperature Phases comparison chart		
Composition % Rh	Experimental (Massalski [9])	<i>Ab initio</i> result
33	solid solution Ru-A3	$\text{RhRu}_2^{\text{proto}}$ stable both us-lda and <i>paw-gga</i> , $E_f \sim -8.3\text{meV}/\text{atom}$ ( <i>paw-gga</i> ).
50	solid solution Ru-A3	$\text{RhRu}^{\text{proto}}$ stable both us-lda and <i>paw-gga</i> , $E_f \sim -8.8\text{meV}/\text{atom}$ ( <i>paw-gga</i> ).

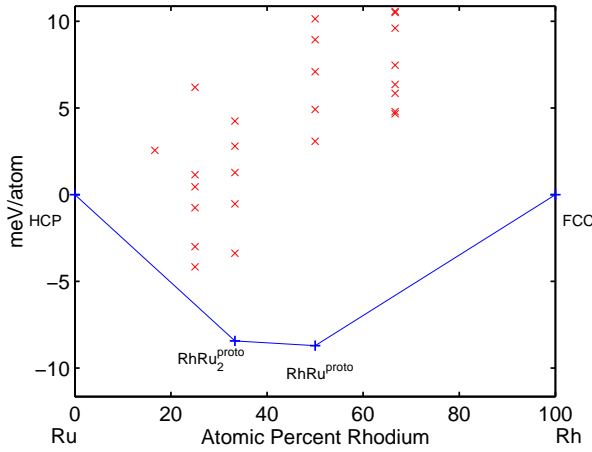


FIG. 46. RhRu (Rhodium - Ruthenium) ground state convex hull.

**Rh-Tc (Rhodium - Technetium).** The phase diagram for the system Rh-Tc is based on the solid solubility data [9,10,43,366,368]. Experimental results report two solid solutions (fcc Rh-rich) and (hcp Tc-rich) with a two-phase region in between. No intermetallic compounds have been reported [366,368]. However, we find three stable phases:  $\text{RhTc}_3\text{-D0}_{19}$ ,  $\text{RhTc-B19}$ , and  $\text{Ru}_2\text{Tc-ZrSi}_2$ . Trends of Tc alloys are further discussed in Section (VIII).

Rh-Tc system		
Low Temperature Phases comparison chart		
Composition % Rh	Experimental (Massalski [9])	<i>Ab initio</i> result
25	solid solution Tc-A3	$\text{RhTc}_3\text{-D0}_{19}$
50	solid solution Tc-A3	$\text{RhTc-B19}$ B27~29meV/at. above B19 (us-lda).
66.6	two-phase region above $\sim 1000^\circ\text{C}$ Pt-A1 $\leftrightarrow$ Tc-A3	$\text{Rh}_2\text{Tc-ZrSi}_2$

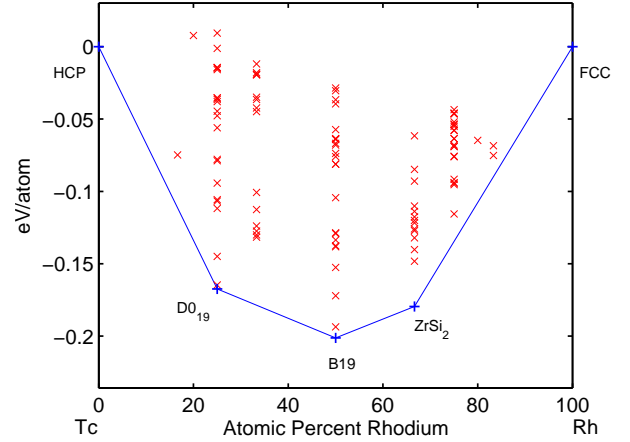


FIG. 47. RhTc (Rhodium - Technetium) ground state convex hull.



**Rh-Ti (Rhodium - Titanium).** There are qualitative disagreements about the phase diagram of the Rh-Ti system [9,10,48,322,328-332]. We confirm the stable phases that were found by all investigators [328-331]:  $\text{RhTi}_2$ ,  $\alpha\text{RhTi-L1}_0$ , and  $\text{Rh}_3\text{Ti-L1}_2$ . References [10,322,332] report  $\text{RhTi}_2\text{-CuZr}_2$  instead of  $\text{RhTi}_2\text{-C11}_b$ . The prototype  $\text{CuZr}_2$  is a distortion of  $\text{C11}_b$  and has the same lattice type (tetragonal,  $tI6$ ) and space group ( $I4/mmm$  #139) [10]. We find  $\text{RhTi}_2\text{-C11}_b$  and  $\text{RhTi}_2\text{-CuZr}_2$  to have degenerate energy. In the Rh-rich part of the phase diagram we find a stable phase  $\text{Rh}_2\text{Ti-C37}$ . However, we do not have  $\text{Rh}_5\text{Ti}_3$  in our library, so C37 might likely be unstable with respect to the two-phase field  $\text{Rh}_5\text{Ti}_3\leftrightarrow\text{L1}_2$ . At concentration  $\approx 84\%$  Rh, we do not find any stable compound, in agreement with [330] and in contrast with [328]. *To address the degenerate structures  $\text{RhTi}_2\text{-C11}_b/\text{CuZr}_2$ , we further investigate  $\text{RhTi}_2$  with PAW-GGA potentials, as described in Section (III). Also with PAW,  $\text{C11}_b$  and  $\text{CuZr}_2$  remain degenerate.*

Other *ab initio* studies, relevant for this system, can be found in references [232,292].

Rh-Ti system		
Low Temperature Phases comparison chart		
Composition % Rh	Experimental (Massalski [9])	<i>Ab initio</i> result
33.3	$\text{C11}_b$ [9]/ $\text{CuZr}_2$ [10]	$\text{RhTi}_2$ $\text{C11}_b/\text{CuZr}_2$ (us-lda,) $\text{C11}_b/\text{CuZr}_2$ (paw-gga)
$\sim 38$ to $58$	$\alpha\text{RhTi-L1}_0$	$\text{RhTi-L1}_0$
62.5	$\text{Rh}_5\text{Ti}_3\text{-Ge}_3\text{Rh}_5$	unavailable
66.6	two-phase region above $600^\circ\text{C}$	$\text{Rh}_2\text{Ti-C37}$
73 to 78	$\text{L1}_2$	$\text{Rh}_3\text{Ti-L1}_2$
$\sim 83.8$	$\text{Rh}_5\text{Ti}$ (unknown)	nothing stable

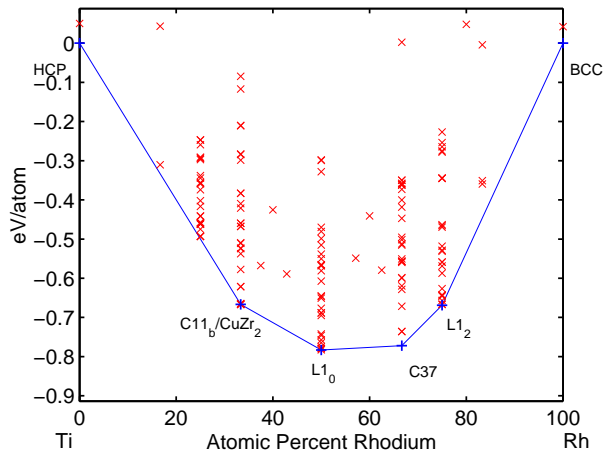


FIG. 48. RhTi (Rhodium - Titanium) ground state convex hull.

**Rh-Y (Rhodium - Yttrium).** Several compounds have been reported for the system Rh-Y at low-temperature [9,10,43,333,277,334,335,337]. The stability of  $\text{Rh}_2\text{Y-C15}$ ,  $\text{RhY-B2}$ ,  $\text{RhY}_3\text{-D0}_{11}$  is confirmed. At composition  $\text{Rh}_5\text{Y}$ , where a  $\text{D2}_d$  structure has been seen at high-temperature (but not stable at low-temperature), we find the  $\text{D2}_d$  to be the lowest energy structure (of all the structures at that composition), even though it is metastable with respect to the phase separation into  $\text{Rh}_2\text{Y-C15}\leftrightarrow\text{Rh}$ . At composition  $\text{Rh}_3\text{Y}$  one compound has been reported to be stable with prototype  $\text{CeNi}_3$  and space group  $\text{P6}_3/\text{mmc}$  #194 [10,336,338]. We do not have such prototype in our library and we do not find any stable phase:  $\text{Rh}_3\text{Y-D0}_{19}$  is the least metastable prototype we obtain.  $\text{Rh}_3\text{Y-D0}_{19}$  is higher by 130 meV/atom with respect the tie-line, which is at least one order of magnitude bigger than the accuracy of the calculations. We also find  $\text{RhY}_2\text{-C37}$ , which appears in a concentration between two known compounds,  $\text{Rh}_3\text{Y}_5$  and  $\text{Rh}_3\text{Y}_7$ , that are not present in our set of calculations. Therefore C37 might be unstable with respect to the two-phase region  $\text{Rh}_3\text{Y}_5\leftrightarrow\text{Rh}_3\text{Y}_7$ .

Rh-Y system		
Low Temperature Phases comparison chart		
Composition % Rh	Experimental (Massalski [9])	<i>Ab initio</i> result
25	$\text{D0}_{11}$	$\text{RhY}_3\text{-D0}_{11}$
30	$\text{Rh}_3\text{Y}_7\text{-D10}_2$	unavailable
33.3	two-phase region above $0^\circ\text{C}$	$\text{RhY}_2\text{-C37}$ (uncertain)
37.5	$\text{Rh}_3\text{Y}_5$ (unknown)	unavailable
40	$\text{Rh}_2\text{Y}_3$ (unknown) $tI140\text{-I4/mcm}$	unavailable
50	$\text{B2}$	$\text{RhY-B2}$
66.6	$\text{C15}$	$\text{Rh}_2\text{Y-C15}$
75	$\text{Rh}_3\text{Y}$ (unknown) $hP24\text{-P6}_3/\text{mmc}$	$\text{D0}_{19}\sim 130\text{meV/at.}$ above tie-line
83.5	$\text{Rh}_5\text{Y-D2}_d$ (high-temperature)	$\text{D2}_d\sim 110\text{meV/at.}$ above tie-line

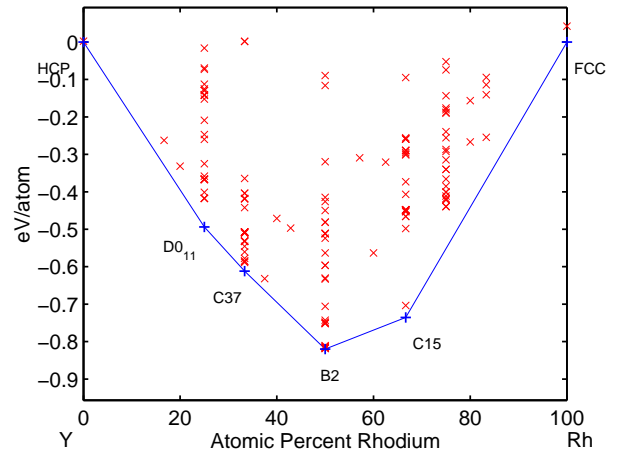


FIG. 49. RhY (Rhodium - Yttrium) ground state convex hull.

**Rh-Zr (Rhodium - Zirconium).** Although the system Zr-Rh is well known for its superconducting phases [9,10,339,342], further investigations are needed to clarify the stability and presence of intermediate phases [340,341]. Our *ab initio* method confirms the stability of  $\text{RhZr}_2\text{-C16}$  and  $\text{Rh}_3\text{Zr-L1}_2$ . Massalski does not report the prototype of the low-temperature phase  $\alpha\text{RhZr}$  [9]. References [342–344] report  $\alpha\text{RhZr-B27}$ . We confirm the stability of  $\alpha\text{RhZr-B27}$  (BFe prototype) with no other metastable compounds with similar energy. In addition, we find three new phases  $\text{Rh}_2\text{Zr-C37}$ ,  $\text{RhZr}_4\text{-D1}_a$  and  $\text{RhZr}_3\text{-FCC}_{AB3}^{[001]}$ , which are degenerate with the two-phase fields  $\text{RhZr}\leftrightarrow\text{Rh}_3\text{Zr}$ ,  $\text{Zr}\leftrightarrow\text{RhZr}$ , and  $\text{Zr}\leftrightarrow\text{RhZr}$ , respectively.

Other *ab initio* studies, relevant for this system, can be found in references [232,345].

Rh-Zr system		
Low Temperature Phases comparison chart		
Composition % Rh	Experimental (Massalski [9])	<i>Ab initio</i> result
20	two-phase region above 0°C	$\text{RhZr}_4\text{-D1}_a$ /tie-line
25	two-phase region above 0°C	$\text{RhZr}_3\text{-FCC}_{AB3}^{[001]}$ /tie-line
33.3	C16	$\text{RhZr}_2\text{-C16}$
50 to ?	$\alpha\text{RhZr}$ unknown [9] B27 [342–344]	$\text{RhZr-B27}$
57.1	$\text{Rh}_4\text{Zr}_3$ (unknown)	unavailable
62.5	$\text{Rh}_5\text{Zr}_3\text{-Pd}_3\text{Pu}_3$	unavailable
66.6	two-phase region above 0°C	$\text{Rh}_2\text{Zr-C37}$ /tie-line
72 to 82	L1 <sub>2</sub>	$\text{Rh}_3\text{Zr-L1}_2$

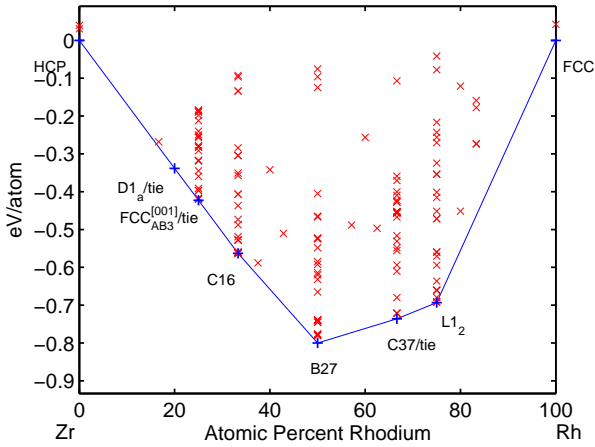


FIG. 50. RhZr (Rhodium - Zirconium) ground state convex hull.

**Ru-Tc (Ruthenium - Technetium).** The phase diagram for the system Ru-Tc is considered to have a continuous disordered hcp solid solution at low-temperature [9,10,365,368,346]. We find three stable ordered phases  $\text{Ru}_3\text{Tc-D0}_{19}$ ,  $\text{RuTc-B19}$ , and  $\text{RuTc}_3\text{-D0}_{19}$ , all of which are hcp superstructures. Hence, it is possible that they are low-temperature phases of the system Ru-Tc. Trends of Tc alloys are further discussed in Section (VIII).

Ru-Tc system		
Low Temperature Phases comparison chart		
Composition % Ru	Experimental (Massalski [9])	<i>Ab initio</i> result
25	disorder solution (Ru,Tc)-A3	$\text{RuTc}_3\text{-D0}_{19}$
50	same as above	$\text{RuTc-B19}$
75	same as above	$\text{Ru}_3\text{Tc-D0}_{19}$

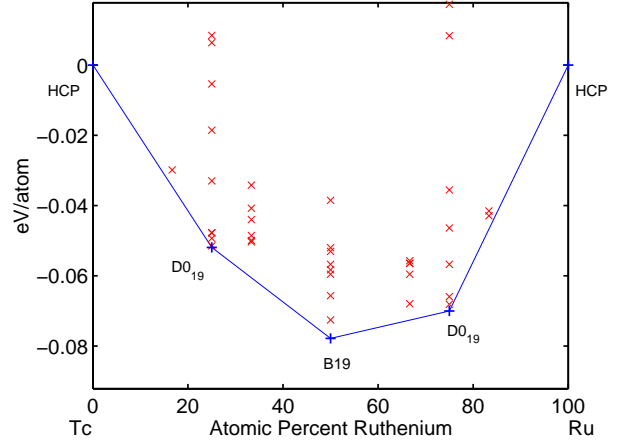


FIG. 51. RuTc (Ruthenium - Technetium) ground state convex hull.

**Ru-Ti (Ruthenium - Titanium).** The phase diagram of Ru-Ti is well determined by several investigators. A single low-temperature compound RuTi-B2 has been reported [9,10,43,285,347,348,350,349,351-354], and our *ab initio* method confirms its stability. In addition, we find two stable phases: RuTi<sub>2</sub>-C49, and orthorhombic RuTi<sub>3</sub> with space group Immm #71, bcc superstructure, and prototype RuTi<sub>3</sub><sup>proto</sup> described in Appendix (XI). Such compounds are close to the tie-line Ti↔RuTi. In fact, for C49 and RuTi<sub>3</sub><sup>proto</sup>, the formation energies are lower by ~34meV/atom and ~37meV/atom with respect to the two-phase field Ti↔RuTi.

Ru-Ti system		
Low Temperature Phases comparison chart		
Composition % Ru	Experimental (Massalski [9])	<i>Ab initio</i> result
25	two-phase region above 600°C	RuTi <sub>3</sub> <sup>proto</sup> Appendix (XI) ~37meV/at. below Ti↔RuTi
33.3	same as above	RuTi <sub>2</sub> -C49 ~34meV/at. below Ti↔RuTi
45 to 52 ±1	B2	RuTi-B2

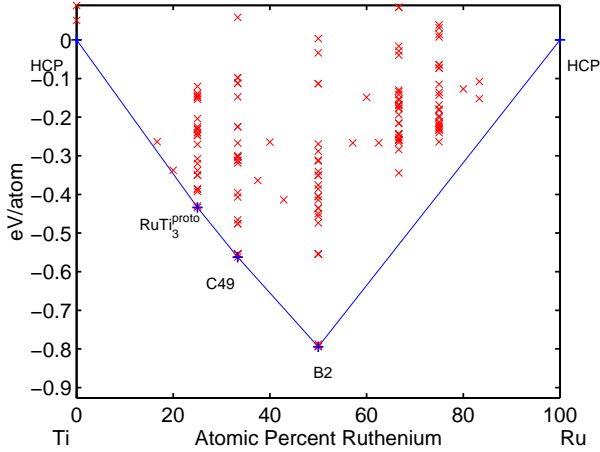


FIG. 52. RuTi (Ruthenium - Titanium) ground state convex hull.

**Ru-Y (Ruthenium - Yttrium).** Several compounds have been reported for the system Ru-Y [9,10,43,333,355-359]. We confirm the stability of RuY<sub>3</sub>-D0<sub>11</sub> and Ru<sub>2</sub>Y-C14. Also, we find RuY<sub>2</sub>-C16, which appears in a concentration between two known compounds Ru<sub>25</sub>Y<sub>44</sub> and Ru<sub>2</sub>Y<sub>5</sub> that are not in our library of calculations. Hence, the existence of RuY<sub>2</sub>-C16 is uncertain. At concentration 50%, we do not find any stable RuY compound, in agreement with [358].

Ru-Y system		
Low Temperature Phases comparison chart		
Composition % Ru	Experimental (Massalski [9])	<i>Ab initio</i> result
25	D0 <sub>11</sub>	RuY <sub>3</sub> -D0 <sub>11</sub>
28.6	Ru <sub>2</sub> Y <sub>5</sub> -C <sub>2</sub> Mn <sub>5</sub> mS28 C12/c1 [10,355,356,358]	unavailable
33.3	two-phase region above 0°C	RuY <sub>2</sub> -C16 (uncertain)
36.2	Ru <sub>25</sub> Y <sub>44</sub> (unknown) oP276 Pnna [10,355,359]	unavailable
40	Ru <sub>2</sub> Y <sub>3</sub> -Er <sub>3</sub> Ru <sub>2</sub> hP10 P6 <sub>3</sub> /m [360]	unavailable
66.6	Ru <sub>2</sub> Y-C14	Ru <sub>2</sub> Y-C14

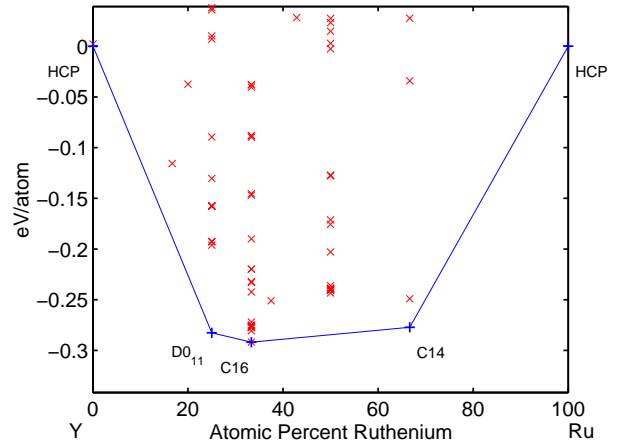


FIG. 53. RuY (Ruthenium - Yttrium) ground state convex hull.

**Ru-Zr (Ruthenium - Zirconium).** The phase diagram of RuZr is known accurately [9,10,362,361]. Our *ab initio* method confirms the stability of the low-temperature phase RuZr-B2. In agreement with experiments, we find no ground state at composition Ru<sub>2</sub>Zr, though the lowest energy structure at that composition in our calculations is C14 which appears in the phase diagram at high-temperature. Ru<sub>2</sub>Zr-C14 is higher by  $\sim 60\text{meV/atom}$  with respect to the two-phase field Ru $\leftrightarrow$ RuZr. In the Zr-rich region we find one stable compound, RuZr<sub>4</sub>-D1<sub>a</sub>, previously unknown. In addition, we find three metastable phases: RuZr<sub>5</sub>, RuZr<sub>3</sub>, and RuZr<sub>2</sub>-C49, with energies higher by 21meV/atom, 16.6meV/atom, and 14meV/atom, with respect to the two-phase fields RuZr<sub>4</sub> $\leftrightarrow$ Zr, RuZr $\leftrightarrow$ RuZr<sub>4</sub>, and RuZr $\leftrightarrow$ RuZr<sub>4</sub>, respectively. The structure of RuZr<sub>5</sub> is similar to MoZr<sub>5</sub><sup>proto</sup> (Appendix (XII)), while the structure of RuZr<sub>3</sub> is similar to RuTi<sub>3</sub><sup>proto</sup> (Appendix (XI)).

Other *ab initio* studies, relevant for this system, can be found in references [238–240,363].

Ru-Zr system		
Low Temperature Phases comparison chart		
Composition % Ru	Experimental (Massalski [9])	<i>Ab initio</i> result
16.6	two-phase region RuZr $\leftrightarrow$ Zr above 400°C	RuZr <sub>5</sub> $\approx$ MoZr <sub>5</sub> <sup>proto</sup> $\sim 21\text{meV/at.}$ above RuZr <sub>4</sub> $\leftrightarrow$ Zr
20	same as above	RuZr <sub>4</sub> -D1 <sub>a</sub>
25	same as above	RuZr <sub>3</sub> $\approx$ RuTi <sub>3</sub> <sup>proto</sup> $\sim 16.6\text{meV/at.}$ above RuZr $\leftrightarrow$ RuZr <sub>4</sub>
33.3	same as above	RuZr <sub>2</sub> -C49 $\sim 14\text{meV/at.}$ above RuZr $\leftrightarrow$ RuZr <sub>4</sub>
48 to 52	B2	RuZr-B2
66 to 68	C14 (high T)	Ru <sub>2</sub> Zr-C14 $\sim 60\text{meV/at.}$ above Ru $\leftrightarrow$ RuZr

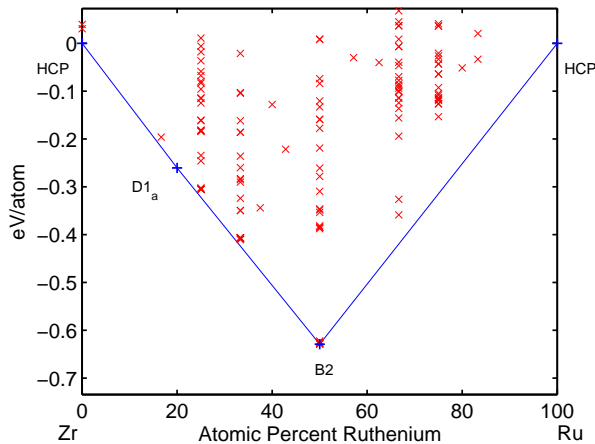


FIG. 54. RuZr (Ruthenium - Zirconium) ground state convex hull.

**Tc-Ti (Technetium - Titanium).** The phase diagram of the system TcTi has been constructed by analogy with chemically related systems [9,10,48,364,365]. Two intermetallic compound, TcTi-B2 and  $\chi$  are reported [364,365]. We confirm the stability of TcTi-B2, but we can not say anything about  $\chi$  since we do not have prototypes at composition 85% Ru. In addition, we find Tc<sub>2</sub>Ti-C11<sub>b</sub>, TcTi<sub>2</sub>-C49, and an orthorhombic phase TcTi<sub>3</sub> with space group Immm #71 and prototype TcTi<sub>3</sub><sup>proto</sup> described in Appendix (XI). These intermetallics have large negative formation energy, therefore they are expected to be very stable. Trends of Tc alloys are further discussed in Section (VIII).

Tc-Ti system		
Low Temperature Phases comparison chart		
Composition % Tc	Experimental (Massalski [9])	<i>Ab initio</i> result
25	disorder $\beta$ Ti-A2	TcTi <sub>3</sub> <sup>proto</sup> Appendix (XI)
33.3	disorder $\beta$ Ti-A2	TcTi <sub>2</sub> -C49
$\sim 50$	B2	TcTi-B2
66.6	two-phase region TcTi $\leftrightarrow$ $\chi$	Tc <sub>2</sub> Ti-C11 <sub>b</sub>
$\sim 85$	$\chi$ -A12	unavailable

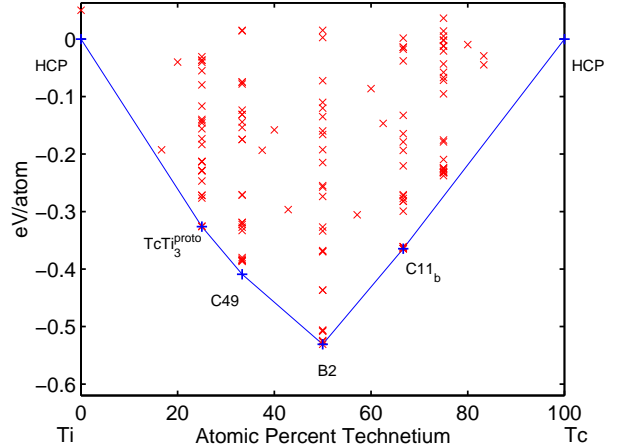


FIG. 55. TcTi (Technetium - Titanium) ground state convex hull.

**Tc-Y (Technetium - Yttrium).** Not enough information exists in order to construct a phase diagram for the system Tc-Y [9,10]. Only one intermetallic compound has been reported:  $\text{Tc}_2\text{Y-C14}$  (Friauf-Laves/Frank-Kasper phase) [367,369]. We confirm the stability of  $\text{Tc}_2\text{Y-C14}$ . In addition, we find another stable phase  $\text{TcY}_3\text{-D0}_{11}$ . Trends of Tc alloys are further discussed in Section (VIII).

Tc-Y system		
Low Temperature Phases comparison chart		
Composition % Tc	Experimental (Massalski [9])	<i>Ab initio</i> result
25	no information	$\text{TcY}_3\text{-D0}_{11}$
66.6	C14 [367,369]	$\text{Tc}_2\text{Y-C14}$ (Laves phase)

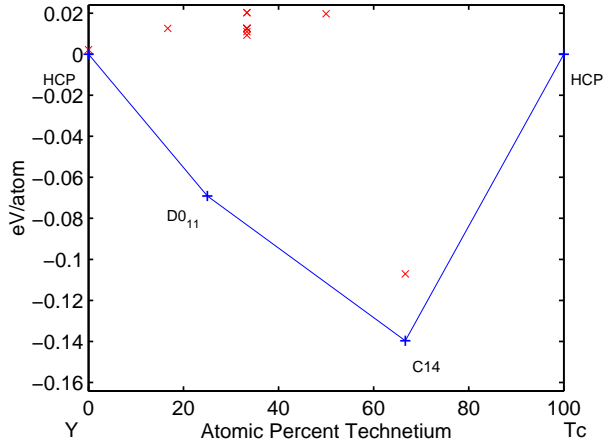


FIG. 56. TcY (Technetium - Yttrium) ground state convex hull.

**Tc-Zr (Technetium - Zirconium).** Not enough information exists in order to construct a phase diagram for the system Tc-Zr [9,10]. Only two intermetallic compounds have been reported:  $\text{Tc}_2\text{Zr-C14}$  (Friauf-Laves/Frank-Kasper phase) and  $\text{Tc}_6\text{Zr-A12}$  [9,10,365,370]. We confirm the stability of  $\text{Tc}_2\text{Zr-C14}$ , but we cannot determine A12 since we do not have the proper prototype in our library. At 50% composition, Miedema *et-al.* reported the existence of a TcZr compound with unknown structure [10,285]. At such composition we find TcZr-B2. In addition, we find other stable phases:  $\text{TcZr}_4\text{-D1}_a$  and  $\text{TcZr}_2\text{-C49}$ . These intermetallics have large negative formation energy, therefore they are expected to be very stable. Trends of Tc alloys are further discussed in Section (VIII).

Tc-Zr system		
Low Temperature Phases comparison chart		
Composition % Tc	Experimental (Massalski [9])	<i>Ab initio</i> result
20	no information	$\text{TcZr}_4\text{-D1}_a$
33.3	no information	$\text{TcZr}_2\text{-C49}$
50	TcZr (unknown) [285]	TcZr-B2
66.6	C14 [365,370]	$\text{Tc}_2\text{Zr-C14}$ (Laves phase)
85.7	$\text{Tc}_6\text{Zr-A12}$	unavailable

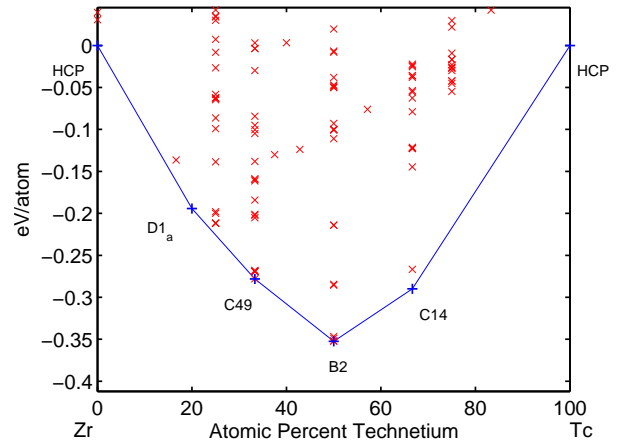


FIG. 57. TcZr (Technetium - Zirconium) ground state convex hull.

## VIII. TREND FOR TECHNETIUM ALLOYS

In our set of calculations, we have noticed that the phase  $\text{D0}_{19}$  appears in systems  $\text{MTc}_3$  where M is a transition metal in the columns on the right of Tc (Tc is in column 7B) while  $\text{D0}_{19}$  is not present if M is in the columns on the left of Tc:  $\text{D0}_{19}$  is stable in  $\text{PdTc}_3$ ,  $\text{PtTc}_3$ ,  $\text{RhTc}_3$ ,  $\text{RuTc}_3$ , and unstable in  $\text{NbTc}$ ,  $\text{TcTi}$ ,  $\text{TcY}$ , and  $\text{TcZr}$ .

## **IX. ACKNOWLEDGMENTS**

The research was supported by the Department of Energy, Office of Basic Energy Science under Contract No. DE-FG02-96ER45571 and National Science Foundation Information Technology Research (NSF-ITR) Grant No. DMR-0312537.

It has benefited from discussion with John Rodgers, Kristin Persson, Frank Hadley Cocks, Chris Fischer, Aleksey Kolmogorov, Vincent Crespi and Zi-Kui Liu.

## X. TABLES OF RESULTS

### A. Experimental compounds in agreement with *ab initio* solutions

Experimental compound $\Leftrightarrow$ <i>ab initio</i> compound					
System	Experimental result	<i>Ab initio</i> result	System	Experimental result	<i>Ab initio</i> result
Ag-Cd	AgCd-B2 [10,67-70]	AgCd-B2/B19/B27	Nb-Pd	NbPd <sub>3</sub> -D0 <sub>22</sub>	NbPd <sub>3</sub> -D0 <sub>22</sub>
Ag-Mg	Ag <sub>3</sub> Mg-D0 <sub>23</sub> [76]	AgMg-D0 <sub>23</sub> /D0 <sub>24</sub>	Nb-Pt	Nb <sub>3</sub> Pt-A15	Nb <sub>3</sub> Pt-A15
Ag-Mg	AgMg-B2	AgMg-B2	Nb-Pt	NbPt <sub>2</sub> -MoPt <sub>2</sub>	NbPt <sub>2</sub> -MoPt <sub>2</sub>
Ag-Na	Ag <sub>2</sub> Na-C15	Ag <sub>2</sub> Na-C15	Nb-Pt	NbPt <sub>3</sub> -D0 <sub><math>\alpha</math></sub>	NbPt <sub>3</sub> -D0 <sub><math>\alpha</math></sub>
Ag-Ti	AgTi <sub>2</sub> -C11 <sub>b</sub>	AgTi <sub>2</sub> -C11 <sub>b</sub>	Nb-Rh	Nb <sub>3</sub> Rh- $\alpha'$ -A15	Nb <sub>3</sub> Rh-A15
Ag-Ti	AgTi-B11	AgTi-B11 ( $\gamma$ CuTi)	Nb-Rh	NbRh-L1 <sub>0</sub>	NbRh-L1 <sub>0</sub>
Ag-Y	AgY-B2	AgY-B2	Nb-Rh	$\epsilon$ (Nb <sub>2</sub> Rh <sub>3</sub> )-B19 (high T)	NbRh-B19
Ag-Y	Ag <sub>2</sub> Y-C11 <sub>b</sub>	Ag <sub>2</sub> Y-C11 <sub>b</sub>	Nb-Rh	$\eta$ (Nb <sub>13</sub> Rh <sub>27</sub> )-Al <sub>3</sub> Pu	NbRh <sub>3</sub> -Al <sub>3</sub> Pu
Ag-Zr	AgZr <sub>2</sub> -C11 <sub>b</sub>	AgZr <sub>2</sub> -C11 <sub>b</sub>	Pd-Ti	PdTi <sub>3</sub> -A15 at 20%	PdTi <sub>3</sub> -A15 at 25%
Ag-Zr	AgZr-B11	AgZr-B11 ( $\gamma$ CuTi)	Pd-Ti	PdTi <sub>2</sub> -C11 <sub>b</sub>	PdTi <sub>2</sub> -C11 <sub>b</sub>
Al-Sc	AlSc <sub>2</sub> -B8 <sub>2</sub>	AlSc <sub>2</sub> -B8 <sub>2</sub>	Pd-Ti	$\alpha$ (TiPd)-B19	PdTi-B19
Al-Sc	AlSc-B2	AlSc-B2	Pd-Ti	Pd <sub>3</sub> Ti-D0 <sub>24</sub>	Pd <sub>3</sub> Ti-D0 <sub>24</sub>
Al-Sc	Al <sub>2</sub> Sc-C15	Al <sub>2</sub> Sc-C15	Pd-Y	PdY <sub>3</sub> -D0 <sub>11</sub>	PdY <sub>3</sub> -D0 <sub>11</sub>
Al-Sc	Al <sub>3</sub> Sc-L1 <sub>2</sub>	Al <sub>3</sub> Sc-L1 <sub>2</sub>	Pd-Y	Pd <sub>3</sub> Y-L1 <sub>2</sub>	Pd <sub>3</sub> Y-L1 <sub>2</sub>
Au-Cd	$\beta'$ AuCd-B19	AuCd-B19	Pd-Zr	PdZr <sub>2</sub> -C11 <sub>b</sub>	PdZr <sub>2</sub> -C11 <sub>b</sub>
Au-Cd	$\beta$ AuCd-B2 (high T)	AuCd-B2	Pd-Zr	PdZr-B33	PdZr-B33
Au-Nb	Au <sub>2</sub> Nb-C32	Au <sub>2</sub> Nb-C32 (paw-gga)	Pd-Zr	Pd <sub>2</sub> Zr-C11 <sub>b</sub>	Pd <sub>2</sub> Zr-C11 <sub>b</sub> /tie-line (paw-gga)
Au-Sc	Au <sub>4</sub> Sc-D1 <sub><math>\alpha</math></sub>	Au <sub>4</sub> Sc-D1 <sub><math>\alpha</math></sub>	Pd-Zr	Pd <sub>3</sub> Zr-D0 <sub>24</sub>	Pd <sub>3</sub> Zr-D0 <sub>24</sub>
Au-Sc	Au <sub>2</sub> Sc-C11 <sub>b</sub>	Au <sub>2</sub> Sc-C11 <sub>b</sub> /MoPt <sub>2</sub>	Pt-Ti	Pt <sub>3</sub> Ti-D0 <sub>24</sub>	Pt <sub>3</sub> Ti-D0 <sub>24</sub>
Au-Sc	AuSc-B2	AuSc-B2/B19	Pt-Ti	$\alpha$ PtTi-B19	PtTi-B19
Au-Ti	Au <sub>4</sub> Ti-D1 <sub><math>\alpha</math></sub>	Au <sub>4</sub> Ti-D1 <sub><math>\alpha</math></sub>	Pt-Ti	PtTi <sub>3</sub> -A15	PtTi <sub>3</sub> -A15
Au-Ti	Au <sub>2</sub> Ti-C11 <sub>b</sub>	Au <sub>2</sub> Ti-C11 <sub>b</sub> /MoPt <sub>2</sub>	Pt-Y	Pt <sub>3</sub> Y <sub>5</sub> -D8 <sub>8</sub>	Pt <sub>3</sub> Y <sub>5</sub> -D8 <sub>8</sub> (paw-gga)
Au-Ti	$\alpha$ AuTi-B11	AuTi-B11	Pt-Y	Pt <sub>3</sub> Y-L1 <sub>2</sub>	Pt <sub>3</sub> Y-L1 <sub>2</sub>
Au-Ti	AuTi <sub>3</sub> -A15	AuTi <sub>3</sub> -A15	Pt-Y	Pt <sub>2</sub> Y-C15	Pt <sub>2</sub> Y-C15
Au-Y	Au <sub>3</sub> Y-D0 <sub><math>\alpha</math></sub>	Au <sub>3</sub> Y-D0 <sub><math>\alpha</math></sub>	Pt-Y	PtY <sub>2</sub> -C37	PtY <sub>2</sub> -C37
Au-Y	Au <sub>2</sub> Y-C11 <sub>b</sub>	Au <sub>2</sub> Y-C11 <sub>b</sub>	Pt-Y	PtY <sub>3</sub> -D0 <sub>11</sub>	PtY <sub>3</sub> -D0 <sub>11</sub>
Au-Zr	Au <sub>3</sub> Zr-D0 <sub><math>\alpha</math></sub>	Au <sub>3</sub> Zr-D0 <sub><math>\alpha</math></sub>	Pt-Zr	Pt <sub>3</sub> Zr-D0 <sub>24</sub>	Pt <sub>3</sub> Zr-D0 <sub>24</sub>
Au-Zr	Au <sub>2</sub> Zr-C11 <sub>b</sub>	Au <sub>2</sub> Zr-C11 <sub>b</sub>	Pt-Zr	PtZr-B33	PtZr-B33
Au-Zr	AuZr <sub>2</sub> -CuZr <sub>2</sub> /C11 <sub>b</sub>	AuZr <sub>2</sub> -CuZr <sub>2</sub> (paw-gga)	Rh-Ti	RhTi <sub>2</sub> -C11 <sub>b</sub> [9]/CuZr <sub>2</sub> [10]	RhTi <sub>2</sub> -C11 <sub>b</sub> /CuZr <sub>2</sub>
Au-Zr	AuZr <sub>3</sub> -A15	AuZr <sub>3</sub> -A15	Rh-Ti	$\alpha$ RhTi-L1 <sub>0</sub>	RhTi-L1 <sub>0</sub>
Cd-Pd	CdPd- $\beta$ <sub>1</sub> -L1 <sub>0</sub>	CdPd-L1 <sub>0</sub>	Rh-Ti	Rh <sub>3</sub> Ti-L1 <sub>2</sub>	Rh <sub>3</sub> Ti-L1 <sub>2</sub>
Cd-Pt	CdPt- $\alpha'$ <sub>1</sub> -L1 <sub>0</sub>	CdPt-L1 <sub>0</sub>	Rh-Y	RhY <sub>3</sub> -D0 <sub>11</sub>	RhY <sub>3</sub> -D0 <sub>11</sub>
Cd-Ti	CdTi <sub>2</sub> -C11 <sub>b</sub>	CdTi <sub>2</sub> -C11 <sub>b</sub>	Rh-Y	RhY-B2	RhY-B2
Cd-Ti	CdTi-B11	CdTi-B11 ( $\gamma$ CuTi)	Rh-Y	Rh <sub>2</sub> Y-C15	Rh <sub>2</sub> Y-C15
Cd-Y	CdY-B2	CdY-B2	Rh-Zr	RhZr <sub>2</sub> -C16	RhZr <sub>2</sub> -C16
Cd-Y	Cd <sub>2</sub> Y-C6	Cd <sub>2</sub> Y-C6	Rh-Zr	$\alpha$ RhZr-B27	RhZr-B27
Cd-Y	Cd <sub>3</sub> Y-Cd <sub>3</sub> Er	Cd <sub>3</sub> Y-Cd <sub>3</sub> Er	Rh-Zr	Rh <sub>3</sub> Zr-L1 <sub>2</sub>	Rh <sub>3</sub> Zr-L1 <sub>2</sub>
Cd-Zr	CdZr <sub>2</sub> -C11 <sub>b</sub>	CdZr <sub>2</sub> -C11 <sub>b</sub>	Ru-Ti	RuTi-B2	RuTi-B2
Cd-Zr	CdZr-B11	CdZr-B11 (paw-gga)	Ru-Y	RuY <sub>3</sub> -D0 <sub>11</sub>	RuY <sub>3</sub> -D0 <sub>11</sub>
Cd-Zr	Cd <sub>3</sub> Zr-L1 <sub>2</sub>	Cd <sub>3</sub> Zr-L1 <sub>2</sub>	Ru-Y	Ru <sub>2</sub> Y-C14	Ru <sub>2</sub> Y-C14
Mo-Pt	MoPt-B19	MoPt-B19	Ru-Zr	RuZr-B2	RuZr-B2
Mo-Pt	MoPt <sub>2</sub>	MoPt <sub>2</sub>	Tc-Ti	TcTi-B2	TcTi-B2
Mo-Rh	MoRh-B19	MoRh-B19	Tc-Y	Tc <sub>2</sub> Y-C14	Tc <sub>2</sub> Y-C14
Mo-Zr	Mo <sub>2</sub> Zr-C15	Mo <sub>2</sub> Zr-C15	Tc-Zr	Tc <sub>2</sub> Zr-C14	Tc <sub>2</sub> Zr-C14
Nb-Pd	NbPd <sub>2</sub> -MoPt <sub>2</sub>	NbPd <sub>2</sub> -MoPt <sub>2</sub>			

TABLE 5: Experimental compounds in agreement with *ab initio* solutions (89 entries).

**B. Experimentally unknown, non-identified or speculated compounds and *ab initio* predictions**

Experimental unknown/speculated compound $\Leftrightarrow$ <i>ab initio</i> compound		
System	Experimental result	<i>Ab initio</i> result
Ag-Cd	$\beta'$ -bcc ordered	AgCd-B2/B19/B27
Ag-Mg	cF* (unknown)	AgMg <sub>3</sub> -D0 <sub>19</sub> (hP8) / D0 <sub>a</sub> (oP8)
Au-Cd	Au <sub>3</sub> Cd- $\alpha_2$ -hP? (unknown)	Au <sub>3</sub> Cd-D0 <sub>24</sub> /D0 <sub>19</sub> /Al <sub>3</sub> Pu
Au-Cd	$\alpha'' \sim$ AuCd (unknown)	AuCd-L1 <sub>0</sub> /FCC <sup>[201]</sup> <sub>A2B2</sub>
Au-Cd	$\epsilon' \sim$ AuCd <sub>3</sub> (unknown)	AuCd <sub>3</sub> -L6 <sub>0</sub>
Au-Pd	Au <sub>3</sub> Pd-L1 <sub>2</sub> (speculated) (wide concentration range)	Au <sub>3</sub> Pd-D0 <sub>23</sub> /D0 <sub>22</sub> /L1 <sub>2</sub> Au <sub>4</sub> Pd-D1 <sub>a</sub> /tie-line
Au-Pd	AuPd (speculated and unknown)	AuPd-FCC <sup>[201]</sup> <sub>A2B2</sub>
Au-Pd	AuPd <sub>3</sub> -L1 <sub>2</sub> (speculated)	AuPd <sub>3</sub> -D0 <sub>23</sub> /D0 <sub>22</sub> /L1 <sub>2</sub> /tie-line
Au-Sc	AuSc <sub>2</sub> -C37 (speculated)	AuSc <sub>2</sub> -C37
Cd-Pd	$\gamma'$ - (unknown)	Cd <sub>3</sub> Pd-D0 <sub>19</sub> /D0 <sub>24</sub> /NbPd <sub>3</sub> /Al <sub>3</sub> Pu
Cd-Pt	$\gamma_1$ - (unknown)	Cd <sub>3</sub> Pt-D0 <sub>11</sub> /D0 <sub>a</sub> /D0 <sub>22</sub>
Cd-Pt	Cd <sub>2</sub> Pt- (unknown)	Cd <sub>2</sub> Pt-C37/C16/tie-line
Cd-Zr	cubic (unknown)	Cd <sub>2</sub> Zr-C11 <sub>b</sub>
Mo-Pd	MoPd <sub>2</sub> $\sim$ MoPt <sub>2</sub>	MoPd <sub>2</sub> -ZrSi <sub>2</sub>
Mo-Rh	MoRh <sub>3</sub> (unknown)	MoRh <sub>3</sub> -CdMg <sub>3</sub>
Nb-Pt	Nb two-phase region <sub>1-x</sub> Pt <sub>1+x</sub> -B19	NbPt-L1 <sub>0</sub>
Pd-Ti	orthorhombic distortion of Pd <sub>2</sub> Ti-C11 <sub>b</sub>	Pd <sub>2</sub> Ti-MoPt <sub>2</sub> (distortion of C11 <sub>b</sub> )
Pd-Y	$\alpha$ PdY (unknown)	PdY-B27
Pt-Ru	PtRu-FCC (unknown)	PtRu-FCC <sup>[001]</sup> <sub>A2B2</sub>
Pt-Y	Pt <sub>5</sub> Y (unknown)	Pt <sub>5</sub> Y-D2 <sub>d</sub> metastable
Tc-Zr	TcZr (unknown)	TcZr-B2

TABLE 6: Experimentally unknown, non-identified or speculated compounds and *ab initio* predictions (21 entries).



C. Experimental solid solutions, two-phases and “not studied” regions and possible *ab initio* predictions

Experimental non-compound $\Leftrightarrow$ <i>ab initio</i> compound		
System	Experimental result	<i>Ab initio</i> result
Ag-Au	short-range order $\gtrsim 950^\circ\text{C}$	Ag <sub>4</sub> Au-D1 <sub>a</sub> /tie-line
Ag-Au	short-range order $\gtrsim 950^\circ\text{C}$	Ag <sub>3</sub> Au-L1 <sub>2</sub> /D0 <sub>23</sub> /Al <sub>3</sub> Pu/NbPd <sub>3</sub> /D0 <sub>22</sub> /D0 <sub>24</sub>
Ag-Au	short-range order $\gtrsim 950^\circ\text{C}$	Ag <sub>2</sub> Au-C37/MoPt <sub>2</sub>
Ag-Au	short-range order $\gtrsim 950^\circ\text{C}$	AgAu-L1 <sub>0</sub>
Ag-Au	short-range order $\gtrsim 950^\circ\text{C}$	AgAu <sub>2</sub> -C37/MoPt <sub>2</sub>
Ag-Au	short-range order $\gtrsim 950^\circ\text{C}$	AgAu <sub>3</sub> -L1 <sub>2</sub> /D0 <sub>22</sub> /D0 <sub>23</sub>
Ag-Cd	fcc solid solution	Ag <sub>3</sub> Cd-D0 <sub>22</sub> /D0 <sub>24</sub>
Ag-Cd	fcc solid solution	Ag <sub>2</sub> Cd-C37
Ag-Cd	none	AgCd <sub>2</sub> -ZrSi <sub>2</sub>
Ag-Cd	hcp solid solution	AgCd <sub>3</sub> -D0 <sub>19</sub>
Ag-Pd	solid solution $\gtrsim 900^\circ\text{C}$	AgPd-L1 <sub>1</sub>
Ag-Pd	solid solution $\gtrsim 900^\circ\text{C}$	Ag <sub>2</sub> Pd-C37
Ag-Pd	solid solution $\gtrsim 900^\circ\text{C}$	Ag <sub>3</sub> Pd- L1 <sub>2</sub> /D0 <sub>22</sub>
Ag-Y	two-phase region above 200°C	AgY <sub>2</sub> -C37/tie-line (uncertain)
Ag-Y	two-phase region above 200°C	Ag <sub>3</sub> Y-D0 <sub>a</sub> (uncertain)
Ag-Zr	two-phase region above 700°C	AgZr <sub>3</sub> -FCC <sub>AB3</sub> <sup>[001]</sup> /tie-line (uncertain)
Ag-Zr	two-phase region above 700°C	Ag <sub>2</sub> Zr-C32
Al-Sc	two-phase region above 0°C	AlSc <sub>3</sub> -D0 <sub>19</sub>
Au-Nb	two-phase region (calculated)	AuNb <sub>2</sub> -BCC <sub>AB2</sub> <sup>[011]</sup>
Au-Pd	solid solution	Au <sub>2</sub> Pd-C49/C37
Au-Ti	two-phase region above 500°C	Au <sub>4</sub> Ti <sub>3</sub> -Cu <sub>4</sub> Ti <sub>3</sub> /tie
Au-Y	not studied	AuY <sub>2</sub> -C37
Au-Zr	two-phase region	Au <sub>4</sub> Zr <sub>3</sub> -Cu <sub>4</sub> Ti <sub>3</sub> (unreliable)
Au-Zr	two-phase region	AuZr-B11/FCC <sub>A2B2</sub> <sup>[001]</sup> (unreliable)
Cd-Pd	Pd phase above 100°C	CdPd <sub>3</sub> -D0 <sub>22</sub> /NbPd <sub>3</sub>
Cd-Pd	two-phase region above 100°C	CdPd <sub>2</sub> -C37
Cd-Rh	not studied	Cd <sub>2</sub> Rh-C37
Cd-Rh	not studied	Cd <sub>3</sub> Rh-Al <sub>3</sub> Pu
Cd-Ti	two-phase region above 200°C	Cu <sub>4</sub> Ti <sub>3</sub> /tie-line
Cd-Y	not studied/two-phase region	CdY <sub>2</sub> -C37
Cd-Zr	not studied/two-phase region	CdZr <sub>3</sub> -A15
Mo-Nb	not studied	MoNb <sub>2</sub> -C11 <sub>b</sub>
Mo-Nb	not studied	MoNb-B2
Mo-Nb	not studied	Mo <sub>2</sub> Nb-C11 <sub>b</sub>
Mo-Nb	not studied	Mo <sub>3</sub> Nb -D0 <sub>3</sub>
Mo-Pd	disorder fcc Pd-A1	MoPd <sub>4</sub> -D1 <sub>a</sub>
Mo-Pt	two-phase region MoPt <sub>2</sub> $\leftrightarrow$ Pt	MoPt <sub>4</sub> -D1 <sub>a</sub>
Mo-Rh	two-phase region above 900°C	Mo <sub>2</sub> Rh-C37
Mo-Ru	disorder hcp Ru-A3 above 800°C	MoRu <sub>3</sub> -D0 <sub>19</sub>
Mo-Ti	not studied/two-phase region above 400°C	MoTi <sub>3</sub> <sup>proto</sup> /tie-line (uncertain), Appendix (XI)
Mo-Ti	not studied/two-phase region above 400°C	MoTi <sub>2</sub> -BCC <sub>AB2</sub> <sup>[211]</sup>
Mo-Ti	not studied/two-phase region above 400°C	MoTi <sup>proto</sup> , Appendix (XI)
Mo-Ti	not studied/two-phase region above 400°C	Mo <sub>2</sub> Ti-C11 <sub>b</sub>
Mo-Ti	not studied/two-phase region above 400°C	Mo <sub>3</sub> Ti <sup>proto</sup> , Appendix (XI)
Mo-Ti	not studied/two-phase region above 400°C	Mo <sub>4</sub> Ti-D1 <sub>a</sub> /tie-line
Mo-Ti	not studied/two-phase region above 400°C	Mo <sub>5</sub> Ti <sup>proto</sup> , Appendix (XII)
Mo-Zr	two-phase region above 400°C	MoZr <sub>5</sub> <sup>proto</sup> /tie-line, Appendix (XII) (uncertain)
Mo-Zr	two-phase region above 400°C	MoZr <sub>3</sub> <sup>proto</sup> /tie-line, Appendix (XII) (uncertain)
Mo-Zr	two-phase region above 400°C	$\sim$ MoTi <sup>proto</sup> (uncertain) ( $\sim 2\text{meV}$ above two-phase reg.)

TABLE 7a: Experimental solid solutions, two-phases and “not studied” regions and possible *ab initio* predictions. The table continues in the next page.

Experimental non-compound $\Leftrightarrow$ <i>ab initio</i> compound		
System	Experimental result	<i>Ab initio</i> result
Nb-Pd	two-phase region above 700°C	Nb <sub>2</sub> Pd-BCC <sub>AB<sub>2</sub></sub> <sup>[011]</sup>
Nb-Ru	disorder Nb-A2	Nb <sub>5</sub> Ru <sup>proto</sup> , Appendix (XII)
Nb-Ru	disorder Nb-A2	Nb <sub>3</sub> Ru-D0 <sub>3</sub>
Nb-Ru	two-phase region above 700°C	NbRu <sub>2</sub> -C37
Nb-Tc	not studied/unknown	Nb <sub>3</sub> Tc <sup>proto</sup> , Appendix (XI)
Nb-Tc	not studied/unknown	Nb <sub>2</sub> Tc-C11 <sub>b</sub>
Nb-Tc	not studied/unknown	NbTc-B2
Pd-Pt	two-phase region Pd $\leftrightarrow$ Pt	Pd <sub>3</sub> Pt <sup>proto</sup> /tie-line (uncertain), Appendix (XI)
Pd-Pt	two-phase region Pd $\leftrightarrow$ Pt	PdPt-L1 <sub>1</sub>
Pd-Pt	two-phase region Pd $\leftrightarrow$ Pt	PdPt <sub>3</sub> <sup>proto</sup> , Appendix (XI)
Pd-Tc	two-phase region above $\sim$ 1000°C	PdTc <sub>3</sub> -D0 <sub>19</sub>
Pd-Y	two-phase region	PdY <sub>2</sub> -C37 (uncertain)
Pd-Zr	two-phase region	PdZr <sub>3</sub> -FCC <sub>AB<sub>3</sub></sub> <sup>[001]</sup> (uncertain)
Pt-Rh	two-phase region Pt $\leftrightarrow$ Rh [9], D1 <sub>a</sub> [262]	Pt <sub>4</sub> Rh-D1 <sub>a</sub>
Pt-Rh	two-phase region Pt $\leftrightarrow$ Rh	Pt <sub>3</sub> Rh-D0 <sub>22</sub>
Pt-Rh	two-phase region Pt $\leftrightarrow$ Rh	PtRh-NbP
Pt-Rh	two-phase region Pt $\leftrightarrow$ Rh	PtRh <sub>2</sub> -C49
Pt-Rh	two-phase region Pt $\leftrightarrow$ Rh	PtRh <sub>3</sub> -D0 <sub>22</sub>
Pt-Rh	two-phase region Pt $\leftrightarrow$ Rh [9], D1 <sub>a</sub> [262]	PtRh <sub>4</sub> -D1 <sub>a</sub>
Pt-Ru	disorder Pt-A1	Pt <sub>3</sub> Ru-FCC <sub>AB<sub>3</sub></sub> <sup>[001]</sup> /tie-line (uncertain)
Pt-Tc	disorder Pt-A1	Pt <sub>3</sub> Tc-FCC <sub>AB<sub>3</sub></sub> <sup>[001]</sup>
Pt-Tc	two-phase region above $\sim$ 1000°C	PtTc <sub>3</sub> -D0 <sub>19</sub>
Pt-Zr	two-phase region above 600°C	PtZr <sub>2</sub> -C16 (uncertain)
Pt-Zr	two-phase region above 600°C	PtZr <sub>3</sub> -A15 (uncertain)
Rh-Ru	solid solution Ru-A3	RhRu <sub>2</sub> <sup>proto</sup>
Rh-Ru	solid solution Ru-A3	RhRu <sup>proto</sup>
Rh-Tc	solid solution Tc-A3	RhTc <sub>3</sub> -D0 <sub>19</sub>
Rh-Tc	solid solution Tc-A3	RhTc-B19
Rh-Tc	two-phase region above 1000°C	Rh <sub>2</sub> Tc <sub>2</sub> -ZrSi <sub>2</sub>
Rh-Ti	two-phase region above 600°C	Rh <sub>2</sub> Ti-C37
Rh-Y	two-phase region above 0°C	RhY <sub>2</sub> -C37 (uncertain)
Rh-Zr	two-phase region above 0°C	RhZr <sub>4</sub> -D1 <sub>a</sub> /tie-line
Rh-Zr	two-phase region above 0°C	RhZr <sub>3</sub> -FCC <sub>AB<sub>3</sub></sub> <sup>[001]</sup> /tie-line
Rh-Zr	two-phase region above 0°C	Rh <sub>2</sub> Zr-C37/tie-line
Ru-Tc	disorder solution (Ru,Tc)-A3	RuTc <sub>3</sub> -D0 <sub>19</sub>
Ru-Tc	disorder solution (Ru,Tc)-A3	RuTc-B19
Ru-Tc	disorder solution (Ru,Tc)-A3	Ru <sub>3</sub> Tc-D0 <sub>19</sub>
Ru-Ti	two-phase region above 600°C	RuTi <sub>3</sub> <sup>proto</sup> , Appendix (XI)
Ru-Ti	two-phase region above 600°C	RuTi <sub>2</sub> -C49
Ru-Y	two-phase region above 0°C	RuY <sub>2</sub> -C16 (uncertain)
Ru-Zr	two-phase region above 400°C	RuZr <sub>4</sub> -D1 <sub>a</sub>
Tc-Ti	disorder $\beta$ Ti-A2	TcTi <sub>3</sub> <sup>proto</sup> , Appendix (XI)
Tc-Ti	disorder $\beta$ Ti-A2	TcTi <sub>2</sub> -C49
Tc-Ti	two-phase region TcTi $\leftrightarrow$ $\chi$	Tc <sub>2</sub> Ti-C11 <sub>b</sub>
Tc-Y	no information	TcY <sub>3</sub> -D0 <sub>11</sub>
Tc-Zr	no information	TcZr <sub>4</sub> -D1 <sub>a</sub>
Tc-Zr	no information	TcZr <sub>2</sub> -C49

TABLE 7b: Experimental solid solutions, two-phases and “not studied” regions and possible *ab initio* predictions (Table 7a + Table 7b = 96 entries). The table starts in the previous page.

#### D. Experimental compounds that could not be checked by our calculations

Experimental compound $\Leftrightarrow$ unavailable compound		
System	Experimental result	<i>Ab initio</i> result
Ag-Mg	AgMg <sub>4</sub> -hP* (unknown)	unknown experimental compound
Ag-Y	Ag <sub>51</sub> Y <sub>14</sub> -Ag <sub>51</sub> Gd <sub>14</sub>	unavailable prototype
Au-Cd	$\eta'$ (unknown)	unknown experimental compound
Au-Cd	$\alpha_1$ Au <sub>3</sub> Cd-Ag <sub>3</sub> Mg	unavailable prototype
Au-Cd	Au <sub>3</sub> Cd <sub>5</sub> -D8 <sub>m</sub>	unknown experimental compound
Au-Nb	Au <sub>2</sub> Nb <sub>3</sub> (unknown)	unknown experimental compound
Au-Ti	$\beta$ AuTi-B19	unavailable prototype off-stoichiometry B19
Au-Y	AuY <sub>3</sub> (unknown)	unknown experimental compound
Au-Zr	Au <sub>4</sub> Zr (oP20 - Pnma)	unavailable prototype
Au-Zr	Au <sub>10</sub> Zr <sub>7</sub> (tI34)	unavailable prototype
Au-Zr	Au <sub>4</sub> Zr <sub>5</sub> (unknown prototype)	unknown experimental compound
Cd-Pd	$\gamma_1$ -(unknown)	unknown experimental compound
Cd-Pd	$\gamma$ -D8 <sub>3</sub>	unavailable prototype
Cd-Pt	$\gamma$ -(unknown)	unknown experimental compound
Cd-Pt	$\gamma_2$ -(unknown)	unknown experimental compound
Cd-Y	Cd <sub>45</sub> Y <sub>11</sub> -Cd <sub>45</sub> Sm <sub>11</sub>	unavailable prototype
Cd-Y	Cd <sub>58</sub> Y <sub>13</sub> -Pu <sub>13</sub> Zn <sub>58</sub>	unavailable prototype
Cd-Y	Cd <sub>6</sub> Y	unavailable prototype
Mo-Pt	$\epsilon'$ -D0 <sub>19</sub> above 1000°C	unavailable prototype off-stoichiometry D0 <sub>19</sub>
Nb-Pt	D8 <sub>b</sub>	unavailable prototype $\sigma$ phase
Nb-Rh	$\sigma$ (Nb <sub>13</sub> Rh <sub>7</sub> )-D8 <sub>b</sub>	unavailable prototype
Nb-Rh	$\xi$ (Nb <sub>2</sub> Rh <sub>3</sub> )-Nb <sub>2</sub> Rh <sub>3</sub>	unavailable prototype
Nb-Tc	NbTc <sub>3</sub> ,Nb <sub>0.15</sub> Tc <sub>0.85</sub> - $\alpha$ Mn	unavailable prototype
Pd-Ti	Pd <sub>3</sub> Ti <sub>2</sub> $\sim$ Au <sub>2</sub> V	unavailable prototype
Pd-Ti	Pd <sub>5</sub> Ti <sub>3</sub> $\sim$ C11 <sub>b</sub>	unavailable prototype
Pd-Y	unknown at 66.6% Pd	unknown experimental compound
Pd-Y	unknown at 87.5% Pd	unknown experimental compound
Pd-Y	Pd <sub>2</sub> Y <sub>5</sub> (unknown)	unknown experimental compound
Pd-Y	Pd <sub>2</sub> Y <sub>3</sub> -hR15 (unknown)	unknown experimental compound
Pd-Y	Pd <sub>4</sub> Y <sub>3</sub> -hR14 (unknown)	unknown experimental compound
Pd-Y	$\alpha$ Pd <sub>3</sub> Y <sub>2</sub> (unknown)	unknown experimental compound
Pt-Ti	Pt <sub>8</sub> Ti-D1 <sub><math>\alpha</math></sub>	unavailable prototype off-stoichiometry D1 <sub><math>\alpha</math></sub>
Pt-Ti	Pt <sub>2</sub> Ti-ReSi <sub>2</sub>	unavailable prototype
Pt-Y	Pt <sub>4</sub> Y <sub>3</sub> -Pd <sub>4</sub> Pu <sub>3</sub>	unavailable prototype
Pt-Y	Pt <sub>4</sub> Y <sub>5</sub> -Pu <sub>5</sub> Rh <sub>4</sub>	unavailable prototype
Pt-Y	Pt <sub>3</sub> Y <sub>7</sub> -D10 <sub>2</sub>	unavailable prototype
Rh-Ti	Rh <sub>5</sub> Ti (unknown)	unknown experimental compound
Rh-Ti	Rh <sub>5</sub> Ti <sub>3</sub> -Ge <sub>3</sub> Rh <sub>5</sub>	unavailable prototype
Rh-Y	Rh <sub>3</sub> Y (unknown), hP24-P6 <sub>3</sub> /mmc	unknown experimental compound
Rh-Y	Rh <sub>3</sub> Y <sub>7</sub> -D10 <sub>2</sub>	unavailable prototype
Rh-Y	Rh <sub>3</sub> Y <sub>5</sub> (unknown)	unknown experimental compound
Rh-Y	Rh <sub>2</sub> Y <sub>3</sub> (unknown), tI140-I4/mcm	unknown experimental compound
Rh-Zr	Rh <sub>4</sub> Zr <sub>3</sub> (unknown)	unknown experimental compound
Rh-Zr	Rh <sub>5</sub> Zr <sub>3</sub> -Pd <sub>3</sub> Pu <sub>3</sub>	unavailable prototype
Ru-Y	Ru <sub>2</sub> Y <sub>5</sub> -C <sub>2</sub> Mn <sub>5</sub>	unavailable prototype
Ru-Y	Ru <sub>25</sub> Y <sub>44</sub> (unknown)	unknown experimental compound
Tc-Ti	$\chi$ -A12	unavailable prototype
Tc-Zr	Tc <sub>6</sub> Zr-A12	unavailable prototype

TABLE 8: Experimental compounds that could not be checked by our calculations, because the proper structure prototype or concentration is not known or not in our library. The table contains 21 “*unknown experimental compounds*” and 27 “*unavailable prototypes*” (48 entries total).

### E. Experimental compounds in disagreement with other *ab initio* compounds or two-phase regions

Experimental compound $\Leftrightarrow$ <i>ab initio</i> wrong compound or two-phases					
System	Experimental result	<i>Ab initio</i> result	$\Delta E_f$ (us-lda) (meV/atom)	$\Delta E_f$ (paw-gga) (meV/atom)	Note
Au-Nb	AuNb <sub>3</sub> -A15	two-phase region	7	6.5	(a)
Au-Y	AuY-B2 [170]	AuY-B33	26	25	(b)
Cd-Nb	Cd <sub>3</sub> Nb-L1 <sub>2</sub>	immiscible system	70	>100	(c)
Cd-Pt	CdPt <sub>3</sub> - $\alpha'$ -L1 <sub>2</sub> [181]	CdPt <sub>3</sub> <sup>proto</sup> , Appendix (XI)	25	10.4	(b)
Nb-Rh	$\kappa$ (NbRh <sub>3</sub> )-L1 <sub>2</sub>	NbRh <sub>3</sub> -Al <sub>3</sub> Pu	8	5.3	(a)
Nb-Ru	NbRu <sub>3</sub> -L1 <sub>2</sub>	NbRu <sub>3</sub> -D0 <sub>24</sub>	8	2.5	(a)
Nb-Ru	NbRu'-L1 <sub>0</sub>	two-phase region	20	4	(a)
Pt-Y	PtY-B27	PtY-B33	50	60	(c)
Pt-Zr	Pt <sub>3</sub> Zr <sub>5</sub> -D8 <sub>8</sub>	two-phase region	36	23	(c)

TABLE 9: Experimental compounds (which we have in the library as prototypes) in disagreement with other *ab initio* compounds or two-phase regions. We include the differences between the formation energies of the phases in disagreement, both for US-LDA and PAW-GGA potentials. (9 entries). Note **(a)**: the *ab initio* ground state is within less than 10meV/atom of the experimental ground state (4). Note **(b)**: the assigned experimental structures are poorly justified (2) [170,181]. Note **(c)**: unambiguous significant disagreement (3).

## XI. APPENDIX: NEW STRUCTURE PROTOTYPES WHICH ARE SUPERSTRUCTURES OF FCC, BCC, HCP

System	CdPt <sub>3</sub> , PdPt <sub>3</sub> , Pd <sub>3</sub> Pt	MoTi,	MoTi <sub>3</sub> , Mo <sub>3</sub> Ti, Nb <sub>3</sub> Tc, RuTi <sub>3</sub> , TcTi <sub>3</sub>	RhRu	RhRu <sub>2</sub>
Superlattice	FCC AB <sub>3</sub>	BCC A <sub>2</sub> B <sub>2</sub>	BCC AB <sub>3</sub>	HCP A <sub>2</sub> B <sub>2</sub>	HCP A <sub>2</sub> B <sub>4</sub>
Lattice	Orthorhombic	Orthorhombic	Orthorhombic	Trigonal	Orthorhombic
Space Group	Cmmm #65	Imma #74	Immm #71	P3m1 #164	Cmcm #63
Pearson symbol	oC8	oI8	oI8	hP4	oC12
Primitive vectors (cart.)					
$\mathbf{a}_1/a$	(1, -1/2, 1/2)	(3/2, 1/2, -1/2)	(3/2, 1/2, -1/2)	(1/2, - $\sqrt{3}/2$ , 0)	(-1/2, 3 $\sqrt{3}/2$ , 0)
$\mathbf{a}_2/a$	(-1, -1/2, 1/2)	(1/2, 3/2, 1/2)	(1/2, 3/2, 1/2)	(1/2, $\sqrt{3}/2$ , 0)	(-1/2, -3 $\sqrt{3}/2$ , 0)
$\mathbf{a}_3/a$	(0 - 1/2, -1/2)	(-1/2, -3/2, 1/2)	(-1/2, -3/2, 1/2)	(0, 0, 2 $\sqrt{8}/3$ )	(0, 0, $\sqrt{8}/3$ )
Atomic positions (fract.)					
<b>A1</b>	(0, 0, 0)	(0, 0, 0)	(0, 0, 0)	(0, 0, 0)	(0, 0, 0)
<b>A2</b>	-	(1/4, 3/4, 1/2)	-	(1/3, 2/3, 1/4)	(5/9, 4/9, 1/2)
<b>B1</b>	(0, 1/2, 1/2)	(1/2, 1/2, 0)	(1/4, 3/4, 1/2)	(0, 0, 1/2)	(2/9, 7/9, 1/2)
<b>B2</b>	(1/2, 0, 1/2)	(3/4, 1/4, 1/2)	(1/2, 1/2, 0)	(1/3, 2/3, 3/4)	(1/3, 2/3, 0)
<b>B3</b>	(1/2, 1/2, 0)	-	(3/4, 1/4, 1/2)	-	(2/3, 1/3, 0)
<b>B4</b>	-	-	-	-	(8/9, 1/9, 1/2)

TABLE 10. Geometry of FCC, BCC, HCP superstructures which appear as new prototypes in our study. Positions are given as unrelaxed positions in the parent lattice.

## XII. APPENDIX: RELAXED STRUCTURE PROTOTYPES

System	MoZr <sub>3</sub> (AB <sub>3</sub> )	Mo <sub>5</sub> Ti* (AB <sub>5</sub> )	MoZr <sub>5</sub> * (AB <sub>5</sub> )	Nb <sub>5</sub> Ru* (AB <sub>5</sub> )
Lattice	Orthorhombic	Monoclinic	Monoclinic	Monoclinic
Space Group	Imma #74	C2/m #12	C2/m #12	C2/m #12
Prototype	MoZr <sub>3</sub>	Mo <sub>5</sub> Ti see note*	Mo <sub>5</sub> Ti see note*	Mo <sub>5</sub> Ti see note*
Primitive vectors				
( $a, b, c$ ) (Å)	(5.678, 5.678, 5.678)	(5.192, 5.192, 9.879)	(5.695, 5.695, 10.881)	(5.339, 5.339, 10.178)
( $\alpha, \beta, \gamma$ ) degrees	(145.5, 128.9, 63.1)	(139.8, 139.8, 35.0)	(138.5, 138.5, 34.1)	(139.8, 139.8, 35.1)
Atomic positions (fract.)				
<b>A1</b>	(0, 0, 0)	(0, 0, 0)	(0, 0, 0)	(0, 0, 0)
<b>B1</b>	(0.259, 0.722, 0.537)	(0.166, 0.166, 0.833)	(0.205, 0.205, 0.864)	(0.170, 0.170, 0.836)
<b>B2</b>	(0.524, 0.500, 0.024)	(0.334, 0.334, 0.665)	(0.349, 0.349, 0.692)	(0.335, 0.335, 0.672)
<b>B3</b>	(0.815, 0.278, 0.537)	(0.500, 0.500, 0.499)	(0.495, 0.495, 0.513)	(0.501, 0.501, 0.500)
<b>B4</b>	-	(0.667, 0.667, 0.334)	(0.642, 0.642, 0.313)	(0.666, 0.666, 0.328)
<b>B5</b>	-	(0.834, 0.834, 0.166)	(0.800, 0.800, 0.160)	(0.831, 0.831, 0.164)

TABLE 11. Geometry of relaxed structures which appear as new prototypes in our study. Positions are given as fractional positions of the primitive vectors. Note \*: Mo<sub>5</sub>Ti, MoZr<sub>5</sub>, and Nb<sub>5</sub>Ru are slight distortion of the prototype Mo<sub>5</sub>Ti<sup>proto</sup>, monoclinic lattice, space group C2/m #12, with atoms in the following Wyckoff positions: Ti in 2a, Mo(1) in 2c, Mo(2) in 4i ( $x = 1/3, z = 1/6$ ), Mo(3) in 4i ( $x = 2/3, z = 1/3$ ), and primitive vectors  $\mathbf{a}_1/a = (3.171, 1, 0)$ ,  $\mathbf{a}_2/a = (-0.315, 1, 0)$ ,  $\mathbf{a}_3/a = (-0.638, -0.201, 1.987)$  [17].

## REFERENCES

---

- [1] D. de Fontaine, in *Solid State Physics*, edited by H. Ehrenreich and D. Turnbull (Academic Press 1994), Vol. 47, pp. 33-176.
- [2] M. Sluiter, P. Turchi, F. Zezhong, and D. de Fontaine, *Tight Binding Calculation of Ti-Rh-Type Phase Diagram*, Phys. Rev. Lett. **60**, 716 (1988).
- [3] S. Curtarolo, D. Morgan, K. Persson, J. Rodgers, and G. Ceder, Phys. Rev. Lett. **91**, 135503 (2003).
- [4] S. Curtarolo, H. Cocks, and A. N. Kolmogorov, *High-Throughput ab initio analysis of the Bi-Mg, Bi-In, In-Mg, Mg-Sb, In-Sb, and Bi-Sb systems*, submitted (2005).
- [5] S. Curtarolo and A. N. Kolmogorov, *Prediction of possible metastable alloy phases in the Mg-B system*, internal report (2004).
- [6] D. Morgan, G. Ceder, and S. Curtarolo, Mat. Res. Soc. Symp. Proc. **804**, JJ9.25 (2004).
- [7] D. Morgan, G. Ceder, and S. Curtarolo, J. Measurement Science & Technology, Special Feature Combinatorial and High-Throughput Materials Research, Meas. Sci. Technol. **16**, 296-301 (2005).
- [8] Y. Wang, S. Curtarolo, C. Jiang, R. Arroyave, T. Wang, G. Ceder, L.-Q. Chen, and Z.-K. Liu, Calphad **28**, 79 (2004).
- [9] *Binary Alloy Phase Diagrams*, edited by T. B. Massalski (ASM International, Metals Park, OH, 1992)
- [10] P. Villars, K. Cenzual, J. L. C. Daams, F. Hulliger, T. B. Massalski, H. Okamoto, K. Osaki, A. Prince, and S. Iwata, Crystal Impact, *Pauling File. Inorganic Materials Database and Design System*, Binaries Edition, ASM International, Metal Park, OH (2003)
- [11] P. S. White, J. R. Rodgers, and Y. Le Page, CRYSTMET: a database of the structures and powder patterns of metals and intermetallics, Acta Cryst. B **58**, 343 (2002).
- [12] J. M. Sanchez and D. de Fontaine, *Theoretical Prediction of Ordered Superstructures in Metallic Alloys*, in "Structure and Bonding in Crystals", Vol. II, Academic Press (1981).
- [13] Z. W. Lu, S.-H. Wei, A. Zunger, S. Frota-Pessoa, and L. G. Ferreira, Phys. Rev. B **44**, 512 (1991).
- [14] C. Wolverton and A. Zunger, Phys. Rev. B **50**, 10548 (1994).
- [15] S. Curtarolo, *Coarse-Graining and Data Mining Approaches to the Prediction of Structures and their Dynamics*, Ph.D. Thesis, MIT (2003).  
Download: burgaz.mit.edu and alpha.mems.duke.edu
- [16] Appendix B, pp. 196-210 of reference [15].
- [17] *International Table of Crystallography*, edited by T. Hahn, (Kluwer Academic Publishers, 2002)
- [18] J. P. Perdew and A. Zunger, Phys. Rev. B **23**, 5048 (1981).
- [19] D. Vanderbilt, Phys. Rev. B **41**, 7892 (1990).
- [20] G. Kresse and J. Furthmuller, Comput. Mater. Sci. **6**, 15 (1996).
- [21] H. J. Monkhorst and J. D. Pack, Phys. Rev. B **13**, 5188 (1976).
- [22] H. J. Monkhorst and J. D. Pack, Phys. Rev. B **16**, 1748 (1977).
- [23] P. E. Blöchl, Phys. Rev. B **50**, 17953 (1994).
- [24] G. Kresse and D. Joubert, Phys. Rev. B **59**, 1758 (1999).
- [25] J. P. Perdew and Y. Wang, Phys. Rev. B **45**, 13244 (1992).
- [26] J. B. Neaton and N. W. Ashcroft, Phys. Rev. Lett. **86**, 2830 (2001).
- [27] A. K. McMahan and J. A. Moriarty, Phys. Rev. B **27**, 3235 (1983).
- [28] J. E. Jaffe, Z. Lin, and A. C. Hess, Phys. Rev. B **57**, 11834 (1998).
- [29] M. M. Dacorogna and M. L. Cohen, Phys. Rev. B **34**, 4996 (1986).
- [30] M. I. Katsnelson, G. V. Sinko, N. A. Smirnov, A. V. Trefilov, and K. Yu. Khromov, Phys. Rev. B **61**, 14420 (2000).
- [31] C. S. Barrett and O. R. Trautz, Trans. Am. Inst. Min. Metall. Pet. Eng. **175**, 579 (1948).
- [32] S. Barrett, Acta Crystallogr. **9**, 671 (1956).
- [33] A. W. Overhauser, Phys. Rev. Lett. **53**, 64 (1984).
- [34] G. Ernst, C. Artner, O. Blaschko, and G. Krexner, Phys. Rev. B **33**, 6465 (1986).
- [35] H. G. Smith, R. Berliner, J. D. Jorgensen, M. Nielsen, and J. Trivisonno, Phys. Rev. B **41**, 1231 (1990).
- [36] W. Schwarz and O. Blaschko, Phys. Rev. Lett. **65**, 3144 (1990).
- [37] W. Schwarz, O. Blaschko, and I. Gorgas, Phys. Rev. B **44**, 6785 (1991).
- [38] O. Blaschko, V. Dmitriev, G. Krexner, P. Tolédano, Phys. Rev. B **59**, 9095 (1999).
- [39] L. Vegard, Z. Phys. **5**, 17 (1921).
- [40] The reference CPU is Compaq/HP - Alpha 21264 EV67 667MHz.
- [41] M. Hansen and K. Anderko, *Constitution of Binary Alloys*, McGraw-Hill, New-York (1958).
- [42] W. B. Pearson, *Handbook of Lattice Spacings and Structures of Metals and Alloys*, Metals Park, Oh: American Society for Metals (1985).
- [43] W. G. Moffatt, Ed., *Handbook of Binary Phase Diagrams*, Business Growth Services, General Electric Co., Schenectady, NY (1976).
- [44] F. A. Shunk, *Constitution of Binary Alloys, Second Supplement*, McGraw-Hill, New-York; General Electric Co., Business Growth Services, Schenectady, New York (1969).
- [45] M. Venkatraman, J. P. Neumann, *Phase Diagrams of Binary Titanium Magnesium*, ASM International (1988).
- [46] L. Brewer, *Molybdenum: Physico-Chemical Properties of its Compounds and Alloys*, edited by O. Kubaschewski, Atomic Energy Review Special Issue No. 7, International Atomic Energy Agency, Vienna (1980).
- [47] V. I. Lavrentev, Ya. I. Gerassimov, P. Feschotte, D.

- T. Livey, O. von Goldbeck, H. Nowotny, K. Seifert, R. Ferro, A. L. Dragoo, *Niobium: Physico-Chemical Properties of its Compounds and Alloys*, edited by O. Kubaschewski, Atomic Energy Review Special Issue No. 2, International Atomic Energy Agency, Vienna (1968).
- [48] J. L. Murray, *Phase Diagrams of Binary Titanium Alloys*, ASM International (1987).
- [49] C. B. Alcock, K. T. Jacob, S. Zador, O. von Goldbeck, H. Nowotny, K. Seifert, O. Kubaschewski, *Zirconium: Physico-Chemical Properties of its Compounds and Alloys*, edited by O. Kubaschewski, Atomic Energy Review Special Issue No. 6, International Atomic Energy Agency, Vienna (1976).
- [50] D. R. Lide (editor), *CRC Handbook of Chemistry and Physics*, CRC Press Inc., Cleveland, OH (2003).
- [51] L. Kaufman, *Calphad* **14**, 163 (1990).
- [52] C. Wagner, *Acta Metall.* **2**(2), 242 (1954).
- [53] J. L. White, R. L. Orr, and R. Hultgren, *Acta Metall.* **5**(12), 747 (1957).
- [54] J. L. White, *Trans. AIME* **215**(1), 178 (1959).
- [55] C. J. Cooke and W. Hume-Rothery, *Acta Metall.* **9**(10), 982 (1961).
- [56] S.-H. Wei, A. A. Mbaye, L. G. Ferreira, and A. Zunger, *Phys. Rev. B* **36**, 4163 (1987).
- [57] T. Mohri, K. Terakura, T. Oguchi, and K. Watanabe, *Acta Metall.* **36**, 547 (1988).
- [58] R. A. Johnson, *Phys. Rev. B* **41**, 9717 (1990).
- [59] T. Mohri, K. Terakura, S. Takizawa, and J. M. Sanchez, *Acta Metall. Mater.* **39**, 493 (1991).
- [60] T. Mohri, S. Takizawa, and K. Terakura, *J. Physics: Cond. Matt.* **5**, 1473 (1993).
- [61] Z. W. Lu, B. M. Klein, and A. Zunger, *Superlattice Microst.* **18**, 161 (1995).
- [62] Z. W. Lu, B. M. Klein, and A. Zunger, *J. Phase Equilib.* **16**, 36 (1995).
- [63] Z. W. Lu, B. M. Klein, and A. Zunger, *Model. Simul. Mater. Sc.* **3**, 753 (1995).
- [64] V. Ozolins, C. Wolverton, and A. Zunger, *Phys. Rev. B* **57**, 4816 (1998).
- [65] V. Ozolins, C. Wolverton, and A. Zunger, *Phys. Rev. B* **57**, 6427 (1998).
- [66] A. Zunger, L. G. Wang, G. L. W. Hart, and M. Sanati, *Model. Simul. Mater. Sc.* **10**, 685 (2002).
- [67] A. Tonejc, A. M. Tonejc, and A. Bonfacic, *Phys. Lett. A* **49**, 145 (1974).
- [68] O. S. Zarechnyuk and V. V. Kinzhbalo, *Russ. Metall.* **6**, 153 (1978).
- [69] Y. Matsuo, S. Minamigawa, and K. Katada, *Scripta Metall.* **12**, 821 (1978).
- [70] Y. Matsuo, T. Makita, T. Suzuki, and A. Nagasawa, *J. Phys. Soc. Japan* **50**, 1209 (1981).
- [71] W. Hume-Rothery and E. Butchers, *J. Inst. Met.* **60**, 345 (1937).
- [72] R. J. M. Payne and J. L. Haughton, *J. Inst. Met.* **60**, 351 (1937).
- [73] K. Schubert, B. Kiefer, M. Wilkens, and R. Haufler, *Z. Metallkd.* **46**, 1692 (1955).
- [74] K. Fujiwara, M. Hirabayashi, D. Watanabe, and S. Ogawa, *J. Phys. Soc. Japan* **13**, 167 (1958).
- [75] M. V. Prokof'ev and V. E. Kolesnichenko, *Inorg. Mater.* **21**(8), 1168 (1985).
- [76] J. Kulik, S. Takeda, and D. de Fontaine, *Acta Metall.* **35**(5), 1137 (1987).
- [77] V. E. Kolesnichenko, V. V. Karonik, S. N. Tsyganova, T. A. Kupriyanova, and L. N. Syssoeva, *Russ. Metall.* (5) 199 (1988).
- [78] Y. Liu, R. G. Jordan, and S. L. Qiu, *Phys. Rev. B* **49**, 4478 (1994).
- [79] O. I. Velikokhatnyi, S. V. Eremeev, I. I. Naumov, and A. I. Potekaev *J. Physics: Cond. Matt.* **12**, 8825 (2000).
- [80] N. M. Rosengaard and H. L. Skriver, *Phys. Rev. B* **49**, 14666 (1994).
- [81] F. V. Linen, *Trans. Metall. Soc. AIME* **175**, 878 (1948).
- [82] X. D. Dai, H. R. Gong, and B. X. Liu, *J. Phys. Soc. Jpn.* **73**, 1222 (2004).
- [83] G. J. Lamprecht and P. Crowther, *Trans. AIME* **242**, 2169 (1968).
- [84] J. R. Weeks, *Trans. ASM* **62**, 304 (1969).
- [85] M. W. Chase, *Bull. Alloy Phase Diagrams* **4**, 124 (1983).
- [86] R. Kieffer, H. Nowotny, *Metallwissenschaft Technick* **17**, 669 (1963).
- [87] M. R. Baren, *Bull. Alloy Phase Diagrams* **10**(6) (1989).
- [88] I. Karakaya, and W. T. Thompson, *Bull. Alloy Phase Diagrams* **9** (3) (1988).
- [89] N. V. Skorodumova, S. I. Simak, E. A. Smirnova, and Yu. Kh. Vekilov, *Phys. Lett. A* **208**, 157-60 (1995).
- [90] E. Bruno, B. Ginatempo, E. S. Giuliano, A. V. Ruban, and Yu. Kh. Vekilov, *Phys. Rep.* **249**, 353 (1994).
- [91] E. Bruno, B. Ginatempo, and E. S. Giuliano, *Phys. Rev. B* **52**, 14544 (1995).
- [92] E. Bruno, B. Ginatempo, and E. S. Giuliano, *Nuovo Cimento D* **20D**, 1367-76 (1998).
- [93] W. Olovsson, I. A. Abrikosova, and B. Johansson, *J. Electron Spectrosc. Relat. Phenom.* **127**, 65-9 (2002).
- [94] A. A. Rudnitskii and A. N. Khotinskaya, *Russ. J. Inorg. Chem.* **4**, 1053 (1959).
- [95] I. Barin, O. Knacke, and O. Kubaschewski, *Thermodynamical Properties of Inorganic Substances (Supplement)*, 590, Springer-Verlag, Berlin (1977).
- [96] I. Karakaya and W. T. Thompson, *Bull. Alloy Phase Diagrams* **7**(4), 259 (1986).
- [97] A. A. Rudnitskii and O. A. Novikova, *Russ. J. Inorg. Chem.* **4**, 719 (1959).
- [98] J. H. Li, L. T. Kong, and B. X. Liu, *J. Phys. Chem. B* **108**, 16071-16076 (2004).
- [99] B. B. Gulyaev and G. F. Dvorshkaya, in *Phase Diagrams of Metallic Systems*, E. M. Savitskii, Ed., Nauka Pub., Moscow, 267 (1968).
- [100] V. N. Emerenko, Y. I. Buyanov, and N. M. Panchenko, *Sov. Powder Metall. Met. Cer.* **8**(7), 562 (1969).
- [101] M. R. Plichta and H. I. Aaronson, *Acta Metall.* **26**, 1293 (1978).
- [102] E. Gebhardt, M. von Erdberg, and U. Lüty, *Nucl. Met.* **10**, 303 (1964).
- [103] K. A. Gschneidner, O. D. McMasters, D. G. Alexander, and R. F. Venteicher, *Metall. Trans.* **1**, 1961 (1970).
- [104] O. D. McMasters, K. A. Gschneidner, and R. F. Venteicher, *Acta Crystallogr.* **B26** 1224 (1970).

- [105] I. Barin, O. Knacke, and O. Kubaschewski, *Thermochemical Properties of Inorganic Substances*, Springer-Verlag, Berlin (1977).
- [106] I. Karakaya and W. T. Thompson, *Bull. Alloy Phase Diagrams* **8**(4), 326 (1987).
- [107] O. P. Naumkin, V. F. Terekhova, and E. M. Savitskii, *Russ. Metall.* (4) 176 (1965).
- [108] M. E. Drits, E. S. Kadaner, T. V. Dobatkina, and N. I. Turkina, *Russ. Metall.* (4) 152 (1973).
- [109] S. Fujikawa, M. Sugaya, H. Takei, and K. Hirano, *J. Less-Common Met.* **63**, 87 (1979).
- [110] H. Anton and P. C. Schmidt, *Intermetallics* **5**, 449-65 (1997).
- [111] M. Asta, S. M. Foiles, and A. A. Quong, *Phys. Rev. B* **57**, 11265 (1998).
- [112] M. Asta and V. Ozolins, *Phys. Rev. B* **64**, 094104 (2001).
- [113] V. Ozolins and M. Asta, *Phys. Rev. Lett.* **86**, 448 (2001).
- [114] B. Mayer, H. Anton, E. Bott, M. Methfessel, J. Sticht, J. Harris, and P. C. Schmidt, *P.C. Intermetallics* **11**, 23-32 (2003).
- [115] E. Clouet, M. Nastar, and C. Sigli, *Phys. Rev. B* **69**, 64109 (2004).
- [116] H. Okamoto and T. B. Massalski, *Bull. Alloy Phase Diagrams* **5**(4) (1984).
- [117] H. Okamoto and T. B. Massalski, *Bull. Alloy Phase Diagrams* **6**(1) (1985).
- [118] T. B. Massalski, H. Okamoto, and L. Brewer, *Bull. Alloy Phase Diagrams* **7**(5) (1986).
- [119] T. B. Massalski, H. Okamoto, and L. Brewer, in *Phase Diagrams of Binary Gold Alloys*, ASM International (1987).
- [120] L. Dreibholz, *Z. Phys. Chem.* **108**, 1 (1924).
- [121] G. A. Geach and E. Summersmith, *J. Inst. Met.* **82**, 471 (1953).
- [122] J. A. Rodriguez and M. Kuhn, *Surf. Sci.* **330**, L657-64 (1995).
- [123] H. Hirabayashi and S. Ogawa, *Acta Metall.* **9**(4), 264 (1961).
- [124] J. D. Filby and J. N. Pratt, *Trans. Faraday Soc.* **60**, 1934 (1964).
- [125] M. Hirabayashi, K. Hiraga, S. Yamaguchi, and N. Ino, *J. Phys. Soc. Jpn.* **27**(1), 80 (1969).
- [126] K. L. Komarek, E. Reiffenstein, and G. Stummerer, *Monatsh. Chem.* **104**(6), 1570 (1973).
- [127] E. A. Wood and B. T. Matthias, *Acta Crystallogr.* **9**, 534 (1956).
- [128] A. E. Dwight, *Metall. Soc. Conf. Proc.* **10**, 383 (1961).
- [129] R. Flükiger, P. Spitzli, F. Helmiger, and J. Muller, *Phys. Lett. A* **29**, 407 (1969).
- [130] M. Bernasson, P. Descouts, R. Flükiger, and A. Trevaud, *Solid State Comm.* **8**, 837 (1970).
- [131] E. Ehrenfreund, A. C. Gossard, and J. H. Wernick, *Solid State Comm.* **8**, 1925 (1970).
- [132] E. Röschel, C. J. Raub, and O. Loebich, Jr., *Z. Metallkd.* **64**(5), 359 (1973).
- [133] H. R. Khan, E. Röschel, and C. J. Raub, *Z. Physik* **262**, 279 (1973).
- [134] E. Z. Kurmaev, F. Werfel, O. Brümmer, and R. Flükiger, *Solid State Comm.* **21**, 239 (1977).
- [135] R. Flükiger, S. Foner, E. J. McNiff Jr., and O. Fischer, *Solid State Comm.* **30**, 723 (1979).
- [136] M. S. Wire and G. W. Webb, *J. Phys. Chem. Solids* **42**, 233 (1981).
- [137] N. Savvides, C. M. Hurd, and S. P. McAlister, *Solid State Comm.* **41**, 735 (1982).
- [138] M. S. Wire, G. W. Webb, D. E. Cox, C. L. Snead Jr., and A. R. Sweedler, *Solid State Comm.* **48**, 125 (1983).
- [139] S. Ramakrishnan, G. Chandra, and M. C. Saxena, *Physica B & C* **141**, 185 (1986).
- [140] L. M. Di and H. Bakker, *J. Phys. Cond. Matt.* **3**, 9319 (1991).
- [141] M. Baier, R. Wordel, F. E. Wagner, T. E. Antonova, aV. E. Antonov, *J. Less-Common Met.* **172/174**, 358 (1991).
- [142] R. Ruer, *Z. Anorg. Chem.* **51**, 391 (1906).
- [143] A. Nagasawa, Y. Matsuo, and J. Kakinoki, *J. Phys. Soc. Jpn.* **20**(10), 1881 (1965).
- [144] Y. Matsuo, A. Nagasawa, and J. Kakinoki, *J. Phys. Soc. Jpn.* **21**(12), 2633 (1966).
- [145] Y. Kawasaki, S. Ino, and S. Ogawa, *J. Phys. Soc. Jpn.* **30**(6), 1758 (1971).
- [146] F. Doerinckel, *Z. Anorg. Allg. Chem.* **34**, 333 (1907).
- [147] C. H. Johansson and J. O. Linde, *Ann. Phys.* **5**(6), 762 (1930).
- [148] A. S. Darling, R. A. Mintern, and J. C. Chaston, *J. Inst. Met.* **81**, 125 (1952-1953).
- [149] A. A. Rudnitskii and A. N. Khotinskaya, *Zh. Neorg. Khim.* **4**, 2518 (1959); TR: *Russ. J. Inorg. Chem.* **4**, 1160 (1969).
- [150] E. Raub and G. Falkenburgh, *Z. Metallkd.* **55**(7), 392 (1964).
- [151] A. A. Rudnitskii and A. N. Khotinskaya, *Zh. Neorg. Khim.* **4**, 1601 (1959); TR: *Russ. J. Inorg. Chem.* **4**, 722 (1969).
- [152] M. Kuhn, J. A. Rodriguez, J. Hrbek, A. Bzowski, and T. K. Sham, *Surf. Sci.* **341**, L1011-18 (1995).
- [153] A. T. Aldred, *Trans. AIME* **224**, 1082 (1962).
- [154] H. Reule, S. Steeb, and C. Donolato, *J. Less-Common Met.* **24**, 108 (1971).
- [155] P. E. Rider and K. A. Gschneidner, Jr., O. D. McMasters, *Trans. AIME* **233**, 1488 (1965).
- [156] A. R. Miedema, *J. Less-Common Met.* **46**, 67 (1976).
- [157] B. T. Matthias, E. Corenzwit, J. M. Vandenberg, H. Barz, M. B. Maple, and R. N. Shelton, *J. Less-Common Met.* **46**, 339 (1976).
- [158] A. E. Dwight, J. W. Downey, and R. A. Conner, Jr., *Acta Crystallogr.* **22**, 745 (1967).
- [159] H. J. M. van Rongen, B. Knook, and G. G. van den Berg, *Low-Temperature Physics LT9*, Proc. IXth Int. Conf. on Low-Temperature Physics, Columbus, OH, B1041 (1964).
- [160] E. Raub, P. Walter, and M. Engel, *Z. Metallkd.* **43**, 112 (1952).
- [161] M. K. McQuillan, *J. Inst. Metals* **82**, 511 (1954).
- [162] P. Pietrokowsky, E. P. Frink, and P. Duwez, *Trans. AIME* **206**, 930 (1956).



- [163] K. Schubert, H. G. Meissner, M. Pötzschke, W. Rossteutscher, and E. Stolz, *Naturwissenschaften* **49**, 57 (1962).
- [164] P. Pietrokowsky, *J. Inst. Metals* **90**, 434 (1961/62).
- [165] H. Vonphilipsborn and F. Laves, *Acta Crystallogr.* **17**, 213 (1964).
- [166] E. Vielhaber and H. L. Luom, *Solid State Comm.* **5**, 221 (1967).
- [167] J. B. Vetrano, G. L. Guthrie, and H. E. Kissinger, *Phys. Lett. A* **26** 45 (1967).
- [168] P. Pietrokowsky, *Scripta Metall.* **2**, 379 (1968).
- [169] S. A. Shabalovskaya, *Solid State Comm.* **70**, 23-26 (1989).
- [170] C. C. Chao, H. L. Luo, and P. Dumez, *J. Appl. Phys.* **34**, 1971 (1963).
- [171] H. R. Kirchmayr, *Z. Metallkd.* **56**, 767 (1965).
- [172] J. B. Kusma and E. Laube, *Monatsh. Chem.* **96**, 1496 (1965).
- [173] Y. Sadagopan, B. C. Giessen, and N. J. Grant, *J. Less-Common Met.* **14**, 279 (1968).
- [174] E. Raub and M. Engel, *Z. Metallkd.* **39**, 172 (1948).
- [175] K. Schubert, M. Balk, S. Bhan, M. Breimer, P. Esslinger, and E. Stolz, *Naturwissenschaften* **49**, 647 (1962).
- [176] M. V. Nevitt and J. W. Downey, *Trans. AIME* **224**, 194 (1962).
- [177] E. Stolz and K. Schubert, *Z. Metallkd.* **53**, 433 (1962).
- [178] H. Holleck, *Acta Crystallogr.* **21**(3), 451 (1966).
- [179] I. Arnberg, *Acta Crystallogr. B* **36**, 527 (1980).
- [180] J. P. Neumann, A. Mikula, and Y. A. Chang, *Metall. Trans. A* **13**(7), 1123 (1982).
- [181] H. Nowotny, E. Bauer, A. Stampfl, and H. Bittner, *Monatsh. Chem.* **83**, 221 (1952).
- [182] M. G. Chasanov, I. Johnson, and R. V. Schablaske, *J. Less-Common Met.* **7**, 1127 (1964).
- [183] M. G. Chasanov, P. D. Hunt, I. Johnson, and H. M. Feder, *Trans. AIME* **224**, 935 (1962).
- [184] W. M. Robertson, *Metall. Trans.* **3** 1443 (1972).
- [185] R. Elmendorf and E. Ryba, *Acta Crystallogr. B* **24**, 462 (1968).
- [186] E. Ryba, P. K. Kejriwal, and R. Elmendorf, *J. Less-Common Met.* **18**, 419 (1969).
- [187] G. Bruzzone, M. L. Fornasini, and F. Merlo, *J. Less-Common Met.* **30**, 361 (1973).
- [188] Y. Ishii, K. Nozawa, and T. Fujiwara, *Mat. Res. Soc. Symp. Proc.* **805**, 129-134 (2003)
- [189] W. Rossteutscher, K. Schubert, *Z. Metallkd.* **56**, 730 (1965).
- [190] Arunsingh and B. Dayal, *Acta Crystallogr. B* **25**, 1010 (1969).
- [191] E. Montignie, *Bull. Soc. Chim. Fr. Mem.* **5**, 567 (1938).
- [192] J. D. Grogan and J. L. Haughton, *J. Inst. Met.* **69**, 241-248 (1943).
- [193] N. Tiner, *Trans. Am. Inst. Mining, Metallurgical and Petroleum Eng.* **161**, 351-359 (1945).
- [194] H. Nowotny, *Z. Metallkd.* **37**, 130-136 (1946).
- [195] N. I. Varich and B. N. Litvin, *Phys. Met. Metallogr.* **16**(4), 29-32 (1963).
- [196] J. J. Hauser, J. V. Waszczak, and B. A. Davidson, *Solid State Comm.* **62**, 835-836 (1987).
- [197] E. Rudy, *Compendium of Phase Diagram Data*, Air Force Materials Laboratory, Wright-Patterson AFB, OH, Rep. No. AFML-TR-65-2, Part V (1969).
- [198] J. Chao, C. Wolverton, J. Sofo, L.-Q. Chen, and Z.-K. Liu, *Phys. Rev. B* **69**, 214202 (2004).
- [199] S. S. Rajput, R. Prasad, R. M. Singru, S. Kaprzyk, and A. Bansil, *Mater. Sci. Forum* **175-178**, 925 (1995).
- [200] C. MoBecker and J. Hafner, *J. Physics: Cond. Matt.* **7**, 5843-56 (1995).
- [201] A. Maldonado and K. Shubert, *Z. Metallkd.* **55**, 619 (1964).
- [202] E. Raub, *Z. Metallkd.* **45**, 23-30 (1954).
- [203] K. Schubert, W. Burkhardt, P. Esslinger, E. Günzel, H. G. Meissner, W. Schütt, J. Wegst, and M. Wilkens, *Naturwissenschaften* **43**, 248-249 (1956).
- [204] A. G. Knapton, *Planseeber. Pulvermet.* **7**, 2-3 (1959).
- [205] K. Schubert, K. Frank, R. Gohle, A. Maldonado, H. G. Meissner, A. Raman, and W. Rossteutscher, *Naturwissenschaften* **50**, 41 (1963).
- [206] H. P. Rooksby and B. Lewis, *J. Less-Common Met.* **6**, 451-460 (1964).
- [207] H. Ocken and J. H. N. Van Vucht, *J. Less-Common Met.* **15**, 193-199 (1968).
- [208] R. Flükiger, A. Paoli, R. Roggen, K. Yvon, and J. Müller, *Solid State Comm.* **11**, 61-63 (1972).
- [209] R. Flükiger, K. Yvon, C. Susz, R. Roggen, A. Paoli, and J. Müller, *J. Less-Common Met.*, **32**, 207 (1973).
- [210] R. Flükiger, A. Paoli, and J. Müller, *Solid State Comm.* **14**, 443-447 (1974).
- [211] C. W. Haworth and W. Hume-Rothery, *J. Inst. Met.* **87**, 265 (1958/1959).
- [212] E. Anderson and W. Hume-Rothery, *J. Less-Common Met.* **2**, 19 (1960).
- [213] B. C. Giessen, U. Jaehnigen and N. J. Grant, *J. Less-Common Met.* **10**, 147 (1966).
- [214] R. Gurler and J. N. Pratt, *J. Alloys Compd.* **177**, 321 (1991).
- [215] H. Kleykamp, *J. Less-Common Met.* **136**, 271 (1988).
- [216] S. Ferreira, J. Duarte Jr., and S. Frota-Pessoa, *Phys. Rev. B* **41**, 5627 (1990).
- [217] P. Souvatzis, M. I. Katsnelson, S. Simak, R. Ahuja, O. Eriksson, and P. Mohn, *Phys. Rev. B* **70**, 12201 (2004).
- [218] G. N. Ronami, *Krist. Tech.* **7**(6), 615 (1972).
- [219] R. G. Baggerly, *Metallography* **8**, 361 (1975).
- [220] D. L. Moffatt and U. R. Kattner, *Metall. Trans.* **19**, 2389 (1988).
- [221] G. Rubin and A. Finel, *J. Physics: Cond. Matt.* **7**, 3139-52 (1995).
- [222] K. A. Gschneidner, Jr. *Rare Earth Alloys*, Van Nostrand, Princeton, NJ, 221 (1961).
- [223] L. T. Kong, J. B. Liu, and B. X. Liu, *J. Mater. Res.* **17**, 528-531 (2002).
- [224] R. E. Watson, M. Weinert, and M. Alatalo, *Phys. Rev. B* **65**, 014103 (2002).
- [225] B. T. Matthias, V. B. Compton, and E. Corenzwit, *Phys. Chem. Solids* **19**, 130 (1961).
- [226] B. C. Giessen and N. J. Grant, *Acta Crystallogr.* **17** 615 (1964).

- [227] A. Maldonado and K. Shubert, *Z. Metallkd.* **55**, 619 (1964).
- [228] B. C. Giessen and N. J. Grant, *J. Less-Common Met.* **8**, 114 (1965).
- [229] R. M. Waterstrat and B. C. Giessen, *Metall. Trans. A* **16**(11), 1943 (1985).
- [230] D. L. Ritter, B. C. Giessen, and N. J. Grant, *Trans. AIME* **230**, 1250 (1964).
- [231] D. L. Ritter, B. C. Giessen, and N. J. Grant, *Trans. AIME* **230**, 1259 (1964).
- [232] M. Rajagopalan and M. Sundareswari, *J. Alloys Compd.* **379**, 8-15 (2004).
- [233] D. Bender, E. Bucher, and J. Muller, *Phys. Kondens. Mater.* **1**, 225 (1963).
- [234] E. Raub and W. Fritzsche, *Z. Metallkd.* **54** 317 (1963).
- [235] G. F. Hurley and J. H. Brophy, *J. Less-Common Met.* **7**, 267 (1964).
- [236] T. Tsukamoto, K. Koyama, A. Oota, and S. Noguchi, *Nippon Kinzoku Gakkai-shi* **53**(3), 253 (1989).
- [237] B. H. Chen, H. F. Franzen, *J. Less-Common Met.* **153**, L13 (1989).
- [238] J. M. Sanchez and J. D. Becker, *Mat. Res. Soc. Symp. Proc.* **291**, 115-27 (1993).
- [239] J. D. Becker and J. M. Sanchez, *J. Mater. Sci.* **A170**, 161-167 (1993).
- [240] J. D. Becker, J. M. Sanchez, and J. K. Tien, *Mat. Res. Soc. Symp. Proc.* **213**, 113-18 (1991).
- [241] V.B. Compton, E. Corenzwit, J. P. Maita, B. T. Matthias, and F. J. Morin, *Phys. Rev.* **123**, 1567 (1961).
- [242] D. O. Van Ostenburg, D. J. Lam, M. Shimizu, and A. Katsuki, *J. Phys. Soc. Japan* **18**, 1744-1754 (1963).
- [243] A. L. Giorgi and E. G. Szklarz, *J. Less-Common Met.* **20**(2), 173-175 (1970).
- [244] O. N. Carlson, V. C. Marcotte, and D. E. Williams, *USAEC Rep. ISC-1050*, 53 (1959).
- [245] O. N. Carlson, W. L. Larsen, V. C. Marcotte, and D. E. Williams, *USAEC Rep. IS-17*, 76 (1959).
- [246] C. E. Lundin and D. T. Klodt, *J. Inst. Met.* **90**, 341 (1961).
- [247] A. Taylor, W. M. Hickam, and N. J. Doyle, *J. Less-Common Met.* **9**, 214 (1965).
- [248] L. T. Kong, J. B. Liu and B. X. Liu, *J. Phys. Soc. Jpn.* **71**, 141-3 (2002).
- [249] A. G. Rabinkin, L. A. Klishanova, and L. N. Pronina, *Problems of Superconducting Materials* **141** (1970).
- [250] P. Van Effenterre, Report CEA0R04330, Atomic Energy Commission, Saclay, France (1972).
- [251] P. E. J. Flewitt, *J. Appl. Crystallogr.* **5**, 423 (1972).
- [252] P. E. J. Flewitt, *Acta Metall.* **22**, 47 (1974).
- [253] J. P. Abriata and J. C. Bolcich, *Bull. Alloy Phase Diagrams* **3**(1) (1982).
- [254] H. v. Leuken, A. Lodder, M. T. Czyzyk, F. Springelkamp, and R. A. de Groot, *Phys. Rev. B* **41**, 5613 (1990).
- [255] J. M. Sanchez and J. D. Becker, *Prog. Theor. Phys. Sul.* **115**, 131-45 (1994).
- [256] G. B. Grad, A. F. Guillermet, and J. R. Granada, *Z. Metallkd.* **87**, 726-731 (1996).
- [257] G. B. Grad, G. M. Benites, G. Aurelio, and A. F. Guillermet, *Mat. Sci. Eng. A-Struct.* **A273-275**, 175-180 (1999).
- [258] J. Kudrnovsky and V. Drchal, *Z. Phys. B Cond. Mat.* **73**, 489-93 (1989).
- [259] B. C. Giessen, N. J. Grant, D. P. Parker, R. C. Manuszewski, and R. M. Waterstrat, *Metall. Trans. A* **11**, 709 (1980).
- [260] E. Raub, *J. Less-Common Met.* **1**(1), 3 (1959).
- [261] D. T. Hawkins, in *Metals Handbook, Metallography, Structures and Phase Diagrams*, Vol. 8, 8th ed., American Society for Metals, Metal Park, Ohio (1973).
- [262] Z. W. Lu, S.-H. Wei, and A. Zunger, *Phys. Rev. Lett.* **66**, 1753 (1991).
- [263] E. Raub, *J. Less-Common Met.* **1**(1), 3 (1959).
- [264] E. Raub, H. Beeskow, and D. Menzel, *Z. Metallkd.* **50**, 428 (1959).
- [265] P. E. A. Turchi, G. M. Stocks, W. H. Butler, D. M. Nicholson, and A. Gonis, *Phys. Rev. B* **37**, 5982 (1988).
- [266] J. E. Shield, and R. K. Williams, *Scr. Metall.* **21**, 1475 (1987).
- [267] M. Asato, T. Hoshino, and K. Masuda-Jindo, *J. Magn. Mater.* **226-230**, 1051-2 (2001).
- [268] M. Asato, T. Mizuno, T. Hoshino, and H. Sawada *Mater. Trans.* **42**, 2216-2224 (2001).
- [269] C. Wolverton and D. de Fontaine, *Mat. Res. Soc. Symp. Proc.* **291**, 431-6 (1993).
- [270] F. M. Marquez, C. Cienfuegos, B. K. Pongsai, M. Yu. Lavrentiev, N. L. Allan, J. A. Purton, and G. D. Barrera, *Model. Simul. Mater. Sc.* **11**, 115-26 (2003).
- [271] A. A. Rudnitskii and R. S. Plyakova, *Zh. Neorg. Khim.* **4**, 1014 (1959); *Russ. J. Inorg. Chem.* **4**, 631 (1959).
- [272] A. S. Darling and J. M. Yorke, *Platinum Met. Rev.* **4**, 104 (1960).
- [273] H. Kleykamp, *J. Nucl. Mater.* **167**, 49 (1989).
- [274] H.B. Guo, X.Y. Li, and B. X. Liu, *J. Phys. Soc. Jpn.* **71**, 2933-5 (2002).
- [275] H. R. Haines, P. E. Potter, and M. H. Rand, *Thermodynamics of Nuclear Materials, Proceedings of a Symposium, 4th, Vienna* **1**, 471-501 (1980).
- [276] A. A. Rudnitskii and N. A. Birun, *Russ. J. Inorg. Chem.* **5**, 1169-1173 (1960).
- [277] A. E. Dwight, R. A. Jr. Conner, and J. W. Downey, *Acta Crystallogr.* **18**, 835-839 (1965).
- [278] H. W. Rosenberg and D. B. Hunter, *Trans. AIME* **233**, 681-685 (1965).
- [279] E. Raub and E. Röschel, *Z. Metallkd.* **59**, 112-114 (1968).
- [280] P. Krautwasser, S. Bhan, and K. Schubert, *Z. Metallkd.* **59**, 724-729 (1968).
- [281] H. Schulz, K. Ritapal, W. Bronger, and W. Klemm, *Z. Anorg. und Allg. Chem.* **358**, 299-313 (1968).
- [282] I. R. Harris and M. Norman, *J. Less-Common Met.* **22**, 127-130 (1970).
- [283] H. C. Donkersloot and J. H. N. Van Vucht, *J. Less-Common Met.* **20**, 83-91 (1970).
- [284] V. N. Eremenko and T. D. Shtepa, *Sov. Powder Metall. Metal Cer.* **11**, 228-233 (1972).
- [285] A. R. Miedema, K. H. J. Buschow, and H. H. Van Mal, *J. Less-Common Met.* **49**, 463-472 (1976).

- [286] V. P. Sivokha, A. S. Savvinov, V. P. Voronin, and V. N. Khachin, *Phys. Met. Metallogr.*, translated from *Fizika Metallov, Metallovedenie* **56**(3), 112-116 (1983).
- [287] S. A. Shabalovskaya, A. I. Lotkov, A. G. Narmonev, and A. I. Zakharov, *Solid State Comm.* **62**, 93-95 (1987).
- [288] N. Selhaoui, J. C. Gachon, and J. Hertz, *J. Less-Common Met.* **154**, 137-147 (1989).
- [289] S. Pick and P. Mikusik, *Solid State Comm.* **80**, 897-899 (1991).
- [290] P. Mikusik and S. Pick, *Solid State Comm.* **86**, 467-469 (1993).
- [291] J. M. Zhang and G. Y. Guo, *J. Phys. Cont. Mat.* **7**, 6001-60017 (1995).
- [292] C. Wolverton, G. Ceder, D. de Fontaine, and H. Dreysse, *Phys. Rev. B* **48**, 726 (1993).
- [293] O. Loebich and E. Raub, *J. Less-Common Met.* **30**(1), 47 (1973).
- [294] J. Le Roy, J. M. Moreau, and D. Paccard, *Acta Crystallogr. B* **33**(8), 2414 (1977).
- [295] R. Sanjines-Zeballos, R. Chabot, and E. Parthé, *J. Less-Common Met.* **72**(1), P17 (1980).
- [296] K. Takao, Y. Sakamoto, and M. Yoshida, *J. Less-Common Met.* **152**, 115 (1989).
- [297] K. Anderko, *Z. Metallkd.* **50**, 681 (1959).
- [298] E. Stolz and K. Schubert, *Z. Metallkd.* **53**, 433 (1962).
- [299] I. R. Harris and M. Norman, *J. Less-Common Met.* **18**, 333 (1969).
- [300] E. M. Savitsky, V. P. Polyakova, N. Gorina, and N. Roshan, *Physical Metallurgy of Platinum Metals*, MIR, Moscow (1978).
- [301] M. S. Chandrasekharaiah, M. J. Stickney, K. A. Gingerich, and J. A. Speed, *J. Alloy Phase Diagrams* **6**, 59 (1990).
- [302] V. N. Kuznetsov, G. P. Zhmurko, and E. M. Sokolovskaya, *J. Less-Common Met.* **163**, 1 (1990).
- [303] S. Stolen and T. Matsui, *J. Nucl. Mater.* **186**, 242 (1992).
- [304] L. A. Bendersky, J. K. Stalick, R. Portier, and R. M. Waterstrat, *J. Alloys Compd.* **236**, 19 (1996).
- [305] E. Gaganidze, P. Esquinazi, and R. König, *Europhys. Lett.* **31**, 13 (1995).
- [306] J. M. Hutchinson, *Platinum Met. Rev.* **16**, 88 (1972).
- [307] G. A. Camara, M. J. Giz, V. A. Paganin, and E. A. Ticianelli, *J. Electroanal. Chem.* **537**, 21 (2002).
- [308] N. Nishimura and T. Hiramatsu, *Nippon Kinzoku Gakkaishi* **21**, 469 (1957).
- [309] T. Sato, S. Hukai, and Y. C. Huang, *J. Austr. Inst. Met.* **5**(2), 149 (1960).
- [310] P. Pietrokowsky, *Nature* **206**, 291 (1965).
- [311] A. K. Sinha, *Trans. AIME* **245**, 237 (1969).
- [312] P. J. Meschter and W. L. Worrell, *Metall. Trans. A* **7**, 299 (1976).
- [313] V.B. Compton and B. T. Matthias, *Acta Crystallogr.* **12**, 651 (1959).
- [314] T. H. Geballe, B. T. Matthias, V.B. Compton, E. Corenzwit, G. W. Hull, and L. D. Longinotti, *Phys. Rev.* **137**, 119 (1965).
- [315] W. Bronger, *J. Less-Common Met.* **12**, 63 (1967).
- [316] N. H. Krikorian, *J. Less-Common Met.* **23**, 271 (1971).
- [317] A. Raman, *J. Less-Common Met.* **26**, 199 (1972).
- [318] B. Erdmann and C. Keller, *J. Solid State Chem.* **7**, 40 (1973).
- [319] J. Le Roy, J. M. Moreau, D. Paccard, and E. Parthé, *Acta Crystallogr. B* **34**, 3315 (1978).
- [320] X. Yifen and O. Loebich, *J. Less-Common Met.* **144**, 301 (1988).
- [321] H. J. Wallbaum, *Naturwissenschaften* **31**, 91 (1943).
- [322] A. Raman and K. Schubert, *Z. Metallkd.* **55**, 704 (1964).
- [323] K. Shubert, S. Bhan, T. K. Biswas, K. Frank, and P. K. Pandey, *Naturwissenschaften* **55**, 542 (1968).
- [324] A. R. Miedema, R. Boom, and F. R. De Boer, *J. Less-Common Met.* **41**, 283 (1975).
- [325] A. Hellawell, and W. Hume Rothery, *Phil. Mag.* **45**, 797 (1954).
- [326] J. O. A. Paschoal, H. Kleykamp, and F. Thmmler, *J. Less-Common Met.* **98**, 279 (1984).
- [327] R. Gurler, *J. Alloys Compd.* **191**, 31 (1993).
- [328] E. Raub and E. Roeschel, *Z. Metallkd.* **57** 546 (1966).
- [329] V. N. Eremenko, T. D. Shtepa, and V. G. Sirotenko, *Sov. Powder Metall. Metal Cer.* **5**, 487 (1966).
- [330] V. N. Eremenko and T. D. Shtepa, *Colloq. Int. CNRS* **205**, 403 (1972).
- [331] T. D. Shtepa, *Fiz. Khim. Kondens. Faz. Sverkhverd. Mater.* 175 (1975).
- [332] R. Kuentzler and R. M. Waterstrat, *Solid State Comm.* **68**, 85 (1988).
- [333] V. B. Compton and B. T. Matthias, *Acta Crystallogr.* **12**, 651 (1959).
- [334] T. H. Geballe, B. T. Matthias, V. B. Compton, E. Corenzwit, G. W. Hull, and L. D. Longinotti, *Phys. Rev. A* **137**, 119 (1965).
- [335] A. Raman, *J. Less-Common Met.* **26**(2), 199 (1972).
- [336] H. Ghassem and A. Raman, *Z. Metallkd.* **64**(3), 197 (1973).
- [337] J. M. Moreau, D. Paccard, and E. Parthé, *Acta Crystallogr. B* **32**, 1767 (1976).
- [338] O. Loebich and E. Raub, *J. Less-Common Met.* **46**, 1 (1976).
- [339] S. T. Ziegler, *J. Phys. Chem. Solids* **26**, 1347 (1965).
- [340] V. N. Eremenko, E. L. Semenova, and T. D. Shtepa, *Russ. Metall.* (2), 158 (1978).
- [341] V. N. Eremenko, E. L. Semenova, and T. D. Shtepa, *Diag. Sostoyaniya Tugoplavk Sistem Kiev*, 119 (1980).
- [342] J. L. Jorda, T. Graf, L. Schellenberg, J. Müller, K. Cenuzal, J. C. Gachon, and J. Hertz, *J. Less-Common Met.* **136**, 313 (1988).
- [343] R. Kuentzler and R. M. Waterstrat, *Solid State Comm.* **68**, 85 (1988).
- [344] E. L. Semenova and Y. V. Kudryavtsev, *J. Alloys Compd.* **203**, 165 (1994).
- [345] A. Szajek and A. Jezierski, *Solid State Commun.* **71**, 917-22 (1989).
- [346] N. Y. Alekseyevskiy, O. A. Balakhovskii, and I. V. Kirillov, *Phys. Met. Metallogr.*, translated from *Fizika Metallov, Metallovedenie* **40**, 38 (1975).
- [347] C. B. Jordan, *Trans. Am. Inst. Mining, Metallurgical and Petroleum Eng.* **203**, 832-833 (1955).
- [348] A. E. Dwight, *Trans. Am. Inst. Mining, Metallurgical*

- and Petroleum Eng. **215**, 283-286 (1959).
- [349] D. D. Gulamova, M. V. Raevskaya, I. G. Sokolova, F. S. Litvak, and E. M. Sokolovskaya, Moscow Univ. Chem. Bull. **27**(4), 96 (1972).
- [350] E. Raub and E. Roeschel, Z. Metallkd. **54**(8) 455 (1963).
- [351] Y. Tamminga, B. Barkman, and F. R. De Boer, Solid State Comm. **12**, 731-735 (1973).
- [352] V. N. Eremenko, T. D. Shtepa, and V. T. Khoruzhaya, Russ. Metall. (2), 155-156 (1973).
- [353] N. G. Boriskina and I. I. Kornilov, Russ. Metall. (2), 162 (1976).
- [354] J. M. Zhang and G. Y. Guo, J. Phys. Cond. Matt. **7**, 6001-6017 (1995).
- [355] O. Loebich and E. Raub, J. Less-Common Met. **46**, 7 (1976).
- [356] K. Cenzual, A. Palenzona, and E. Parthé, Acta Crystallogr. B **36**(7), 1631 (1980).
- [357] R. Sanjines-Zaballos, B. Chabot, and E. Parthé, J. Less-Common Met. **72**, P17 (1980).
- [358] P. Sharifrazi, R. C. Mohanty, and A. Raman, Z. Metallkd. **75**(10), 801 (1984).
- [359] M. L. Fornasini, A. Mugnoli, and A. Palenzona, J. Less-Common Met. **154**, 149 (1989).
- [360] A. Palenzona and E. Canepa, J. Less-Common Met. **162**, 267 (1990).
- [361] V. N. Eremenko, E. L. Semenova, and T. D. Shtepa, Russ. Metall. (2), 177 (1980).
- [362] V. N. Eremenko, V. T. Khoruzhaya, and T. D. Shtepa, Russ. Metall. (1), 194 (1988).
- [363] M. J. Mehl, J. E. Osburn, D. A. Papaconstantopoulos, and B. M. Klein, Mat. Res. Soc. Symp. Proc. **186**, 277-82 (1991).
- [364] C. C. Koch, J. Less-Common Met. **6**, 177 (1976).
- [365] J. B. Darby, Jr., D. J. Lam, L. J. Norton, and J. W. Downey, J. Less-Common Met. **4**, 558 (1962).
- [366] J. B. Darby, Jr., L. J. Norton, and J. W. Downey, J. Less-Common Met. **5**, 397 (1963).
- [367] J. B. Darby, Jr., L. J. Norton, and J. W. Downey, J. Less-Common Met. **6**, 165 (1964).
- [368] J. Niemiec, Bull. Acad. Pol. Sci. Ser. Sci. Chem. **11**. 665 (1963).
- [369] E. G. Szklarz and A. L. Giorgi, J. Less-Common Met. **81**, 2349 (1981).
- [370] A. L. Giorgi and E. G. Szklarz, J. Less-Common Met. **22**, 246 (1970).
- [371] P. A. Farrar and S. Adler, Trans. AIME **236**, 1061 (1966).
- [372] D. Chatterji, M. T. Hepworth, and S. J. Hruska, Metall. Trans. **2**, 1271 (1971).
- [373] J. Etchessahar and J. Debuigne, Mem. Sci. Rev. Metall. **74**(3), 195 (1977).
- [374] J. P. Auffredic, E. Etchessahar, and J. Debuigne, J. Less-Common Met. **84**, 49 (1982).
- [375] C. E. Lundin, *Rare Earth Symposium*, Annual Meeting, Am. Soc. Metals, Chicago (1959).
- [376] J. C. Uy, D. J. Lam, L. C. Ianiello, R. A. Proebstle, A. P. Lee, B. T. M. Loh, and A. A. Burr, Final Report AT(30-1)-2159, Rensselaer Polytechnic Institute (1961).
- [377] C. E. Lundin, D. T. Klodt, Trans. AIME **224**, 367 (1962).
- [378] R. Wang, Metall. Trans. **3**, 1213 (1972).
- [379] R. Wang and Y. B. Kim, Metall. Trans. **5**, 1973 (1974).
- [380] R. Wang, Mater. Sci. Eng. **23**, 135 (1976).
- [381] A. van de Walle and G. Ceder, Rev. Mod. Phys. **74**(1), 11 (2002).
- [382] C. Wolverton and V. Ozolins, Phys. Rev. Lett. **86**, 5518 (2001).